Technical Report

TR-99-23

SR 97

Radionuclide transport calculations

Maria Lindgren
Kemakta Konsult AB

Fredrik Lindström
Svensk Kärnbränslehantering AB

December 1999

Svensk Kärnbränslehantering AB
Swedish Nuclear Fuel
and Waste Management Co
Box 5864
SE-102 40 Stockholm Sweden
Tel 08-459 84 00
+46 8 459 84 00
Fax 08-661 57 19
+46 8 661 57 19

SR 97

Radionuclide transport calculations

Maria Lindgren
Kemakta Konsult AB

Fredrik Lindström
Svensk Kärnbränslehantering AB

December 1999

Summary

An essential component of a safety assessment is to calculate radionuclide release and dose consequences for different scenarios and cases. The SKB tools for such a quantitative assessment are used to calculate the maximum releases and doses for the hypothetical repository sites Aberg, Beberg and Ceberg for the initial canister defect scenario and also for the glacial melting case for Aberg.

The reasonable cases, i.e. all parameters take reasonable values, results in maximum biosphere doses of $5 \cdot 10^{-8}$ Sv/yr for Aberg, $3 \cdot 10^{-8}$ Sv/yr for Beberg and $1 \cdot 10^{-8}$ Sv/yr for Ceberg for peat area. These doses lie significantly below 0.15 mSv/yr. (A dose of 0.15 mSv/yr for unit probability corresponds to the risk limit of 10^{-5} per year for the most exposed individuals recommended in regulations.)

The conclusion that the maximum risk would lie well below 10^{-5} per year is also demonstrated by results from the probabilistic calculations, which directly assess the resulting risk by combining dose and probability estimates. The analyses indicate that the risk is $2 \cdot 10^{-5}$ Sv/yr for Aberg, $8 \cdot 10^{-7}$ Sv/yr for Beberg and $3 \cdot 10^{-8}$ Sv/yr for Ceberg.

The analysis shows that the most important parameters in the near field are the number of defective canisters and the instant release fraction. The influence from varying one parameter never changes the doses as much as an order of magnitude. In the far field the most important uncertainties affecting release and retention are associated with permeability and connectivity of the fractures in the rock. These properties affect several parameters. Highly permeable and well connected fractures imply high groundwater fluxes and short groundwater travel times. Sparsely connected or highly variable fracture properties implies low flow wetted surface along migration paths. It should, however, be remembered that the far-field parameters have little importance if the near-field parameters take their reasonable values. In that case almost all radionuclides will be contained in the near field. The dose rate in the biosphere is essentially controlled by the possibilities of dilution. If the release occurs to an inner bay or open coast, the dose rates will be several orders of magnitude lower than if the release occurs to a drinking water well or peat area.

Sammanfattning

En grundläggande del av en säkerhetsanalys är att beräkna radionuklidutsläpp och doskonsekvenser för olika scenarier och fall. SKB's verktyg för denna kvantitativa analys har använts för att beräkna maximala utsläpp och doser för de tre hypotetiska förvarsplatserna Aberg, Beberg och Ceberg för kapseldefektscenariot och för ett fall inkluderande smältning av inlandsisen för Aberg.

Det rimliga fallet, dvs. alla parametrar har rimliga värden, resulterar i maximala biosfärsdoser på $5 \cdot 10^{-8}$ Sv/yr för Aberg, $3 \cdot 10^{-8}$ Sv/år för Beberg och $1 \cdot 10^{-8}$ Sv/år för Ceberg för torvmark. Dessa doser ligger signifikant under 0.15 mSv/år. (En dos på 0.15 mSv/år motsvarar en riskgräns på 10^{-5} per år för de mest exponerade individerna om exponering säkert inträffar, vilket är ett stipulerat acceptanskriterium.)

Slutsatsen att den maximala risken ligger väl under 10^{-5} per år stöds också av resultaten från de probabilistiska beräkningarna, som direkt ger risken genom kombinering av dos och sannolikhet. Analysen indikerar att risken är $2 \cdot 10^{-5}$ Sv/år för Aberg, $8 \cdot 10^{-7}$ Sv/år för Beberg och $3 \cdot 10^{-8}$ Sv/år för Ceberg. Denna analys ger dock bara en indikation och behöver utökas i en säkerhetsanalys som skall stödja en licensansökan.

Analysen visar att de viktigaste parametrarna i närzonen är antalet defekta kapslar och den omedelbart tillgängliga fraktionen. Inverkan av att variera en parameter i taget ändrar aldrig dosen så mycket som en tiopotens. I fjärrzonen är den viktigaste osäkerheten som påverkar utsläpp och fördröjning relaterade till sprickornas permeabilitet och hur väl de är sammanbundna. Dessa egenskaper påverkar flera parametrar. Högpermeabla och väl sammanbundna sprickor medför höga grundvattenflöden och korta gångtider. Sparsamt sammanbundna sprickor eller kraftigt varierande sprickegenskaper medför en liten flödesvätt yta längs transportvägen. Det skall emellertid noteras att fjärrzonsparametrarna har liten betydelse om närzonsparametrarna antar sina rimliga värden. Dosen i biosfären bestäms huvudsakligen av utspädningen. Om utsläppet sker till en vik eller öppen kust är dosen flera tiopotenser lägre än om utsläppet sker till en dricksvattenbrunn eller torvmark.

Contents

1 Introduction

The objective of this report is to describe how the radionuclide release calculations for the canister defect scenario within the Safety Report 97 have been carried out. The information used in the calculations is documented and the results are presented and discussed.

The aims of the radionuclide release calculations are to:

- Quantitatively describe the radionuclide transport.
- Show the impact of uncertainty in input data and show which parameters that governs the calculated release rates.
- Compare three hypothetical sites (Aberg, Beberg and Ceberg) with each other and with risk limits recommended in regulations.
- Illustrate the impact of the different barriers in the system.

By performing several calculation cases for each site, enough knowledge and understanding about the system is achieved to fulfil these aims.

The calculation results are reported up to a time period of one million years, in accordance with SKI´s draft regulations.

1.1 Scenarios

The scenario analysis of SR 97 is provided in the SR 97 Main Report. Some results of this analysis have implications for the work discussed in this report and are thus summarised here.

The base scenario in SR 97 assumes the following conditions:

- All canisters are manufactured and sealed without defects. The repository is constructed according to specifications.
- Present day climate will prevail also in the future.
- Present day site-specific groundwater chemistry and groundwater flow are assumed to be valid also in the future. Effects of land rise and other transients clearly observable today may still be considered.
- Rock mechanical conditions, including the stress field, will remain as they are today although the repository induced effects on creep, thermal expansion or contractions etc. is to be considered. However, future seismic events or changes to the mechanical boundary conditions are not considered.
- The conditions of present day site-specific biospheres will prevail also in the future. Effects of land rise and other transients clearly observable today may still be considered.

The evaluation of the base scenario, covered in the SR 97 Main Report and in supporting documents, particularly concerns evaluation of the canister life time.

Post-closure radiological consequences can only occur in case canisters break and release radionuclides. Thus, the base scenario may not result in any consequences for an

extremely long period of time. In order to explore the function of the other barriers of the repository system SR 97 also considers a scenario postulating some initially defective canisters. In addition, the scenario is also relevant since such initial defects may not be totally avoided. The initial canister defect scenario builds upon the assumptions that all conditions, except those concerning the initial state of the canisters, are as for the base scenario.

Apart from these two scenarios, SR 97 evaluates scenarios describing e.g. changing climate and earthquakes.

1.2 Models and data

The models and data used in the calculations are described in Chapters 2 and 3 respectively. The understanding of the various transport processes and phenomena underlying the formulation of the computer models is described in the SR 97 Process Report and summarised in the SR 97 Main Report. The data and data uncertainties/variabilities are presented in detail in the SR 97 Data Report (Andersson, 1999). Most of the underlying analyses yielding input to the model chain are in the SR 97 Main Report.

2 Models

In this chapter the steps taken in performing radionuclide release calculations for a safety assessment are described.

Evaluation of the consequences is made with a series of coupled models, which in turn require input from analyses of the state of the barriers and the rock. This chapter briefly outlines the main components and the information flow in this chain of models.

2.1 Near-field geometry and exit paths

A schematic view of the near field assumed for the canister defect scenario is given in Figure 2-1. The nuclides may escape from the canister through a small hole into the bentonite by diffusion. The transport continues to one of the four possible exit paths, indicated in the figure as Q1-Q4. Q1 is a fracture around the deposit hole at the top of the canister. Q2 is a fractured zone around the upper part of the deposition hole. Q3 is a fracture through the deposition tunnel (disturbed zone). Exit through Q2 and Q3 also include transport through crushed rock-bentonite. Q4 is a fracture zone below the deposition hole with good rock between and therefore exit through Q4 also includes transport through rock.

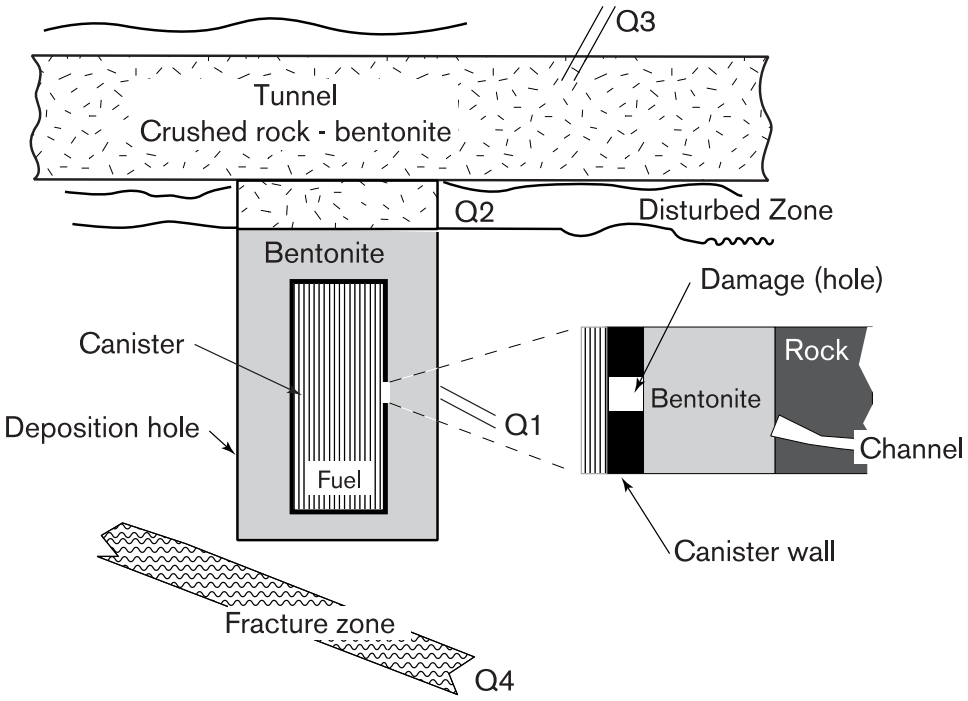

Figure 2-1. *Schematic view of the near field, showing a small hole in the canister and the location of various transport paths into the near-field rock. (Q1 is a fracture around the deposition hole at the top of the canister. Q2 is a fractured zone around the upper part of the deposition hole. Q3 is a fracture through the deposition tunnel (disturbed zone). Q4 is a fracture zone below the deposition hole with good rock between.)*

2.2 The chain of models

The primary model used for evaluating the radiological consequences of the initially damaged canister is made up of a series of coupled (sub-) models as illustrated in Figure 2-2.

The hydrological calculations were performed with HYDRASTAR and saved for use in this study with HYDRABOOT. The direct radiological consequence analyses are performed by the near-field model COMP23 (Romero, 1995), the far-field migration code FARF31 (Norman and Kjellbert, 1990) and the code BIO42/SUM41 which transforms radionuclide flow into dose using pre-calculated dose conversion factors. The programs PREBAT and BATEMAN are used to prepare the inventory for use in the near-field model. TULLGARN is an older steady-state near-field model not used in SR 97.

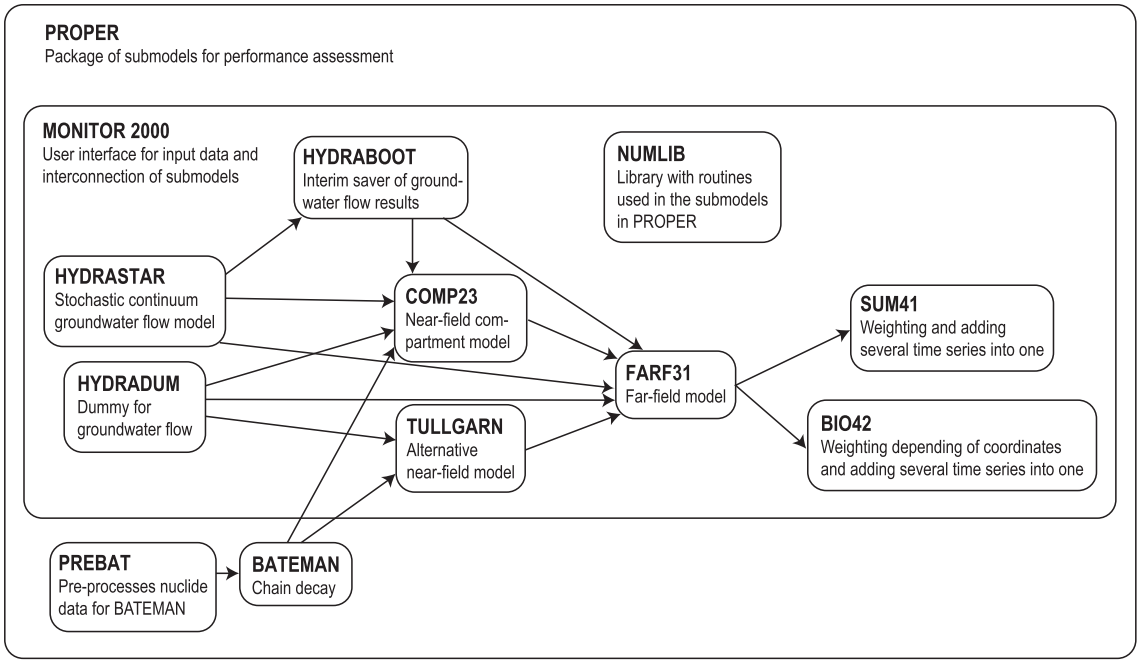

Figure 2-2. *Schematic view of the different submodels included in the PROPER package that is used in the calculations.*

2.2.1 HYDRADUM/HYDRABOOT

HYDRADUM is a simple model used in the deterministic calculations. The model gives the groundwater flow data to the near-field and far-field model in a correct format.

HYDRABOOT is used in the probabilistic calculations. The model is an interim saver for groundwater flow results to give the possibility to divide the calculations into two parts. In the calculations performed with groundwater flow model HYDRASTAR (Walker and Gylling, 1998; Gylling et al., 1999; Walker and Gylling, 1999) the results are saved by HYDRABOOT in a file for later use in the radionuclide release calculations. When the radionuclide release calculations are performed the saved data is fetched by HYDRABOOT.

For a number of representative canister positions in the repository (typically 120), HYDRASTAR calculates:

- the near-field groundwater flux
- the groundwater travel time from the canister position to the surface exit point
- the coordinates of the exit points.

The results for only limited number of canister positions are used in the radionuclide transport calculations since only limited numbers of canisters are assumed to be defective. Therefore, HYDRABOOT also contains a function for random choice of a limited number of the canister positions. This is done by random choice of one position and then a second one from all positions including also the first one. This process is repeated until the desired amount of defective canisters is represented. Every position represents several canisters and hence every choice is made among all positions.

2.2.2 COMP23

The near-field model COMP23 is a compartment model that is developed from the NUCTRAN-code (Romero, 1995 and Romero et al., 1999). COMP23 is a multiple path model that calculates the instationary nuclide transport in the near field of a repository as occurring through a network of resistances and capacitances coupled together in analogy with an electrical circuit network. Analytical solutions instead of fine discretization at sensitive zones, for example at the exit point of the canister hole and at the entrance to fractures, are embedded to speed up the calculations.

The used near-field model COMP23 does only take into account transport due to diffusion. In Moreno (1999) the potential effects of flow in the backfill were studied. Moreno concluded that the impact of flow has little effect on the release since the main transport resistance in the near field is not located in the tunnel.

To represent the barrier system, through which the species are transported, COMP23 makes use of the integrated finite difference method and of the concept of compartments. The barrier system is discretized into compartments. The material balance over a compartment connected to some other compartment for a dissolved single nuclide is described as:

$$V_i K_i \frac{dc_i}{dt} = \sum_{j \neq i} \left(\frac{AD_e}{d} \right)_{i,j} (c_j - c_i) - V_i K_i \lambda c_i$$

where
V_i is the volume of compartment i (m^3)
V_iK_i is the capacity of the compartment, $K = \varepsilon + (1-\varepsilon)K_d \rho_s$
ε is the porosity of the material in the compartment (-)
K_d is the distribution coefficient (m^3/kg)
ρ_s is the solid density of the material in the compartment (kg/m^3)
c_i, c_j is the concentration in compartment i and j respectively (mol/m^3)
A is the diffusion area (m^2)
D_e is the effective diffusivity (m^2/s)
d is the diffusion length (m)
λ is the decay constant (s^{-1}).

The left-hand side of the equation accounts for the accumulation of nuclides in the water and the solid by sorption. The right hand side accounts for the diffusive transport from one compartment to the adjacent compartments and the radionuclide decay.

The compartments are defined by their volume, their diffusion length and cross sectional area used by the diffusion and material data, such as porosity, density and diffusivities.

Fuel dissolution

The major part of the radionuclides in the spent fuel is embedded in the fuel matrix, which must be dissolved before nuclides are free for transport. A certain fraction of some nuclides are though directly available since they are located either on the surface of the fuel matrix or in the structural parts of the fuel elements which are assumed to be immediately corroded upon water contact. This instant release fraction (IRF) can be specified in COMP23 for each nuclide.

The remainders of the nuclides are assumed to become free for transport as the fuel matrix is dissolved. Three models for the fuel dissolution process is available in COMP23:

- Constant dissolution rate
- Dissolution limited by outward transport of uranium
- Dissolution rate proportional to the radiolysis due to alpha-particles.

Dissolution/precipitation

Many of the radionuclides in the fuel are elements of extremely low solubility under the chemical conditions assumed to be prevailing in the void water. These elements might thus reach a solubility limit in the void water when released from the fuel matrix. In this situation, release of additional amounts of the element will result in precipitation as a solid phase in the void volume. No solubility limitations are taken into account further out in the system.

This is handled by COMP23 by imposing solubility limits on the concentrations of elements in the void water. Additional amounts of an element are collected in a separate compartment in COMP23 that handles the turnover of precipitated elements. If several nuclides of an element are present, they all share the same elemental solubility, but this is not taken into account by the model. Daughter nuclides formed in the precipitated part of the mother nuclide are free for release.

Transport from the hole into the bentonite

The transport of species through the canister hole would require a fine discretization in a pure compartment model. To make the model more computationally effective, the transport out through the canister hole is instead treated analytically.

Species diffusing out from a circular hole are spread out spherically. Near the hole, the cross sectional area is still of the order of the size of the hole. Further away, the cross section increases as the ”sphere” grows. Thus most of the resistance to diffusion is concentrated near the mouth of the hole. In the model this is handled by using a plug with a resistance, R_p, between the compartments representing the water in the hole and the bentonite outside the canister (Romero, 1995).

$$R_p = \frac{d}{AD_e} = \left\{ A = A_{hole} = \pi r_{hole}^2, d = \frac{r_{hole}}{\sqrt{2}} \right\} = \frac{1}{\pi r_{hole} D_e \sqrt{2}}$$

where
d is the diffusion length of the plug (m)
A is the diffusion area set equal to the area of the hole, A_{hole} (m^2)

D_e is the effective diffusivity in bentonite (m^2/s)
r_{hole} is the radius of the hole (m).

This expression is valid for a small hole, while the resistance is overestimated for larger holes.

Transport into a narrow fracture

For the diffusive transport into a narrow fracture, most of the resistance to transport will be located nearest to the fracture. Again, a fine discretization is avoided by adding a plug. An analytical model (Neretnieks, 1986), solving the steady-state two-dimensional diffusion equations for a sector of the bentonite barrier representing half the fracture spacing, was used to derive a simplified expression for the plug resistance. The resulting expression is written as:

$$R_f = \frac{\left(F_{x,0} / \delta\right)\delta}{D_e A_f}$$

where
δ is the fracture aperture (m)
D_e is the effective diffusivity (m^2/s)
A_f is the diffusion area set equal to the area of the fracture (m^2)
$F_{x,0}/\delta$ is a factor.

Neretnieks (1986) evaluated the value of the $F_{x,0}/\delta$ factor for this system with variations in the input parameters. According to Neretnieks the following relationship gives a good approximation to the exact solution:

$$F_{x,0} / \delta = 1 - 1.35 \log \delta / a + 1.6 \log d / a$$

in the regime $10^{-6} < \delta/a < 10^{-1}$ and $0.03 < d/a < 1$.

A is the height of the compartment in connection with the fracture (m)
d is the thickness of the bentonite/backfill (m).

Input to COMP23 is a plug length, corresponding to $(F_{x,0}/\delta)\ \delta$, and a plug area corresponding to the diffusion area set equal to the area of the fracture opening in contact with the bentonite/backfill.

Diffusion from the bentonite into the fractures

For the near-field compartments that are in contact with fractures in the near-field rock, the rate of transport is modelled by the use of Q_{eq}. This fictitious flow rate can be visualised as the flow rate of water that carries away dissolved species with the concentration at the compartment interface resulting in the release of radionuclides. It has been derived by solving the equations for diffusive transport to the passing water by boundary layer theory. The value of Q_{eq} depends on the geometry of the contact area, the water flux, the flow porosity and the diffusivity.

For the case of a fracture covering the full circumference of the deposition hole, the following equations are used (Romero, 1995)

$$Q_{eq} = q_0\ W\ \overline{\eta} = q_0\ W\ \sqrt{\frac{4 D_w t}{\pi}}$$

where
q_0 is the water flux or Darcy velocity (m^3/m^2, yr)

W is the width of the opening (m)
$\overline{\eta}$ is the mean depth of the penetration in the fracture by diffusion (m)
D_w is the diffusivity in water (m^2/yr)
t is the time the water is in contact with the compartment (yr).

The contact time with the flowing water is determined from the water flux q_0, the flow porosity ε_f and the length of the pathway in contact with the flowing water, L:

$$t = \frac{L\varepsilon_f}{q_0}$$

giving

$$Q_{eq} = \sqrt{q_0}\, W \sqrt{\frac{4 D_w L \varepsilon_f}{\pi}}$$

A specific value for Q_{eq} must be determined for each interface with the near-field rock, a total of four for the situation in this study. Each of these has its own values of q_0, W, L and ε_f.

In COMP23 the following expression is used to describe Q_{eq}:

$$Q_{eq}^i = A^i q_0^b$$

where A is a lumped parameter and b is a parameter often set to 0.5 in accordance with the equations above giving a square root dependency of q_0. Due to the large scale in the groundwater flow models only one water flux is calculated at the canister position. Since that water flux is used for the calculation of all four Q_{eq} values, the A values include the differences in water flux expected at the different release paths.

2.2.3 FARF31

The model FARF31 (Norman and Kjellbert, 1990) calculates the transport of dissolved radionuclides through the fractured rock, the retention caused by interactions between the nuclides and the rock matrix, and the radioactive chain decay. The processes included are:
advection - transport of radionuclides by water flowing through fractures in the rock
dispersion - the spreading caused by velocity variations in different fractures or in different parts of a fracture
matrix diffusion and sorption - the diffusive transport of radionuclides from the water in the fracture into pores and microfissures of the rock matrix where the nuclides may sorb on the solid surfaces
radioactive chain decay - the decay and in-growth of radionuclides that are members of a decay chain.
The basis for the modelling is a stream tube, i.e. a volume of rock including fractures with flowing water. The walls of the stream tube are defined by streamlines. As a consequence, no water is allowed to pass through walls of the stream tube and thus all mass entering one end of a stream tube will subsequently be discharged at the other end. FARF31 does not explicitly consider the transport in individual fractures and flow paths contained within the stream tube. Instead, the transport properties of the water bearing fractures and the rock matrix available through diffusion are averaged over the stream tube, using the dual porosity continuum approach. The stream tube concept greatly facilitates the radionuclide transport modelling. The complex three-dimensional flow field is thus divided into a set of one-dimensional stream tubes.

FARF31 is based on the one-dimensional advection-dispersion equation with one-dimensional diffusion perpendicular to the flow into a matrix of finite depth. The equation is formulated in flux averaged quantities of concentration, water velocity, dispersivity and the exchange rate between flowing water and the pores of the rock matrix. The distance in the flow direction is transformed into accumulated groundwater travel time. Thus, the parameters determining the advection-dispersion are the groundwater travel time (t_w) and the Peclet number (Pe). This allowing for the use of groundwater travel times computed externally (in HYDRASTAR or by some other hydrological code). The retention mechanism considered by FARF31 is the diffusion of radionuclides into the rock matrix where they may sorb on the inner surface of the rock. Since the rock volume encompassed by a stream tube will contain many flow paths, it is useful to employ the concept of specific flow wetted surface, e.g. by defining the contact area between the flowing water and the fracture surfaces per unit volume of flowing water (a_w). Retention of radionuclides in fractured rock has been found to depend strongly on the relation between the flow wetted surface and the water flow rate. This may be taken into account in FARF31 by using the F factor, which can be expressed as the product of the groundwater travel time and the flow wetted surface per volume of water in the transport pathway ($t_w \cdot a_w$). One should note, however, that t_w is essentially proportional to the flow porosity whereas a_w is essentially inversely proportional to the flow porosity, making the product $t_w \cdot a_w$ almost insensitive to the flow porosity (Andersson, et al., 1998). Consequently, the F factor is not directly dependent on the groundwater travel time but rather the groundwater flux and on the geometrical distribution of the flow in the fractures.

In order to describe matrix diffusion and sorption data is required for matrix diffusivity (D_e), matrix porosity (ε), maximum penetration depth (x_0) and distribution coefficients for the different radionuclides (K_d). A new version of FARF31 that includes the capability of using radionuclide specific values for the matrix diffusivity has been developed within SR 97 (Eriksson et al., 1999).

The equations on which FARF31 is based are in summary:

$$\frac{\partial c_i}{\partial t} = -\frac{\partial c_i}{\partial \zeta} + \frac{t_w}{Pe}\frac{\partial^2 c_i}{\partial \zeta^2} + a_w D_e \left.\frac{\partial c_i}{\partial x}\right|_{x=0} - \lambda_i c_i + \lambda_{i-1} c_{i-1}$$

$$R_i \frac{\partial c_{p,i}}{\partial t} = D_e \frac{\partial^2 c_{p,i}}{\partial x^2} - R\lambda_i c_{p,i} + R_{i-1}\lambda_{i-1} c_{p,i-1}$$

where:

c_i is the flux-averaged concentration in the flowing water
$c_{p,i}$ is the surface and flux-averaged concentration of radionuclide i in the pore water
t_w is the groundwater travel time in the flowing water
t is the time
a_w is the flow wetted surface per volume of water
ζ is the distance in the flow direction expressed in terms of accumulated groundwater travel time
Pe is the Peclet number
D_e is the effective matrix diffusivity of radionuclide i
x is the penetration depth into the rock matrix
x_0 is the maximum penetration depth in the matrix
R_i is the retardation factor for radionuclide i ($R_i = \varepsilon + K_d \rho$)
ε is the matrix porosity

K_d is the distribution coefficient of radionuclide *i*
ρ is the bulk density of the rock
λ_i is the decay constant for radionuclide *i*

The following initial and boundary conditions are applied:

at $t = 0$ $c_{p,i} = 0$ and $c_i = 0$

when $\zeta \rightarrow \infty$ $c_i = 0$.

The inlet flow is given by:

$$F_{in}^{i}(t) = Q_{tube}\left(c_i(\zeta,t) - \frac{t_w}{Pe}\frac{\partial c_i(\zeta,t)}{\partial \zeta}\right)\Bigg|_{\zeta=0} .$$

The boundary conditions for the diffusional tubes are:

$$\frac{\partial c_{p,i}}{\partial x}\Bigg|_{x=x_0} = 0$$

$$c_{p,i}(x,\zeta,t)\Big|_{x=0} = c_i(\zeta,t) .$$

2.2.4 BIO42/SUM41

The dose conversion model BIO42 calculates the dose by multiplying the release from the far field (Bq/yr) with an ecosystem specific dose conversion factor, EDF, (Sv/Bq). The dose conversion factors are evaluated in the biosphere modelling (Nordlinder et al., 1999). That modelling starts with a division of the site into different modules based on the ecosystem. For each type of module dose conversion factors are calculated. The modules used here are well, lake, stream, river, peat, soil, inner bay and open coast.

The type of module could either be given directly as input or as a function of where the releases occur. The simplified usage of the BIO42, with module data given directly as input data, corresponds to the function of the model SUM41. This latter model was actually used in the calculations.

2.2.5 PROPER

A control program called PROPER administers execution of the chain of sub-models described in the previous sections. The PROPER program allows both deterministic (single) executions of the model chain and probabilistic calculations.

In the latter case, a selection of the input parameters is given as distributions rather than as fixed values. The distributions are chosen so as to express uncertainties in the input parameters. The probabilistic calculations consist of many executions or realizations of the model chain. In each of these, a new set of values of the input parameters is sampled from the input distributions. Each realization results in e.g. estimates of dose to man as a function of time. The ensemble of results from the different realizations can then be post processed to provide a statistical distribution of e.g. the maximum dose over time. In this way uncertainties in input parameters are reflected in the resulting distributions.

2.2.6 Monitor 2000

Input to the sub-models and to the PROPER control program is handled via the recently developed graphic user interface Monitor 2000.

3 Input Data

The need of input data is briefly described in Figure 3-1. Evaluation of suitable input data to the model chain has been performed by Andersson (1999). The data are given as "reasonable" and also for most of the parameters as defendable "pessimistic" estimates. Some parameters that are modelled (hydrogeological and biosphere) are given as a statistical distribution. Some data are dependent of the radionuclide's chemical and/or radioactive properties and therefore become element and/or nuclide specific. Some data are site specific and are hence different for Aberg, Beberg and Ceberg.

The purpose of the determination of reasonable data is to describe the supposed function of the repository system. There is no strict definition of the term reasonable. The aim has been to choose parameter values that are based on model analyses or direct measurements. The pessimistic values are chosen as an upper limit of the parameters negative influence on the calculation result. Many pessimistic values must thus be regarded as highly improbable.

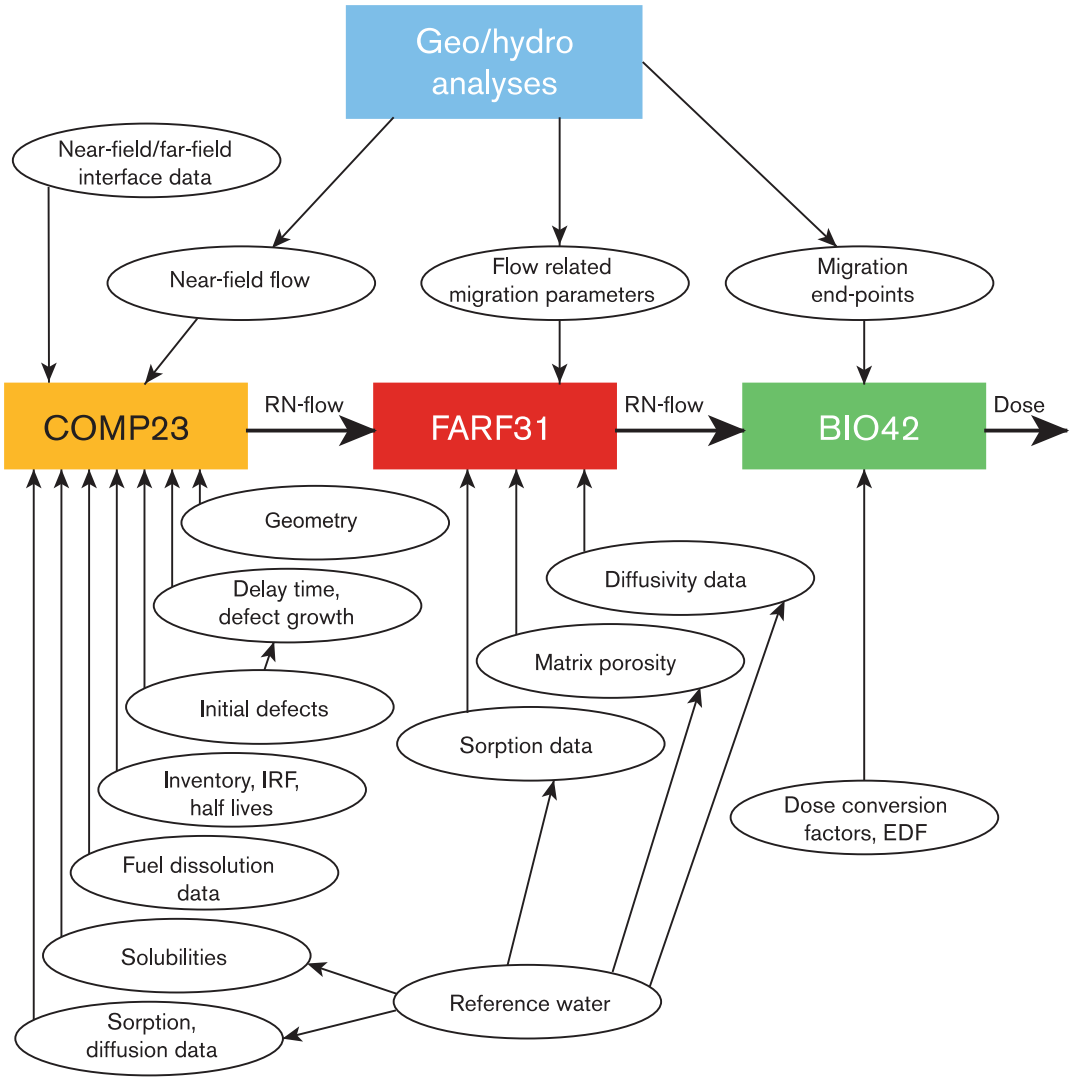

Figure 3-1. *The chain of models used for evaluating radiological consequences and the primary sources of information for these models.*

The following sections give short descriptions of the input parameters, more details are provided in Andersson (1999). Table 3-1 gives an overview of all available parameters. Most of the data used in special cases, glacial melting case and probabilistic calculations are given in connection with the description of those calculations.

Table 3-1. Overview of input parameters to the release calculations. (R=reasonable, P=pessimistic, D=distribution in probabilistic calculations, E/N=element/nuclide specific, S=site specific, C=calculated distribution).

Parameter	R	P	D	E/N	S
Geometry	X				
Inventory	X			X	
IRF	X	X	X	X	
Fuel conversion	X				
Number of defective canisters	X	X	X		
Defect growth	X	X			
Delay time for transport	X	X			
Solubility	X	X	X	X	X
Sorption in bentonite	X	X	X	X	X
Diffusivity in bentonite	X			X	X
Porosity in bentonite	X			X	X
Density in bentonite	X			X	X
Sorption in backfill	X	X	X	X	X
Diffusivity in backfill	X				
Porosity in backfill	X				
Density in backfill	X				
Sorption in rock	X	X	X	X	X
Diffusivity in rock	X	X	X	X	X
Porosity in rock	X				
Density in rock	X				
Q_{eq}-parameters	X	X			
Near-field water flux	X	X	C		X
Travel time	X	X	C		X
Flow wetted surface	X	X	X		X
Maximum penetration depth	X	X			X
Peclet number	X	X			X
EDF-factors	X	X	X	X	X

3.1 Geometry

The geometry data of importance for this study is summarised in Table 3-2.

Table 3-2. Dimensions used to describe the geometry of the KBS 3-repository.

Height of the canister	4.83 m
Outer diameter of the copper	1.05 m
Inner diameter of the copper	0.95 m
Void inside canister	1 m^3
Depth of the canister hole	7.83 m
Diameter of the deposition hole	1.75 m
Height of bentonite below canister in deposition hole	0.5 m
Thickness of bentonite outside canister	0.35 m
Height of bentonite above the canister in the deposition hole	1.5 m
Height of backfill above canister and bentonite in the deposition hole	1.0 m
Distance between deposition hole centres	6 m (at least)
Height of the tunnel	4 m
Width of the tunnel	3.6 m

The near-field model has been set up with nine model blocks, two water blocks representing the void inside the canister and the hole through the canister wall, four blocks representing the bentonite, two blocks representing the crushed rock-bentonite and one for the rock below the deposition hole. Some blocks are further divided and there are totally 19 compartments in the model. The interior of the canister is only assigned a volume but no transport resistance. The geometry of the compartments was evaluated in a pre-study (Lindgren and Widén, 1998). The resulting division into compartments is shown in Figure 3-2. The dimensions of the compartments are given in Appendix A.

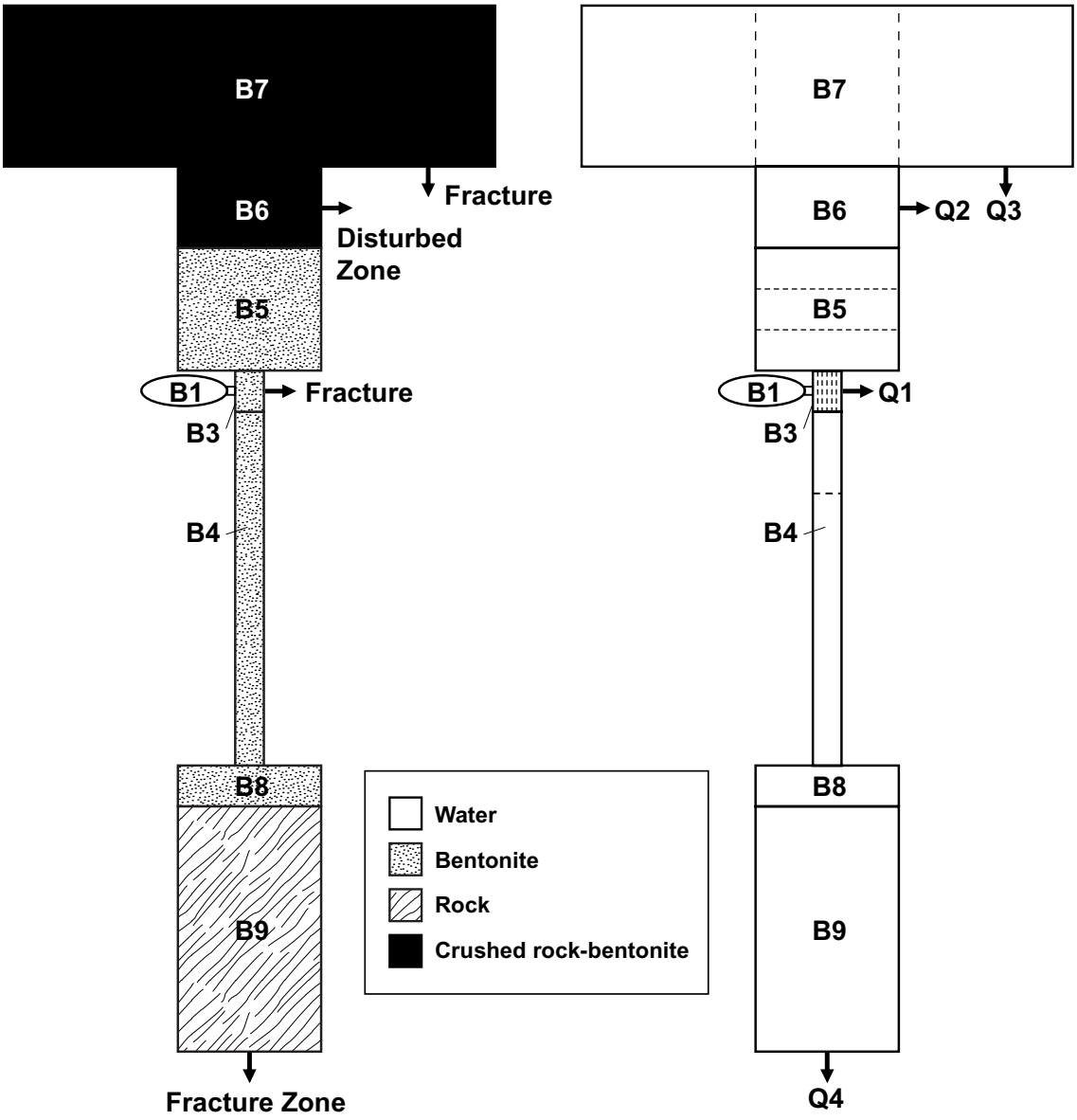

Figure 3-2. *The division of the near field into model blocks of the four different materials (left) and the subdivision of the model blocks 3, 4 and 7 into compartments (right).*

3.2 Inventory

The fuel composition is constrained by the heat load and the space available in the canister, which limits the variability of the possible inventory in a canister. The reasonable estimate of the inventory is that calculated by Håkansson (1998) for 12 BWR fuel elements (SVEA-96) with a burn-up of 38 MWd/kgU. One canister contains

2.04 tU. The inventory is given in Table 3-3 tabulated as the activity in Bq/tU and also as the content in mol/canister 40 years after discharge for the studied nuclides. The latter is used as input to the calculations. The inventory is also shown as a function of time in Figure 3-3 and 3-4. Input to COMP23 is given in an unformatted direct access file containing the contents of all radionuclides in a canister as time series. The preparation of the input files is described in Lindgren and Widén (1999).

Based on earlier studies (e.g. SR95) many nuclides have been concluded to have negligible impact on the final dose and hence the number of nuclides in this study has been limited to 32. These nuclides are chain 4N+1: Cm-245 → Am-241 → Np-237 → U-233 → Th-229, chain 4N+2: Pu-242 → U-238 → U-234 → Th-230 → Ra-226, chain 4N+3: Am-243 → Pu-239 → U-235 → Pa-231 and the single nuclides: C-14, Cl-36, Ni-59, Ni-63, Se-79, Sr-90, Zr-93, Nb-94, Tc-99, Pd-107, Ag-108m, Sn-126, I-129, Cs-135, Cs-137, Sm-151, Ho-166m and Pu-240.

Table 3-3. Inventory of the studied nuclides 40 years after discharge.

Nuclide	Half-life (yr) (Firestone et al., 1998)	Inventory at 40 years after discharge (Bq/tU)	Inventory at 40 years after discharge (mol/canister)
C-14	5730	$5.0 \cdot 10^{10}$	$4.4 \cdot 10^{-2}$
Cl-36	$3.010 \cdot 10^{5}$	$5.5 \cdot 10^{8}$	$2.5 \cdot 10^{-2}$
Ni-59	$7.600 \cdot 10^{4}$	$8.8 \cdot 10^{10}$	$1.1 \cdot 10^{0}$
Ni-63	100.1	$9.3 \cdot 10^{12}$	$1.3 \cdot 10^{-1}$
Se-79	$1.13 \cdot 10^{6}$	$2.8 \cdot 10^{9}$	$2.8 \cdot 10^{-2}$
Sr-90	28.78	$1.2 \cdot 10^{15}$	$5.4 \cdot 10^{0}$
Zr-93	$1.53 \cdot 10^{6}$	$5.6 \cdot 10^{10}$	$1.3 \cdot 10^{1}$
Nb-94	$2.030 \cdot 10^{4}$	$2.9 \cdot 10^{9}$	$9.0 \cdot 10^{-3}$
Tc-99	$2.111 \cdot 10^{5}$	$5.7 \cdot 10^{11}$	$1.9 \cdot 10^{1}$
Pd-107	$6.5 \cdot 10^{6}$	$4.9 \cdot 10^{9}$	$4.9 \cdot 10^{0}$
Ag-108m	418	$5.0 \cdot 10^{8}$	$9.8 \cdot 10^{-6}$
Sn-126	$1.000 \cdot 10^{5}$	$2.3 \cdot 10^{10}$	$3.5 \cdot 10^{-1}$
I-129	$1.57 \cdot 10^{7}$	$1.3 \cdot 10^{9}$	$3.2 \cdot 10^{0}$
Cs-135	$2.3 \cdot 10^{6}$	$2.1 \cdot 10^{10}$	$7.3 \cdot 10^{0}$
Cs-137	30.07	$1.8 \cdot 10^{15}$	$8.3 \cdot 10^{0}$
Sm-151	90	$9.4 \cdot 10^{12}$	$1.3 \cdot 10^{-1}$
Ho-166m	1200	$7.5 \cdot 10^{7}$	$1.4 \cdot 10^{-5}$
Pu-240	6580	$1.2 \cdot 10^{13}$	$1.2 \cdot 10^{1}$
Cm-245	8500	$9.4 \cdot 10^{9}$	$1.2 \cdot 10^{-2}$
Am-241	432.2	$1.5 \cdot 10^{14}$	$1.0 \cdot 10^{1}$
Np-237	$2.144 \cdot 10^{6}$	$1.5 \cdot 10^{10}$	$5.0 \cdot 10^{0}$
U-233	$1.592 \cdot 10^{5}$	$3.1 \cdot 10^{6}$	$7.6 \cdot 10^{-5}$
Th-229	7340	$1.0 \cdot 10^{4}$	$1.2 \cdot 10^{-8}$
Pu-242	$3.733 \cdot 10^{5}$	$1.0 \cdot 10^{11}$	$6.0 \cdot 10^{0}$
U-238	$4.468 \cdot 10^{9}$	$1.2 \cdot 10^{10}$	$8.1 \cdot 10^{3}$
U-234	$2.455 \cdot 10^{5}$	$4.6 \cdot 10^{10}$	$1.8 \cdot 10^{0}$
Th-230	$7.538 \cdot 10^{4}$	$1.6 \cdot 10^{7}$	$1.9 \cdot 10^{-4}$
Ra-226	1600	$1.4 \cdot 10^{5}$	$3.5 \cdot 10^{-8}$
Am-243	7370	$1.2 \cdot 10^{12}$	$1.3 \cdot 10^{0}$
Pu-239	$2.411 \cdot 10^{4}$	$9.5 \cdot 10^{12}$	$3.5 \cdot 10^{1}$
U-235	$7.038 \cdot 10^{8}$	$4.5 \cdot 10^{8}$	$4.9 \cdot 10^{1}$
Pa-231	$3.276 \cdot 10^{4}$	$1.8 \cdot 10^{6}$	$9.1 \cdot 10^{-6}$

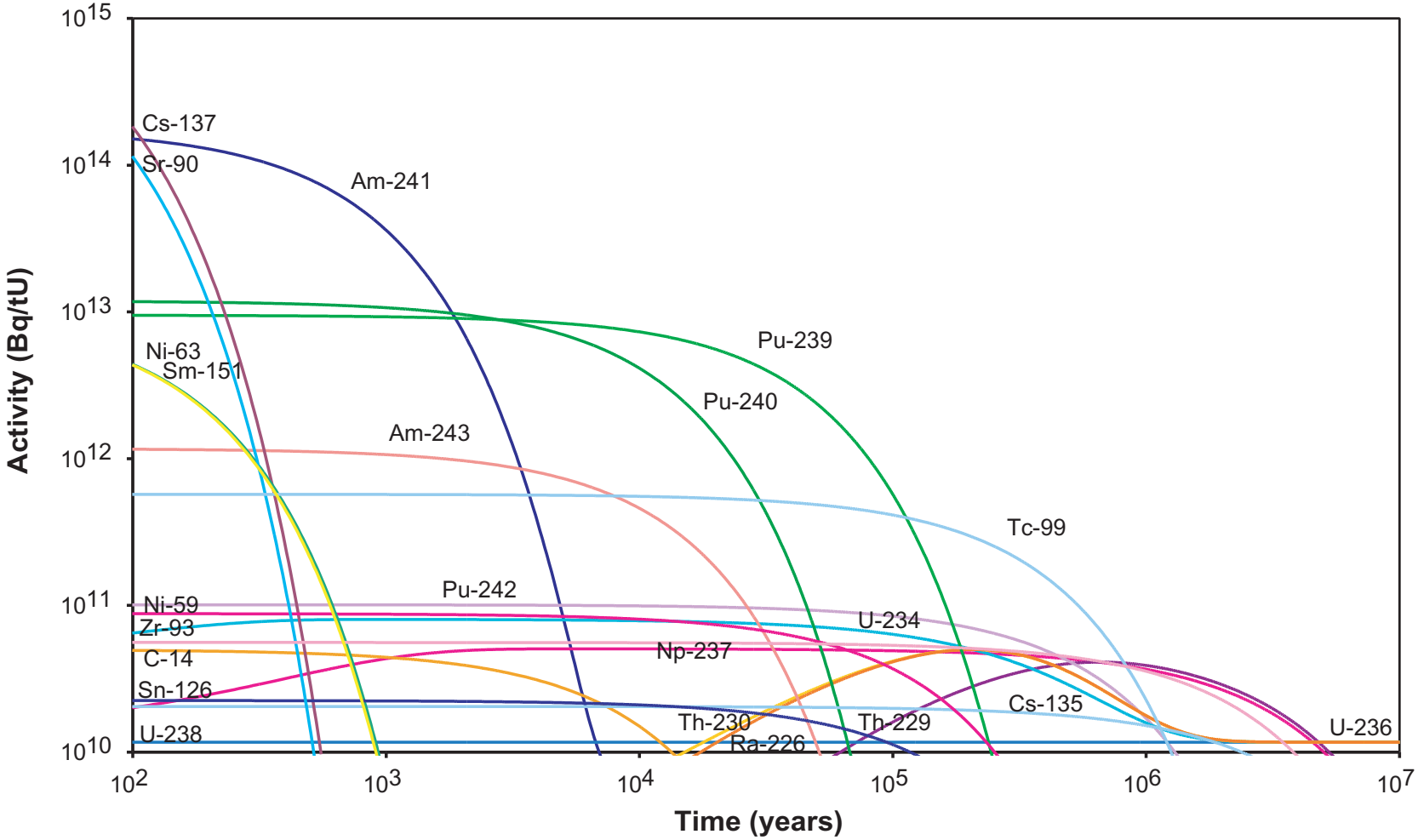

Figure 3-3. *Activity (Bq/tU) as a function of time for the studied nuclides. (Time zero is 40 years after discharge.)*

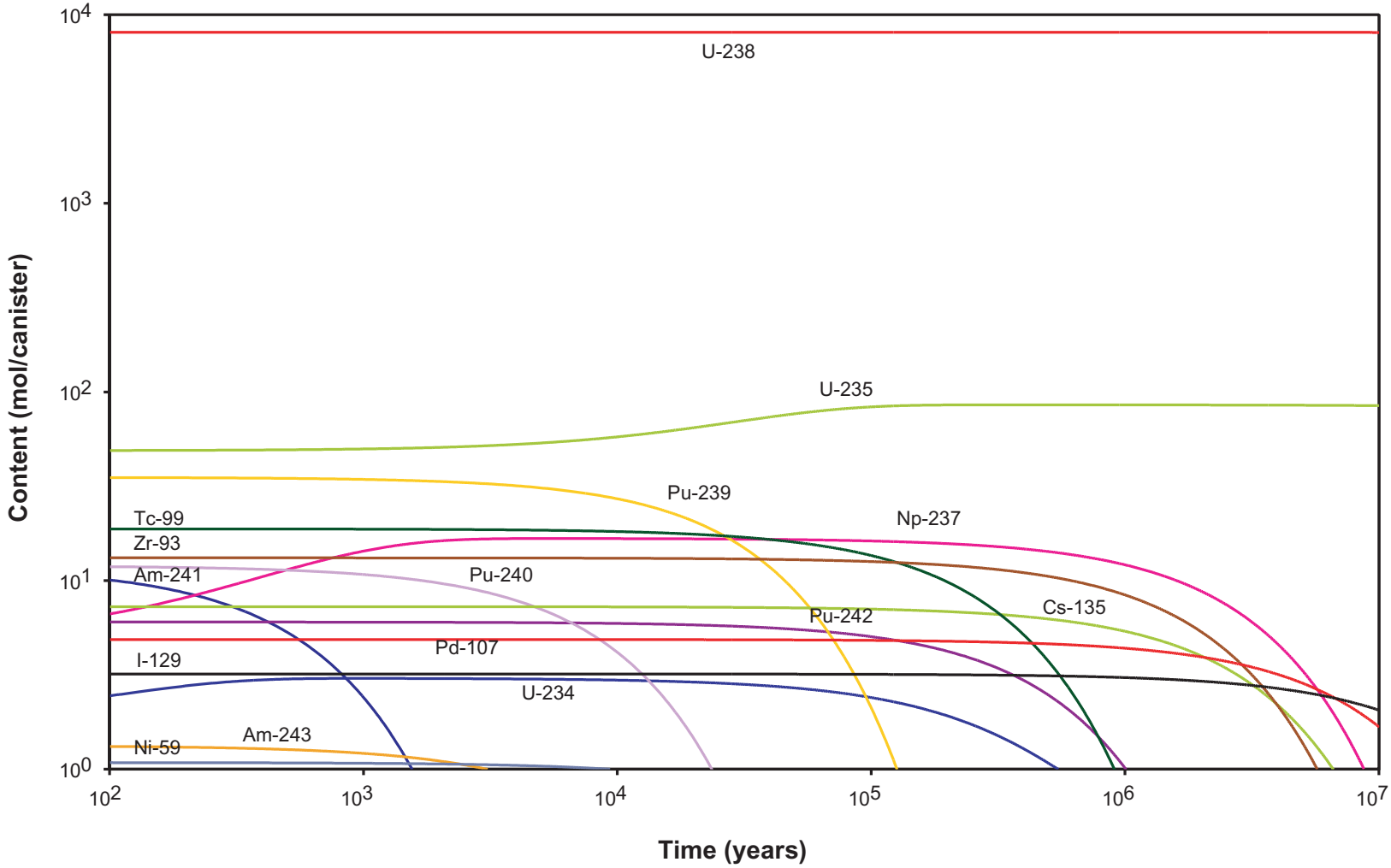

Figure 3-4. *Radionuclide content (mol/canister) as a function of time for the studied nuclides. (Time zero is 40 years after discharge.)*

3.3 Instant release fraction (IRF)

The reasonable estimate of the fraction of the inventory that is instantly free for release of different nuclides has been estimated from measurements of fission gas releases from representative Swedish BWR fuel combined with information from leaching studies on LWR and CANDU fuel (Johnsson and Tait, 1997). The pessimistic values were estimated from the highest values found in these experiments. Nuclides only present in metal parts (Nb-94, Ni-59 and Ni-63) are assumed to be fully available (100 % IRF). C-14 has been assigned a lower IRF-value, since much of the activity is present in the fuel and cladding. The values of the instant release fractions are given in Table 3-4.

Table 3-4. Data used on instant release fraction (IRF).

Nuclide	IRF (%)	
	Reasonable estimate (Aberg, Beberg, Ceberg)	Pessimistic estimate (Aberg, Beberg, Ceberg)
C-14	15	55
Cl-36	6	12
Ni-59	100	100
Ni-63	100	100
Se-79	3	6
Sr-90	0.25	1
Zr-93	0	0
Nb-94	100	100
Tc-99	0.2	1
Pd-107	0.2	1
Ag-108m	100	100
Sn-126	2	4
I-129	3	6
Cs-135	3	6
Cs-137	3	6
Sm-151	0	0
Ho-166m	0	0
Actinides[a)]	0	0

[a)] Pu-240, Cm-245, Am-241, Np-237, U-233, Th-229, Pu-242, U-238, U-234, Th-230, Ra-226, Am-243, Pu-239, U-235, Pa-231.

3.4 Fuel conversion

A refined fuel conversion model, based on dissolution experiments with spent fuel in reducing environments, attempts at a realistic description of the fuel oxidation and resulting dissolution rate. This model implies a dissolution rate of 10^{-8} yr^{-1}, which is used as reasonable value. No pessimistic value has been assigned. Clearly, immediate dissolution of the fuel is a theoretical upper bound, but this "rate" is too extreme and unrealistic to be used as a meaningful pessimistic value.

3.5 Canister defects and delay time

The canister is designed so that it will fully isolate the waste and such that no known corrosion process would lead to failure before 100 000 years. A remaining possibility is initial defects not discovered by the quality control. The most likely position of such a defect would be at the weld of the lid. It is suggested that this defect would not exceed 1 μm and not extend more than half a circumference, i.e. about 1m. This results in a defect size of 1 mm^2. Even tough the risk of not detecting such a defect is close to zero, it is assumed as a reasonable estimate that one single canister has such a defect. The pessimistic value is that 0.1% of the canisters could have such a defect. The total

number of canister is more than 4000 and hence five canisters are used as a pessimistic value.

The defect will grow due to corrosion of the steel vessel when water from the bentonite enters the canister. With a reasonable estimate of the iron corrosion rate a large damage will not occur before $2 \cdot 10^5$ years. For a very pessimistic estimate of the corrosion rate (1 μm/year) the damage will occur after around 22 000 year. The two failure times are used as reasonable and pessimistic estimates respectively.

Radionuclides may migrate from the failed canister already when there is a small defect, but first a continuous water pathway between the fuel rods and the defect must be developed. The time it takes for development of such a pathway is called the delay time. The delay time is controlled by the bentonite permeability, the size of the defect and also by the overpressure due to corrosion. Model calculations for a water inflow combined with hydrogen formation due to corrosion for a 1 mm^2 circular defect suggest a delay time of $2 \cdot 10^5$ years (Bond et al., 1997). This time is taken as reasonable estimate. Accounting for uncertainties in bentonite permeability and in the shape of the defect would imply a pessimistic choice of the delay time of 300 years.

In summary the reasonable estimate is one single canister with an initially small defect (1 mm^2) that does not permit any transport until $2 \cdot 10^5$ years. At this time the defect is large and only provide limited resistance to transport. In the pessimistic case five canisters will have a small defect (1 mm^2) that will be connected to the fuel after 300 years and the defect will grow at 20 000 years when it immediately become large (0.01 m^2). The large defect is assumed to be circular. The reasonable and pessimistic estimates are summarised in Table 3-5.The transport through the hole is calculated assuming diffusion through water. The effective diffusivity is assumed to be 10^{-9} m^2/s for all nuclides.

Table 3-5. Data used on canister defects and delay time for transport.

Parameter	Reasonable estimate	Pessimistic estimate
Number of defective canisters	1	5
Delay time for transport (yr)	200 000	300
Defect growth	Large(0.01 m^2) at 200 000 yr	1 mm^2 at 300 yr growing stepwise at 20 000 yr to 0.01 m^2
Effective diffusivity in water (m^2/s)	10^{-9}	10^{-9}

3.6 Solubilities

Solubilities have been calculated with the speciation code EQ3NR for the Aberg, Beberg and Ceberg reference waters and for a bentonite water (Bruno et al., 1997). The uncertainties associated with co-precipitation and selection of solubility controlling solid phases makes it necessary to select the phases leading to the highest solubility as reasonable estimate. Regarding the uncertainty of the future chemical conditions the pessimistic solubilities are chosen as the highest solubility of each element calculated for any of the different waters. If the uncertainty estimates (Bruno et al., 1997) show potential for even higher solubilities, these higher values are selected. For Selenium two different pessimistic solubilities have been assigned. The solubility limit $4 \cdot 10^{-6}$ mol/m^3 chosen as the highest calculated solubility, as for all the other nuclides. The uncertainty of the redox state of Selenium, imply potential oxidation of Selenium during fuel conversion and essentially infinite solubility, which was chosen as an alternative pessimistic solubility. The solubility data used is given in Table 3-6.

Table 3-6. Solubilities used in the calculations.

Element	Solubility (mol/m^3)			
	Reasonable estimate			Pessimistic
	Aberg	Beberg	Ceberg	All sites
Ag	$2.96 \cdot 10^{-2}$	$9.39 \cdot 10^{-4}$	$7.12 \cdot 10^{-4}$	$3 \cdot 10^{-2}$
Am	$6.87 \cdot 10^{-4}$	$9.36 \cdot 10^{-5}$	$9.34 \cdot 10^{-5}$	$7 \cdot 10^{-3}$
C	high	high	high	high
Cl	high	high	high	high
Cm	$2.22 \cdot 10^{-4}$	$2.02 \cdot 10^{-6}$	$9.01 \cdot 10^{-7}$	$2 \cdot 10^{-3}$
Cs	high	high	high	high
Ho	$6.27 \cdot 10^{-3}$	$5.58 \cdot 10^{-3}$	$5.58 \cdot 10^{-3}$	$6 \cdot 10^{-2}$
I	high	high	high	high
Nb	1.37	1.37	1.39	40
Ni	high	high	high	high
Np	$5.87 \cdot 10^{-5}$	$1.05 \cdot 10^{-4}$	$5.87 \cdot 10^{-5}$	$2 \cdot 10^{-4}$
Pa	$3.16 \cdot 10^{-4}$	$3.16 \cdot 10^{-4}$	$3.16 \cdot 10^{-4}$	$4 \cdot 10^{-4}$
Pd	$4.21 \cdot 10^{-6}$	$4.17 \cdot 10^{-6}$	$4.18 \cdot 10^{-6}$	$8 \cdot 10^{-6}$
Pu	$6.56 \cdot 10^{-6}$	$5.35 \cdot 10^{-7}$	$1.38 \cdot 10^{-7}$	$3 \cdot 10^{-3}$
Ra	$2.86 \cdot 10^{-4}$	$5.02 \cdot 10^{-4}$	$1.20 \cdot 10^{-1}$	$2 \cdot 10^{-1}$
Se	$2.59 \cdot 10^{-6}$	$2.59 \cdot 10^{-6}$	$2.59 \cdot 10^{-6}$	high/$4 \cdot 10^{-6}$
Sm	$2.13 \cdot 10^{-3}$	$8.03 \cdot 10^{-4}$	$8.03 \cdot 10^{-4}$	$2 \cdot 10^{-2}$
Sn	$4.49 \cdot 10^{-6}$	$4.49 \cdot 10^{-6}$	$4.68 \cdot 10^{-6}$	$1 \cdot 10^{-2}$
Sr	6.88	3.09	$1.21 \cdot 10^{-1}$	40
Tc	$7.67 \cdot 10^{-6}$	$7.92 \cdot 10^{-6}$	$7.67 \cdot 10^{-6}$	$5 \cdot 10^{-5}$
Th	$1.22 \cdot 10^{-6}$	$1.22 \cdot 10^{-6}$	$1.22 \cdot 10^{-6}$	$2 \cdot 10^{-6}$
U	$1.28 \cdot 10^{-4}$	$1.29 \cdot 10^{-4}$	$1.29 \cdot 10^{-4}$	$2 \cdot 10^{-4}$
Zr	$2.50 \cdot 10^{-6}$	$2.51 \cdot 10^{-6}$	$2.51 \cdot 10^{-6}$	$3 \cdot 10^{-6}$

3.7 Sorption, porosity and diffusivity in bentonite

(Yu and Neretnieks, 1997) and (Ochs, 1997) have evaluated published results from studies of diffusion and sorption properties in saturated compacted bentonite. These studies give the basis for the choice of reasonable estimate for the distribution coefficients, K_d, and the effective diffusivity, D_e. The pessimistic values were chosen as the lowest values in the uncertainty interval. Both the reasonable and pessimistic values are based on saline and reducing conditions.

The porosity for most of the elements are given by the porosity of the bentonite, i.e. 0.41, but for the anions Cl^- and I^- the effective porosity must be lower, 0.05, to represent anion exclusion. It is, however, not possible to give element specific porosities as input to the current version of the near-field model COMP23. The storage capacities for the anions are thus overestimated, affecting the duration of the transient transport in the buffer. This is however of minor importance since the anions in question are long-lived compared to the transient time and thus the maximum release is almost independent of the porosity.

The dry density of the bentonite type to be used is 1590 kg/m^3 (Bäckblom, 1996). This corresponds to a bulk density for saturated bentonite of 2000 kg/m^3 and a solid density of 2695 kg/m^3 using a porosity of 0.41. The input data used in COMP23 is the solid density.

Element specific distribution coefficients and effective diffusivities are given in Table 3-7. Non element specific data are given in Table 3-8.

Table 3-7. Distribution coefficients and effective diffusivities used for bentonite.

Element	K_d (m^3/kg)		D_e (m^2/s)
	Reasonable estimate All sites	Pessimistic All sites	All sites
Ag	0	0	$2 \cdot 10^{-10}$
Am	3	1	$7 \cdot 10^{-11}$
C	0	0	$3 \cdot 10^{-11}$
Cl	0	0	$1 \cdot 10^{-12}$
Cm	3	1	$7 \cdot 10^{-11}$
Cs	0.05	0.005	$6 \cdot 10^{-10}$
Ho	1	0.2	$2 \cdot 10^{-10}$
I	0	0	$3 \cdot 10^{-12}$
Nb	0.2	0	$5 \cdot 10^{-10}$
Ni	0.1	0.02	$1 \cdot 10^{-9}$
Np	3	0.1	$1 \cdot 10^{-9}$
Pa	0.3	0.001	$7 \cdot 10^{-10}$
Pd	0.01	0	$1 \cdot 10^{-10}$
Pu	3	1	$3 \cdot 10^{-10}$
Ra	0.01	0.001	$5 \cdot 10^{-10}$
Se	0.003	0	$7 \cdot 10^{-11}$
Sm	1	0.2	$2 \cdot 10^{-10}$
Sn	3	0.01	$7 \cdot 10^{-11}$
Sr	0.01	0.001	$5 \cdot 10^{-10}$
Tc	0.1	0.01	$5 \cdot 10^{-10}$
Th	3	0.1	$7 \cdot 10^{-11}$
U	1	0.01	$5 \cdot 10^{-10}$
Zr	2	0.05	$5 \cdot 10^{-11}$

Table 3-8. Material data for bentonite (all elements).

Parameter	All sites, All cases	Comment
Porosity (m^3/m^3)	0.41	Constant value used (i.e. anion exclusion not included)
Solid density (kg/m^3)	2695	

3.8 Sorption, porosity and diffusivity in backfill

The backfill is in the SR 97 study assumed to consist of a mixture of 15 % bentonite and 85 % crushed rock. Sorption data is obtained from a proportional contribution of 15 % of the bentonite values and 85% of the rock values. In the backfill the ion strength of the pore water is assumed to be equal to the groundwater in the rock. This implies that the reasonable estimate for Aberg is saline conditions and for Beberg and Ceberg non-saline conditions.

Since the clay is diluted the ion-exclusion effects are disregarded, and hence all ions are assigned the same porosity, 30%. The effective diffusivity is 10^{-10} m^2/s for all nuclides. The dry density is 1900 kg/m^3 (Bäckblom, 1996). This corresponds to a bulk density for saturated backfill of 2200 kg/m^3 and a solid density of 2714 kg/m^3 using a porosity of 0.3. The input data used in COMP23 is the solid density.

Element specific distribution coefficients are given in Table 3-9. Non element specific data are given in Table 3-10.

Table 3-9. Distribution coefficients used for crushed rock-bentonite backfill.

Element	K_d (m^3/kg)		
	Reasonable estimate Aberg	Reasonable estimate Beberg, Ceberg	Pessimistic All sites
Ag	0.005	0.5	0.009
Am	3	3	1
C	0.0009	0.0009	0.0004
Cl	0	0	0
Cm	3	3	1
Cs	0.05	0.5	0.009
Ho	2	2	0.9
I	0	0	0
Nb	0.9	0.9	0.4
Ni	0.03	0.1	0.01
Np	5	5	0.9
Pa	0.9	1	0.4
Pd	0.01	0.09	0.0009
Pu	5	5	1
Ra	0.02	0.2	0.009
Se	0.001	0.001	0.0004
Sm	2	2	0.9
Sn	0.5	0.5	0.002
Sr	0.002	0.08	0.002
Tc	0.9	0.9	0.3
Th	5	5	0.9
U	4	4	0.9
Zr	1	1	0.5

Table 3-10. Material data for backfill (non element specific).

Parameter	All sites, All cases
Porosity (m^3/m^3)	0.3
Solid density (kg/m^3)	2714
Effective diffusivity (m^2/s)	10^{-10}

3.9 Sorption, porosity and diffusivity in rock

Sorption data in terms of distribution coefficients, K_d, are obtained from different experimental databases, while considering the water chemistry at the different sites (Carbol and Engkvist, 1997). It is mainly the salinity of the water that has influence on the sorption. Difference in the mineralogy is of minor importance. The reasonable estimate is to choose saline values for Aberg and non-saline values for Beberg and Ceberg. For Aberg and Beberg the pessimistic values are chosen as the lowest values found in the studies. For Ceberg it appears evident that non-saline conditions will prevail even in the future and hence the lowest non-saline values are chosen.

Element specific data for the diffusivity has been estimated from diffusion experiments with tritiated water and some cations in salty water in rock samples from Äspö (i.e. Aberg). Diffusivities for other nuclides were assessed from their theoretical relation to tritiated water diffusivity by considering differences in free water diffusivities and possibilities for anion exclusion or surface diffusions (Ohlsson and Neretnieks, 1997). Reasonable values are chosen by including all these effects. Pessimistic values are chosen by omitting effects leading to high diffusivities and by choosing pessimistic water composition.

The diffusion analysis of Ohlsson and Neretnieks builds on the porosity $5 \cdot 10^{-3}$ and this value is also chosen as reasonable estimate for the porosity. However, to account for ion exclusion in low ionic strength waters of Beberg and Ceberg a ten times lower value is to be used for the anions C, Cl and I. It is however not possible to use element specific porosities as input to the current version of the model. No pessimistic values are assigned. The solid density of the rock has been assumed to be 2700 kg/m^3.

Distribution coefficients used for the rock are given in Table 3-11 and effective diffusivities are given in Table 3-12. Non element specific data are given in Table 3-13.

Table 3-11. Distribution coefficients, K_d, used for the rock.

Element	K_d (m^3/kg)			
	Reasonable estimate		Pessimistic	
	Aberg	Beberg, Ceberg	Aberg, Beberg	Ceberg
Ag	0.05	0.5	0.01	0.1
Am	3	3	1	1
C	0.001	0.001	0.0005	0.0005
Cl	0	0	0	0
Cm	3	3	1	1
Cs	0.05	0.5	0.01	0.1
Ho	2	2	1	1
I	0	0	0	0
Nb	1	1	0.5	0.5
Ni	0.02	0.1	0.01	0.05
Np	5	5	1	1
Pa	1	1	0.5	0.5
Pd	0.01	0.1	0.001	0.01
Pu	5	5	1	1
Ra	0.02	0.1	0.01	0.05
Se	0.001	0.001	0.0005	0.0005
Sm	2	2	1	1
Sn	0.001	0.001	0	0
Sr	0.0002	0.01	0.0001	0.0001
Tc	1	1	0.3	0.3
Th	5	5	1	1
U	5	5	1	1
Zr	1	1	0.5	0.5

Table 3-12. Effective diffusivity used for the rock.

Element	D_e (m^2/s)		
	Reasonable estimate		Pessimistic
	Aberg	Beberg, Ceberg	All sites
Ag	$7.1 \cdot 10^{-14}$	$7.1 \cdot 10^{-14}$	$7.1 \cdot 10^{-15}$
Am	$4.0 \cdot 10^{-14}$	$4.0 \cdot 10^{-14}$	$4.0 \cdot 10^{-15}$
C	$5.0 \cdot 10^{-14}$	$5.0 \cdot 10^{-15}$	$5.0 \cdot 10^{-16}$
Cl	$8.3 \cdot 10^{-14}$	$8.0 \cdot 10^{-15}$	$8.0 \cdot 10^{-16}$
Cm	$4.0 \cdot 10^{-14}$	$4.0 \cdot 10^{-14}$	$4.0 \cdot 10^{-15}$
Cs	$8.8 \cdot 10^{-14}$	$9.0 \cdot 10^{-13}$	$9.0 \cdot 10^{-15}$
Ho	$4.0 \cdot 10^{-14}$	$4.0 \cdot 10^{-14}$	$4.0 \cdot 10^{-15}$
I	$8.3 \cdot 10^{-14}$	$8.0 \cdot 10^{-15}$	$8.0 \cdot 10^{-16}$
Nb	$4.0 \cdot 10^{-14}$	$4.0 \cdot 10^{-14}$	$4.0 \cdot 10^{-15}$
Ni	$2.8 \cdot 10^{-14}$	$2.8 \cdot 10^{-14}$	$2.8 \cdot 10^{-15}$
Np	$4.0 \cdot 10^{-14}$	$4.0 \cdot 10^{-14}$	$4.0 \cdot 10^{-15}$
Pa	$4.0 \cdot 10^{-14}$	$4.0 \cdot 10^{-14}$	$4.0 \cdot 10^{-15}$
Pd	$4.0 \cdot 10^{-14}$	$4.0 \cdot 10^{-14}$	$4.0 \cdot 10^{-15}$
Pu	$4.0 \cdot 10^{-14}$	$4.0 \cdot 10^{-14}$	$4.0 \cdot 10^{-15}$
Ra	$3.7 \cdot 10^{-14}$	$3.7 \cdot 10^{-14}$	$3.7 \cdot 10^{-15}$
Se	$4.0 \cdot 10^{-14}$	$4.0 \cdot 10^{-14}$	$4.0 \cdot 10^{-15}$
Sm	$4.0 \cdot 10^{-14}$	$4.0 \cdot 10^{-14}$	$4.0 \cdot 10^{-15}$
Sn	$4.0 \cdot 10^{-14}$	$4.0 \cdot 10^{-14}$	$4.0 \cdot 10^{-15}$
Sr	$3.3 \cdot 10^{-14}$	$3.0 \cdot 10^{-13}$	$3.0 \cdot 10^{-15}$
Tc	$4.0 \cdot 10^{-14}$	$4.0 \cdot 10^{-14}$	$4.0 \cdot 10^{-15}$
Th	$6.3 \cdot 10^{-15}$	$6.3 \cdot 10^{-15}$	$6.3 \cdot 10^{-16}$
U	$4.0 \cdot 10^{-14}$	$4.0 \cdot 10^{-14}$	$4.0 \cdot 10^{-15}$
Zr	$4.0 \cdot 10^{-14}$	$4.0 \cdot 10^{-14}$	$4.0 \cdot 10^{-15}$

Table 3-13. Material data for rock (non element specific).

Parameter	All sites, All cases
Porosity (m^3/m^3)	$5 \cdot 10^{-3}$
Solid density (kg/m^3)	2700

3.10 Other near-field parameters

Parameters determining transport into narrow fractures

In the near-field model an analytical expression is used to calculate the diffusion resistance between the bentonite/backfill and fractures in the rock as described in Section 2.2.2. Input to COMP23 is a plug length, corresponding to ($F_{x,0}/\delta$) δ, and a plug area corresponding to the diffusion area set equal to the area of the fracture opening in contact with the bentonite/backfill.

The near field is assumed to be intersected by two fractures, one crossing the deposition hole outside the hole in the canister and one crossing the deposition tunnel. Both fractures are assumed to be in contact with the bentonite/backfill the whole way around and therefore the area is calculated as the circumference times the fracture aperture.

According to Neretnieks (1986) the following relationship gives a good approximation to the exact solution of $F_{x,0}/\delta$:

$$F_{x,0} / \delta = 1 - 1.35 \log \delta / a + 1.6 \log d / a$$

in the regime $10^{-6} < \delta/a < 10^{-1}$ and $0.03 < d/a < 1$.

δ is the fracture aperture (m)
a is the height of the compartment in connection with the fracture (m)
d is the thickness of the backfill (m).

The parameters used to calculate the plug lengths and plug areas for the connections outside Q1 and Q3 are given in Table 3-14. [1]

Qeq-parameters

Moreno and Gylling (1998) evaluated Qeq for the studied system based on the groundwater flow calculations on site scale (Walker and Gylling, 1998, Gylling et al., 1999 and Walker and Gylling, 1999). This is described in Section 2.2.2. In the near-field model COMP23 two parameters (A and b) are used to describe Qeq according to:

$$Q_{eq}^{i} = A^{i} q_0^{b}$$

The parameter A was assigned both reasonable and pessimistic values for each site, while the parameter b was set to 0.5 for all cases. The parameter A is a lumped parameter that takes into account differences in for example water flux and porosity at the different entries.

Near-field water flux

The near-field water fluxes are determined in the groundwater flow calculations in site scale (Walker and Gylling, 1998, Gylling et al., 1999 and Walker and Gylling, 1999). Reasonable near-field water fluxes are chosen as the median from the results from the base cases for the three different sites. The pessimistic near-field water fluxes are chosen as the 5 percentile from the anisotropy variant for Aberg, the environmental head variant for Beberg and the base case for Ceberg.

The near-field water flux that has been calculated with the continuum model (Walker and Gylling, 1998, Gylling et al., 1999 and Walker and Gylling, 1999) is a mean value for a block of about 30×30×30 m^3. The fluxes for the different pathways in COMP23 are calculated as different multiples of this mean value of the near-field flux, q_0. The flux for the fracture that intersects the deposition hole (q_1) is assumed as a reasonable estimate to be the same as q_0. It is suggests that q_1 may be about five times q_0. q_1 is therefore pessimistically assumed to be $5q_0$. It is assumed that the flux in the EDZ in the tunnel floor (q_2) can be ten times greater than the mean flux and at most 100 times greater than the mean flux (Moreno and Gylling, 1998). The fluxes at the fracture zone intersecting the tunnel (q_3) or at the fracture zone inside the rock (q_4) are of little importance. Reasonable values are assumed to be $q_3 = q_4 = 100q_0$, while pessimistic values are assumed to be $q_3 = 1000q_0$ and $q_4 = 10\ 000q_0$.

The near-field water fluxes and the fluxes for the different pathways in COMP23 related to the near-field water fluxes are shown in Table 3-14.

[1] Due to an error in Neretnieks (1986), where the width of the fissure has been exchanged with the half-width of the fissure in the nomenclature list, the used input data for the plug area and plug length are not consistent. The used areas are twice compared to if calculated with the assumed fracture apertures. This implies that the used resistance is too small, which is thus pessimistic.

Table 3-14. Data used on other near-field parameters.

Parameter	Aberg		Beberg		Ceberg	
	Reason.	Pessim.	Reason.	Pessim.	Reason.	Pessim.
Fracture Q1						
Fracture aperture (m)	$1\cdot10^{-4}$		$1\cdot10^{-4}$		$1\cdot10^{-4}$	
a (m)	0.5		0.5		0.5	
d (m)	0.35		0.35		0.35	
Plug area (m^2)	$5.5\cdot10^{-4}$		$5.5\cdot10^{-4}$		$5.5\cdot10^{-4}$	
Plug length (m)	$5.0\cdot10^{-4}$		$5.0\cdot10^{-4}$		$5.0\cdot10^{-4}$	
Fracture Q3						
Fracture aperture (m)	$5\cdot10^{-4}$		$5\cdot10^{-4}$		$5\cdot10^{-4}$	
a (m)	2.125		2.125		2.125	
d (m)	1.0		1.0		1.0	
Plug area (m^2)	$6\cdot10^{-3}$		$6\cdot10^{-3}$		$6\cdot10^{-3}$	
Plug length (m)	$2\cdot10^{-3}$		$2\cdot10^{-3}$		$2\cdot10^{-3}$	
Qeq-parameter A1	0.03	0.25	0.03	0.25	0.03	0.25
Qeq-parameter A2	0.1	0.5	0.1	0.5	0.1	0.5
Qeq-parameter A3	1	5	1	5	1	5
Qeq-parameter A4	1	10	1	10	1	10
Qeq-parameter b	0.5	0.5	0.5	0.5	0.5	0.5
Near-field water flux, q_0 (m^3/m^2,yr)	$2\cdot10^{-3}$	10^{-1}	$1\cdot10^{-3}$	$2\cdot10^{-2}$	$4\cdot10^{-5}$	$2\cdot10^{-4}$
q_1	q_0	5 q_0	q_0	5 q_0	q_0	5 q_0
q_2	10 q_0	100 q_0	10 q_0	100 q_0	10 q_0	100 q_0
q_3	100 q_0	1000 q_0	100 q_0	1000 q_0	100 q_0	1000 q_0
q_4	100 q_0	1000 q_0	100 q_0	1000 q_0	100 q_0	1000 q_0

3.11 Other far-field parameters

Groundwater travel times, t_w, and Flow wetted surface area per volume of water, a_w

The radionuclide transport through the rock occurs by advection in the open fractures. If the species dissolved in the water do not interact with the rock the transport rate is determined by the groundwater velocity, which may be expressed as the water flux divided by the flow porosity. If the nuclides may diffuse into the rock matrix and sorb there this delays the transport rate. The transport rate is determined by the water flux, the geometry of the fractures as well as the diffusivity and sorption data, while the flow porosity is of minor importance.

In the far-field model FARF31 the product of the groundwater travel time and the flow wetted surface area per volume of water is used to describe the transport resistance. This product is often referred to as the F-ratio. These parameters are thus related to each other and should therefore be correlated.

The stochastic continuum model on site scale (Walker and Gylling, 1998, Gylling et al., 1999 and Walker and Gylling, 1999) calculates groundwater travel times, t_w, from different canister positions through the rock to the discharge in the biosphere. Reasonable estimate travel times are chosen as the median from the results from the base cases for the three different sites. The pessimistic travel times are chosen as the 5 percentile from the base case calculation for Aberg and Ceberg and from the environmental head variant for Beberg. This means that 50 % of all canister positions have longer travel times than the reasonable estimate and 5 % of the canister positions will have shorter travel times than the pessimistic value.

A reasonable estimate for the flow wetted surface area per volume of water was made based on estimates of the conductive fracture frequency, which in turn is estimated from the hydraulic tests. The pessimistic value of the flow wetted surface area is a factor of ten lower than the reasonable value for Aberg and Beberg. No change in the pessimistic value for Ceberg was assigned.

Peclet number

Based on literature data (Elert et al., 1992) a reasonable value of 10 and a pessimistic value of 2 were chosen for the Peclet number. These values are generic rather than site specific.

Penetration depth

The diffusivity data are evaluated for undisturbed rock, i.e. there should not be any physical limits for the diffusion. There is, however a symmetry limit as the migration could not proceed further than half the distance between two active migration paths. This distance is related to the conductive fracture frequency. The reasonable estimate is 2 m for Aberg and Beberg and 20 m for Ceberg. These distances are much longer than the actual penetration of a sorbing nuclide and hence the value of the maximum penetration depth is not very important. The pessimistic values for the maximum penetration depth were assigned to be 1/10 of the reasonable values.

Table 3-15. Data used on other far-field parameters.

Parameter	Aberg		Beberg		Ceberg	
	Reason.	Pessim.	Reason.	Pessim.	Reason.	Pessim.
Groundwater travel time (yr)	10	0.8	60	3.3	2000	400
a_w (m/m)	10^4	10^3	10^4	10^3	10^3	10^3
Peclet number	10	2	10	2	10	2
Penetration depth (m)	2	0.2	2	0.2	20	2

3.12 Biosphere

Dose conversion factors, EDF

The biosphere modelling has been performed by Nordlinder et al. (1999) resulting in ecosystem specific dose conversion factors (EDF) for different modules at each site. This modelling has been made by dividing the site into sub-areas (250 m × 250 m) and associating a module to each sub-area. EDF-factors are calculated for each such module. The module type is selected from present day conditions, mainly from inspection maps and the well archive of the Swedish Geological Survey. The module types considered are well, lake, stream, bay, open coast, soil and peat area.

The choice of module is based on the exit points obtained in the groundwater flow calculations for the three different sites (Walker and Gylling, 1998, Gylling et al., 1999 and Walker and Gylling, 1999). The reasonable estimates for Aberg are mean values for inner bay since 80 % of the exit points are in that module (Andersson, 1999). However, the groundwater flow calculations represent present day conditions and considering the ongoing land rise the release will most likely occur on land and hence the low EDF-factors for inner bay could not be defended. Therefore in the calculations the reasonable estimate for Aberg have been to use mean EDF-factors for peat area. The peat area is the module on land having the highest EDF-factors and it can not be regarded as improbable. Most of the exit points in Beberg and Ceberg are in forest. The forest is however pessimistically approximated by the module peat area and hence the reasonable estimates for both Beberg and Ceberg are the mean values for peat area.

In the pessimistic estimate, the module that gives the highest dose conversion factor for each nuclide has been chosen. The dose conversion factor has furthermore been chosen as the maximum value instead of the mean value used in the reasonable choice of dose conversion factor. The result for almost all nuclides is the module peat area as in the reasonable case, but with maximum values for the dose conversion factors.

Calculations are also performed with the module standard well. This is a hypothetical site specific well with a capacity of 300 litres/hour used to facilitate comparison between the different sites. EDF-factors for some other site-specific well are scaled in proportion to the capacity to achieve EDF-factors corresponding to the capacity of the standard well.

Table 3-16. EDF-factors used in the reasonable cases.

Nuclide	Reasonable EDF-factors (Sv/Bq)						
	Aberg			Beberg		Ceberg	
	Peat area	Well 300l/h	Inner bay	Peat area	Well 300l/h	Peat area	Well 300l/h
Ag-108m	$1.9\cdot10^{-11}$	$1.3\cdot10^{-12}$	$1.1\cdot10^{-15}$	$1.9\cdot10^{-11}$	$1.3\cdot10^{-12}$	$1.8\cdot10^{-11}$	$1.3\cdot10^{-12}$
Am-241	$2.0\cdot10^{-10}$	$6.8\cdot10^{-11}$	$1.6\cdot10^{-14}$	$2.0\cdot10^{-10}$	$6.8\cdot10^{-11}$	$2.0\cdot10^{-10}$	$6.7\cdot10^{-11}$
Am-243	$1.9\cdot10^{-9}$	$1.3\cdot10^{-10}$	$1.6\cdot10^{-14}$	$1.8\cdot10^{-9}$	$1.3\cdot10^{-10}$	$1.7\cdot10^{-9}$	$1.3\cdot10^{-10}$
C-14	$1.1\cdot10^{-14}$	$2.4\cdot10^{-13}$	$1.7\cdot10^{-15}$	$6.5\cdot10^{-15}$	$2.4\cdot10^{-13}$	$4.6\cdot10^{-15}$	$2.4\cdot10^{-13}$
Cl-36	$3.6\cdot10^{-11}$	$7.3\cdot10^{-13}$	$1.6\cdot10^{-16}$	$2.2\cdot10^{-11}$	$7.2\cdot10^{-13}$	$1.5\cdot10^{-11}$	$6.3\cdot10^{-13}$
Cm-245	$1.2\cdot10^{-9}$	$1.6\cdot10^{-10}$	$1.6\cdot10^{-14}$	$9.8\cdot10^{-10}$	$1.6\cdot10^{-10}$	$8.1\cdot10^{-10}$	$1.6\cdot10^{-10}$
Cs-135	$4.4\cdot10^{-12}$	$1.9\cdot10^{-12}$	$7.8\cdot10^{-16}$	$2.7\cdot10^{-12}$	$1.9\cdot10^{-12}$	$1.8\cdot10^{-12}$	$1.7\cdot10^{-12}$
Cs-137	$4.0\cdot10^{-12}$	$5.6\cdot10^{-12}$	$4.8\cdot10^{-15}$	$3.5\cdot10^{-12}$	$5.6\cdot10^{-12}$	$3.1\cdot10^{-12}$	$5.6\cdot10^{-12}$
Ho-166m	$2.3\cdot10^{-12}$	$2.0\cdot10^{-12}$	$1.3\cdot10^{-16}$	$1.9\cdot10^{-12}$	$2.0\cdot10^{-12}$	$1.6\cdot10^{-12}$	$2.0\cdot10^{-12}$
I-129	$5.0\cdot10^{-11}$	$9.2\cdot10^{-11}$	$1.8\cdot10^{-14}$	$3.0\cdot10^{-11}$	$9.1\cdot10^{-11}$	$2.1\cdot10^{-11}$	$7.7\cdot10^{-11}$
Nb-94	$3.0\cdot10^{-12}$	$3.4\cdot10^{-12}$	$2.1\cdot10^{-16}$	$2.0\cdot10^{-12}$	$3.3\cdot10^{-12}$	$1.5\cdot10^{-12}$	$2.8\cdot10^{-12}$
Ni-59	$4.5\cdot10^{-13}$	$5.9\cdot10^{-14}$	$2.2\cdot10^{-17}$	$2.7\cdot10^{-13}$	$5.9\cdot10^{-14}$	$1.9\cdot10^{-13}$	$5.1\cdot10^{-14}$
Ni-63	$1.8\cdot10^{-13}$	$6.2\cdot10^{-14}$	$5.2\cdot10^{-17}$	$1.6\cdot10^{-13}$	$6.3\cdot10^{-14}$	$1.4\cdot10^{-13}$	$6.1\cdot10^{-14}$
Np-237	$1.8\cdot10^{-10}$	$4.7\cdot10^{-11}$	$2.0\cdot10^{-15}$	$1.1\cdot10^{-10}$	$4.7\cdot10^{-11}$	$7.5\cdot10^{-11}$	$4.3\cdot10^{-11}$
Pa-231	$4.7\cdot10^{-9}$	$6.8\cdot10^{-10}$	$1.3\cdot10^{-14}$	$3.5\cdot10^{-9}$	$6.8\cdot10^{-10}$	$2.7\cdot10^{-9}$	$6.7\cdot10^{-10}$
Pd-107	$1.0\cdot10^{-13}$	$2.3\cdot10^{-14}$	$1.2\cdot10^{-18}$	$6.4\cdot10^{-14}$	$2.3\cdot10^{-14}$	$4.4\cdot10^{-14}$	$2.0\cdot10^{-14}$
Pu-239	$6.2\cdot10^{-10}$	$2.2\cdot10^{-10}$	$6.4\cdot10^{-15}$	$4.1\cdot10^{-10}$	$2.3\cdot10^{-10}$	$3.0\cdot10^{-10}$	$2.3\cdot10^{-10}$
Pu-240	$5.2\cdot10^{-10}$	$1.8\cdot10^{-10}$	$6.3\cdot10^{-15}$	$3.6\cdot10^{-10}$	$1.9\cdot10^{-10}$	$2.7\cdot10^{-10}$	$1.9\cdot10^{-10}$
Pu-242	$6.3\cdot10^{-10}$	$2.3\cdot10^{-10}$	$6.1\cdot10^{-15}$	$4.1\cdot10^{-10}$	$2.4\cdot10^{-10}$	$3.0\cdot10^{-10}$	$2.3\cdot10^{-10}$
Ra-226	$1.7\cdot10^{-9}$	$1.2\cdot10^{-10}$	$1.6\cdot10^{-14}$	$1.2\cdot10^{-9}$	$1.1\cdot10^{-10}$	$9.4\cdot10^{-10}$	$1.1\cdot10^{-10}$
Se-79	$2.7\cdot10^{-9}$	$2.7\cdot10^{-12}$	$1.4\cdot10^{-14}$	$1.7\cdot10^{-9}$	$2.7\cdot10^{-12}$	$1.2\cdot10^{-9}$	$2.1\cdot10^{-12}$
Sm-151	$6.4\cdot10^{-15}$	$3.2\cdot10^{-14}$	$5.9\cdot10^{-18}$	$6.0\cdot10^{-15}$	$3.2\cdot10^{-14}$	$5.7\cdot10^{-15}$	$3.2\cdot10^{-14}$
Sn-126	$1.4\cdot10^{-10}$	$3.9\cdot10^{-12}$	$9.9\cdot10^{-16}$	$8.6\cdot10^{-11}$	$3.9\cdot10^{-12}$	$6.1\cdot10^{-11}$	$3.1\cdot10^{-12}$
Sr-90	$2.1\cdot10^{-11}$	$1.3\cdot10^{-11}$	$1.3\cdot10^{-15}$	$1.8\cdot10^{-11}$	$1.3\cdot10^{-11}$	$1.6\cdot10^{-11}$	$1.2\cdot10^{-11}$
Tc-99	$7.0\cdot10^{-13}$	$5.5\cdot10^{-13}$	$1.7\cdot10^{-17}$	$4.2\cdot10^{-13}$	$5.5\cdot10^{-13}$	$2.9\cdot10^{-13}$	$4.7\cdot10^{-13}$
Th-229	$7.5\cdot10^{-9}$	$4.2\cdot10^{-10}$	$1.3\cdot10^{-14}$	$7.0\cdot10^{-9}$	$4.1\cdot10^{-10}$	$6.5\cdot10^{-9}$	$4.1\cdot10^{-10}$
Th-230	$4.4\cdot10^{-9}$	$2.1\cdot10^{-10}$	$5.4\cdot10^{-15}$	$4.0\cdot10^{-9}$	$2.1\cdot10^{-10}$	$3.7\cdot10^{-9}$	$2.0\cdot10^{-10}$
U-233	$1.0\cdot10^{-11}$	$1.9\cdot10^{-11}$	$2.6\cdot10^{-15}$	$6.1\cdot10^{-12}$	$1.9\cdot10^{-11}$	$4.3\cdot10^{-12}$	$1.7\cdot10^{-11}$
U-234	$9.8\cdot10^{-12}$	$1.8\cdot10^{-11}$	$2.5\cdot10^{-15}$	$5.9\cdot10^{-12}$	$1.7\cdot10^{-11}$	$4.1\cdot10^{-12}$	$1.7\cdot10^{-11}$
U-235	$8.9\cdot10^{-12}$	$1.7\cdot10^{-11}$	$2.4\cdot10^{-15}$	$5.4\cdot10^{-12}$	$1.7\cdot10^{-11}$	$3.7\cdot10^{-12}$	$1.6\cdot10^{-11}$
U-238	$8.3\cdot10^{-12}$	$1.6\cdot10^{-11}$	$2.3\cdot10^{-15}$	$5.1\cdot10^{-12}$	$1.6\cdot10^{-11}$	$3.5\cdot10^{-12}$	$1.6\cdot10^{-11}$
Zr-93	$6.1\cdot10^{-13}$	$3.7\cdot10^{-13}$	$9.0\cdot10^{-17}$	$4.4\cdot10^{-13}$	$3.6\cdot10^{-13}$	$3.3\cdot10^{-13}$	$3.6\cdot10^{-13}$

Table 3-17. Pessimistic EDF-factors used in the calculations.

Nuclide	Pessimistic EDF-factors (Sv/Bq)		
	Aberg	Beberg	Ceberg
Ag-108m	$2.3 \cdot 10^{-10}$	$2.3 \cdot 10^{-10}$	$2.2 \cdot 10^{-10}$
Am-241	$2.6 \cdot 10^{-9}$	$2.6 \cdot 10^{-9}$	$2.6 \cdot 10^{-9}$
Am-243	$2.7 \cdot 10^{-8}$	$2.5 \cdot 10^{-8}$	$2.3 \cdot 10^{-8}$
C-14	$5.4 \cdot 10^{-13}$	$2.6 \cdot 10^{-13}$	$2.6 \cdot 10^{-13}$
Cl-36	$3.3 \cdot 10^{-10}$	$2.0 \cdot 10^{-10}$	$1.4 \cdot 10^{-10}$
Cm-245	$1.4 \cdot 10^{-8}$	$1.2 \cdot 10^{-8}$	$9.4 \cdot 10^{-9}$
Cs-135	$3.7 \cdot 10^{-11}$	$2.2 \cdot 10^{-11}$	$1.5 \cdot 10^{-11}$
Cs-137	$3.6 \cdot 10^{-11}$	$2.9 \cdot 10^{-11}$	$2.6 \cdot 10^{-11}$
Ho-166m	$2.3 \cdot 10^{-11}$	$2.0 \cdot 10^{-11}$	$1.8 \cdot 10^{-11}$
I-129	$8.2 \cdot 10^{-10}$	$4.9 \cdot 10^{-10}$	$3.1 \cdot 10^{-10}$
Nb-94	$3.3 \cdot 10^{-11}$	$2.4 \cdot 10^{-11}$	$1.9 \cdot 10^{-11}$
Ni-59	$4.1 \cdot 10^{-12}$	$2.5 \cdot 10^{-12}$	$1.7 \cdot 10^{-12}$
Ni-63	$2.0 \cdot 10^{-12}$	$1.6 \cdot 10^{-12}$	$1.4 \cdot 10^{-12}$
Np-237	$1.7 \cdot 10^{-9}$	$1.0 \cdot 10^{-9}$	$7.0 \cdot 10^{-10}$
Pa-231	$5.2 \cdot 10^{-8}$	$4.3 \cdot 10^{-8}$	$3.4 \cdot 10^{-8}$
Pd-107	$1.1 \cdot 10^{-12}$	$7.1 \cdot 10^{-13}$	$5.0 \cdot 10^{-13}$
Pu-239	$7.7 \cdot 10^{-9}$	$6.4 \cdot 10^{-9}$	$5.0 \cdot 10^{-9}$
Pu-240	$6.4 \cdot 10^{-9}$	$4.9 \cdot 10^{-9}$	$4.1 \cdot 10^{-9}$
Pu-242	$8.3 \cdot 10^{-9}$	$6.8 \cdot 10^{-9}$	$5.0 \cdot 10^{-9}$
Ra-226	$1.9 \cdot 10^{-8}$	$1.6 \cdot 10^{-8}$	$1.2 \cdot 10^{-8}$
Se-79	$2.6 \cdot 10^{-8}$	$1.7 \cdot 10^{-8}$	$1.2 \cdot 10^{-8}$
Sm-151	$8.4 \cdot 10^{-14}$	$8.1 \cdot 10^{-14}$	$7.7 \cdot 10^{-14}$
Sn-126	$1.4 \cdot 10^{-9}$	$9.1 \cdot 10^{-10}$	$6.3 \cdot 10^{-10}$
Sr-90	$2.2 \cdot 10^{-10}$	$1.8 \cdot 10^{-10}$	$1.6 \cdot 10^{-10}$
Tc-99	$1.8 \cdot 10^{-11}$	$1.1 \cdot 10^{-11}$	$7.4 \cdot 10^{-12}$
Th-229	$9.9 \cdot 10^{-8}$	$8.6 \cdot 10^{-8}$	$8.2 \cdot 10^{-8}$
Th-230	$5.7 \cdot 10^{-8}$	$5.0 \cdot 10^{-8}$	$4.5 \cdot 10^{-8}$
U-233	$1.4 \cdot 10^{-10}$	$8.7 \cdot 10^{-11}$	$6.0 \cdot 10^{-11}$
U-234	$1.4 \cdot 10^{-10}$	$8.4 \cdot 10^{-11}$	$5.9 \cdot 10^{-11}$
U-235	$1.3 \cdot 10^{-10}$	$7.6 \cdot 10^{-11}$	$5.3 \cdot 10^{-11}$
U-238	$1.2 \cdot 10^{-10}$	$7.2 \cdot 10^{-11}$	$5.0 \cdot 10^{-11}$
Zr-93	$4.8 \cdot 10^{-12}$	$3.5 \cdot 10^{-12}$	$2.8 \cdot 10^{-12}$

Table 3-18. Pessimistic EDF-factors used in the probabilistic calculations. (Reasonable EDF-factors are given in Table 3-16).

Nuclide	Pessimistic EDF-factor (Sv/Bq)					
	Aberg		Beberg		Ceberg	
	Peat area	Well 300l/h	Peat area	Well 300l/h	Peat area	Well 300l/h
Ni-59	$4.1 \cdot 10^{-12}$	$2.0 \cdot 10^{-13}$	$2.5 \cdot 10^{-12}$	$2.0 \cdot 10^{-13}$	$1.7 \cdot 10^{-12}$	$1.6 \cdot 10^{-13}$
Nb-94	$3.3 \cdot 10^{-11}$	$8.3 \cdot 10^{-12}$	$2.4 \cdot 10^{-11}$	$8.3 \cdot 10^{-12}$	$1.9 \cdot 10^{-11}$	$7.3 \cdot 10^{-12}$
Sn-126	$1.4 \cdot 10^{-9}$	$1.2 \cdot 10^{-11}$	$9.1 \cdot 10^{-10}$	$1.2 \cdot 10^{-11}$	$6.3 \cdot 10^{-10}$	$8.4 \cdot 10^{-12}$
I-129	$4.7 \cdot 10^{-10}$	$3.7 \cdot 10^{-10}$	$2.8 \cdot 10^{-10}$	$3.6 \cdot 10^{-10}$	$2.0 \cdot 10^{-10}$	$2.7 \cdot 10^{-10}$
Ra-226	$1.9 \cdot 10^{-8}$	$2.2 \cdot 10^{-10}$	$1.6 \cdot 10^{-8}$	$2.1 \cdot 10^{-10}$	$1.2 \cdot 10^{-8}$	$1.9 \cdot 10^{-10}$
Th-230	$5.7 \cdot 10^{-8}$	$5.3 \cdot 10^{-10}$	$5.0 \cdot 10^{-8}$	$5.2 \cdot 10^{-10}$	$4.5 \cdot 10^{-8}$	$5.1 \cdot 10^{-10}$
U-234	$1.4 \cdot 10^{-10}$	$2.9 \cdot 10^{-11}$	$8.4 \cdot 10^{-11}$	$2.9 \cdot 10^{-11}$	$5.9 \cdot 10^{-11}$	$2.7 \cdot 10^{-11}$
U-238	$1.2 \cdot 10^{-10}$	$2.6 \cdot 10^{-11}$	$7.2 \cdot 10^{-11}$	$2.5 \cdot 10^{-11}$	$5.0 \cdot 10^{-11}$	$2.4 \cdot 10^{-11}$
Pu-239	$7.7 \cdot 10^{-9}$	$6.0 \cdot 10^{-10}$	$6.4 \cdot 10^{-9}$	$6.0 \cdot 10^{-10}$	$5.0 \cdot 10^{-9}$	$6.0 \cdot 10^{-10}$

Table 3-19. Reasonable EDF-factors for Open Coast used in the glacial melting case for Aberg.

Nuclide	Reasonable EDF-factor (Sv/Bq) Open Coast Aberg
Ag-108m	$4.3 \cdot 10^{-18}$
Am-241	$2.0 \cdot 10^{-16}$
Am-243	$2.0 \cdot 10^{-16}$
C-14	$6.7 \cdot 10^{-18}$
Cl-36	$5.7 \cdot 10^{-19}$
Cm-245	$2.1 \cdot 10^{-16}$
Cs-135	$2.9 \cdot 10^{-18}$
Cs-137	$1.8 \cdot 10^{-17}$
Ho-166m	$1.9 \cdot 10^{-18}$
I-129	$1.1 \cdot 10^{-16}$
Nb-94	$1.5 \cdot 10^{-18}$
Ni-59	$9.0 \cdot 10^{-20}$
Ni-63	$2.1 \cdot 10^{-19}$
Np-237	$7.6 \cdot 10^{-18}$
Pa-231	$4.8 \cdot 10^{-17}$
Pd-107	$2.6 \cdot 10^{-20}$
Pu-239	$5.5 \cdot 10^{-17}$
Pu-240	$5.5 \cdot 10^{-17}$
Pu-242	$5.3 \cdot 10^{-17}$
Ra-226	$7.0 \cdot 10^{-17}$
Se-79	$5.3 \cdot 10^{-17}$
Sm-151	$9.1 \cdot 10^{-20}$
Sn-126	$3.8 \cdot 10^{-18}$
Sr-90	$5.0 \cdot 10^{-18}$
Tc-99	$6.1 \cdot 10^{-19}$
Th-229	$4.0 \cdot 10^{-16}$
Th-230	$1.7 \cdot 10^{-16}$
U-233	$1.1 \cdot 10^{-17}$
U-234	$1.1 \cdot 10^{-17}$
U-235	$1.0 \cdot 10^{-17}$
U-238	$9.7 \cdot 10^{-18}$
Zr-93	$9.8 \cdot 10^{-19}$

Dose limits

For the ecosystems peat area and well the biosphere calculations include the most exposed individuals within a large region. The acceptance criterion, which the calculation results should be compared with when the EDF-factors are used, is thus a risk of 10^{-5}/yr, i.e. a risk for the most exposed individuals in a population given by SSI. Expressed in dose, the risk is equivalent to $1.5 \cdot 10^{-4}$ Sv/yr for an exposure that is certain to occur.

For the ecosystems inner bay and open coast large populations may be exposed in some cases, which makes it more reasonable to compare with a risk of 10^{-6}/yr, which is equivalent to $1.5 \cdot 10^{-5}$ Sv/yr for an exposure that is certain to occur.

4 Deterministic calculations

The deterministic calculations have been set up to demonstrate the radionuclide transport for reasonable conditions at all three sites. To evaluate the uncertainty the influence of changing parameters to pessimistic values in a systematic way were studied in the uncertainty cases performed for all three sites. Also calculations for special cases and for a scenario based on possible climatic changes are performed for Aberg.

4.1 Reasonable Cases

In Table 4-1 all calculation cases regarded as reasonable cases are summarised. For each site, all parameters are assigned reasonable values. Variations with different biosphere modules have also been performed.

Table 4-1. Summary of the reasonable cases. (R=Reasonable estimate, PA=Peat Area, SW=Standard well, IB=Inner Bay).

Case name	Aberg			Beberg		Ceberg	
	a00	a00sw	a00ib	b00	b00sw	c00	c00sw
Near field							
Inventory	R	R	R	R	R	R	R
IRF	R	R	R	R	R	R	R
Fuel conversion	R	R	R	R	R	R	R
Number of defective canisters	R	R	R	R	R	R	R
Defect growth	R	R	R	R	R	R	R
Delay time for transport	R	R	R	R	R	R	R
Solubility	R	R	R	R	R	R	R
Sorption in bentonite	R	R	R	R	R	R	R
Sorption in backfill	R	R	R	R	R	R	R
Near-field water flux q_0	R	R	R	R	R	R	R
Q_{eq}-parameters	R	R	R	R	R	R	R
Far field							
Sorption in rock	R	R	R	R	R	R	R
Diffusivity in rock	R	R	R	R	R	R	R
Travel time	R	R	R	R	R	R	R
Flow-wetted surface	R	R	R	R	R	R	R
Maximum penetration depth	R	R	R	R	R	R	R
Peclet number	R	R	R	R	R	R	R
Biosphere							
Choice of module	PA	SW	IB	PA	SW	PA	SW
EDF for selected module	R	R	R	R	R	R	R

4.1.1 Aberg

In the reasonable case all parameters are given reasonable values. This means that initially there is one canister with a small defect increasing and after 200 000 years a continuous water path has been formed to the fuel. Thereby the fuel dissolution and the radionuclide transport starts at 200 000 years. Many nuclides have decayed to negligible activity during this time. Only long-lived nuclides and especially those having an instant fraction free for release will influence the total release. The defective canister is supposed to be placed in a deposition hole with barriers with reasonable material data.

The near-field water fluxes and travel times are also given their reasonable estimates. The biosphere data used are the mean values for peat area. Variations have been performed using the mean EDF-factors for standard well and inner bay respectively.

In Figure 4-1 to 4-3 the results are shown for the reasonable cases for Aberg using EDF-factors for peat area, standard well and inner bay, respectively. The three plots given in Figure 4-1 show the release from the near field and far field given in Bq/year and the biosphere dose in Sv/year. The three dominating nuclides are indicated in the text box in the upper right corner of each plot. The two upper plots have the same scale to make the far field release rates easily comparable with the release from the near field. In the biosphere plot the dose limit of 0.15 mSv/year, valid for peat area and wells, see Section 3.12, is shown.

Since it is only the EDF-factors that differs in the two variations of the reasonable case it is only the biosphere dose that differs and hence Figure 4-2 and 4-3 only show the biosphere doses. In Figure 4-3 the dose limit of 0.015 mSv/year, valid for the inner bay, see Section 3.12 is indicated.

The radionuclide release from the near field is dominated by Ni-59, a nuclide present in the metal parts around the fuel. The metal is assumed to be totally corroded and initially free for transport. The fraction of I-129 and Cs-135 that is initially free for release diffuses rather fast through the near field. At longer times the release is dominated by Ra-226, a naturally occurring radionuclide, which is formed by in-growth from the chain decay of U-238 in the fuel matrix.

Detailed study of the output shows that the concentrations of the following nuclides reach their solubility limits in the canister: Pu-242, U-238, Th-230, Th-229, Pd-107, Se-79, Sn-126, Tc-99 and Zr-93.

The shape of the release curves from the near field for Ni-59 and Cs-135 shows the influence of the different exit paths. The peaks at 200 000 years are due to release dominated by the exit path Q1. Thereafter the exit path Q2 dominates the release and finally when the slope of the release curve is changed the exit path Q3 dominates the release. The influence from the different exit paths on the total release is different for all nuclides. The release through Q4 is for all nuclides and all times of minor importance.

The peak on the release curve for I-129 is explained by the IRF and the following constant level corresponds to the matrix dissolution rate.

The release from the far field shows that the three dominating nuclides, Ni-59, Cs-135 and Ra-226, are influenced to a large extent by the transport through the far field due to matrix diffusion and sorption in combination with the decay. The non-sorbing nuclides I-129 and Cl-36 are almost unaffected by the transport through the far field and the releases are almost the same as from the near field.

The curves that show biosphere dose for the different nuclides have the same shape as the release curves from the far field. The relative importance of different nuclides is, on the other hand, different in the biosphere curves, which are obtained by multiplying the far-field curves by the nuclide specific dose conversion factors.

The doses in the biosphere are dominated by I-129 for all three biosphere types. The total dose in the reasonable case with EDF-factors for peat area is $5 \cdot 10^{-8}$ Sv/year, for standard well $9 \cdot 10^{-8}$ Sv/year and $2 \cdot 10^{-11}$ Sv/year in the variation with EDF-factors for inner bay. For all times for all three biosphere types the doses are much lower than both the natural background and the dose limits.

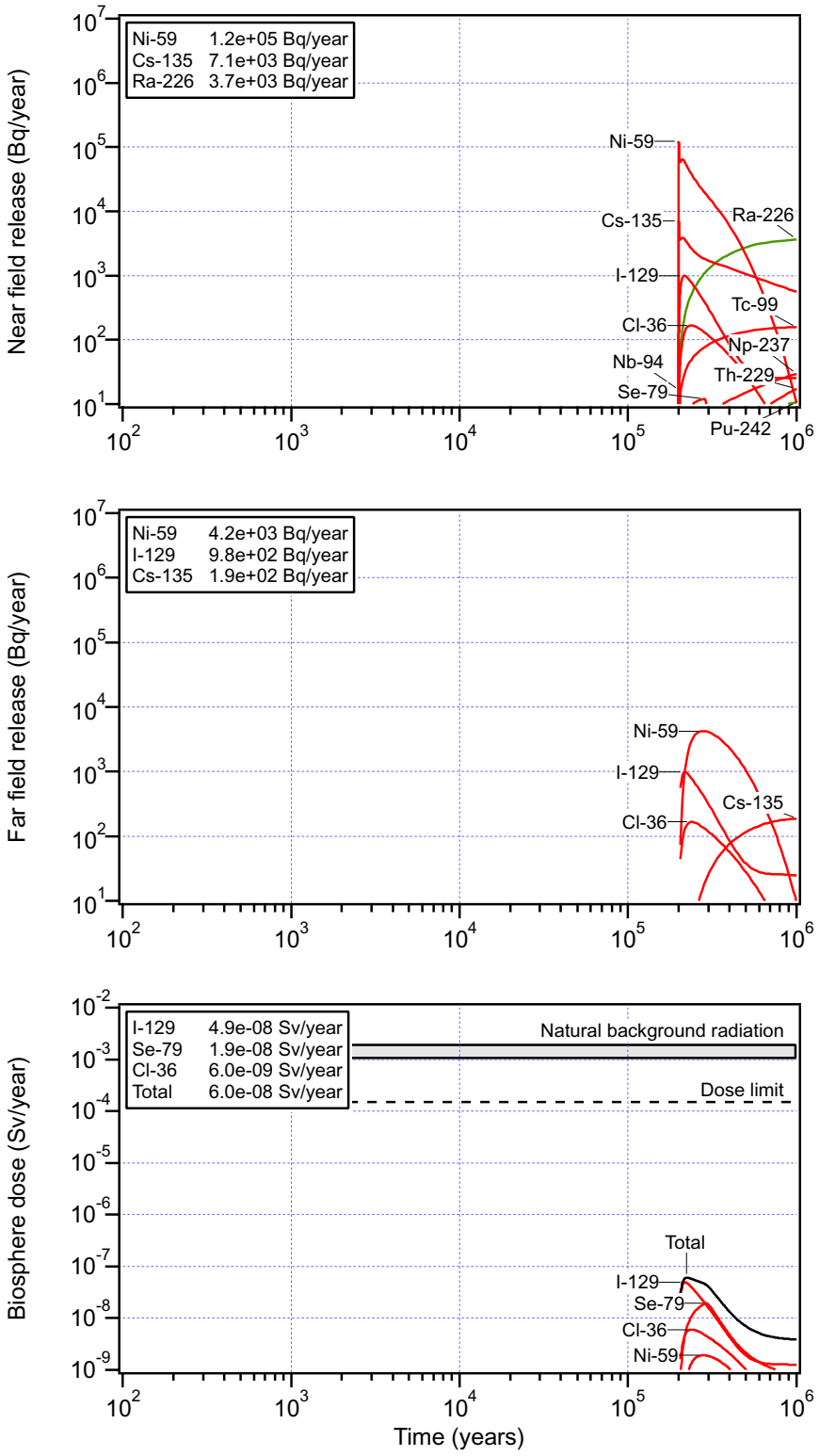

Figure 4-1. *Release from the near and far fields and biosphere doses as a function of time for the reasonable case for Aberg.*

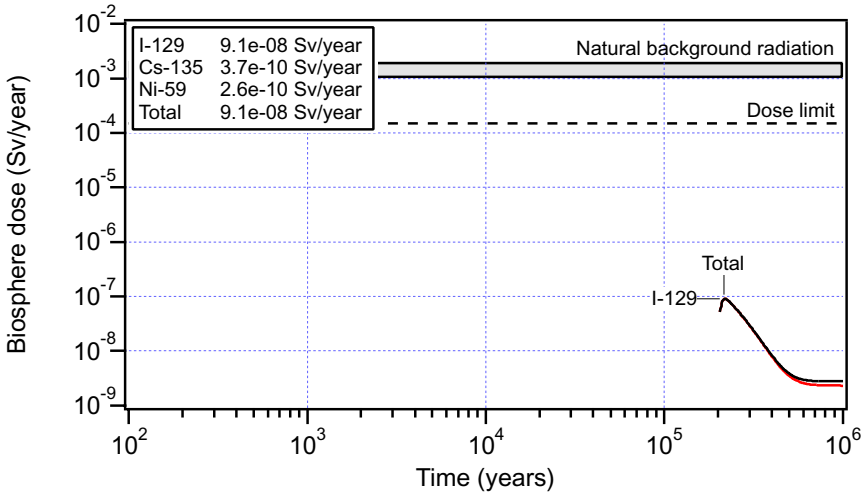

Figure 4-2. *Biosphere doses as a function of time for the reasonable case for Aberg, variation with EDF-factors for standard well.*

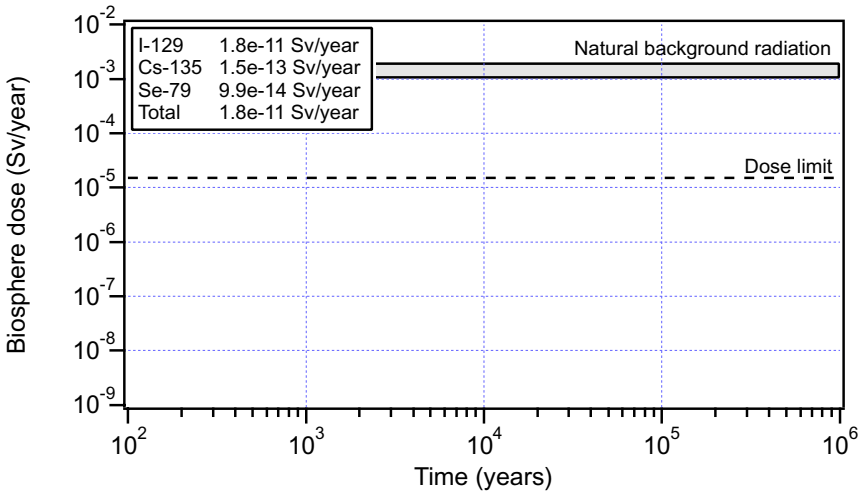

Figure 4-3. *Biosphere doses as a function of time for the reasonable case for Aberg, variation with EDF-factors for inner bay. (Note the different level of the dose limit valid for a large population.)*

4.1.2 Beberg

The corresponding reasonable cases for Beberg are shown in Figures 4-4 (peat area) and 4-5 (standard well).

The release rates from the near field are similar for those for Aberg.

I-129 and Cl-36 dominate the far-field release, both these nuclides are long-lived and do not sorb on any barrier material. Compared to the release from Aberg the release of Ni-59 and Cs-135 are lower in Beberg (below the limits of the diagram). This is due to the increased sorption for these nuclides under the non-saline conditions assumed in the rock in Beberg combined with smaller water fluxes and longer travel times.

The doses in the biosphere are dominated by I-129, Cl-36 and Se-79 that are all long-lived and rather easily transported through the barriers and the far field. The total dose is $3 \cdot 10^{-8}$ Sv/year for the reasonable case with EDF-factors for peat area and $8 \cdot 10^{-8}$ Sv/year for the variation with EDF-factors for the standard well. For all times the doses are much lower than both the natural background and the dose limit. The doses are for all dominating nuclides lower than in Aberg.

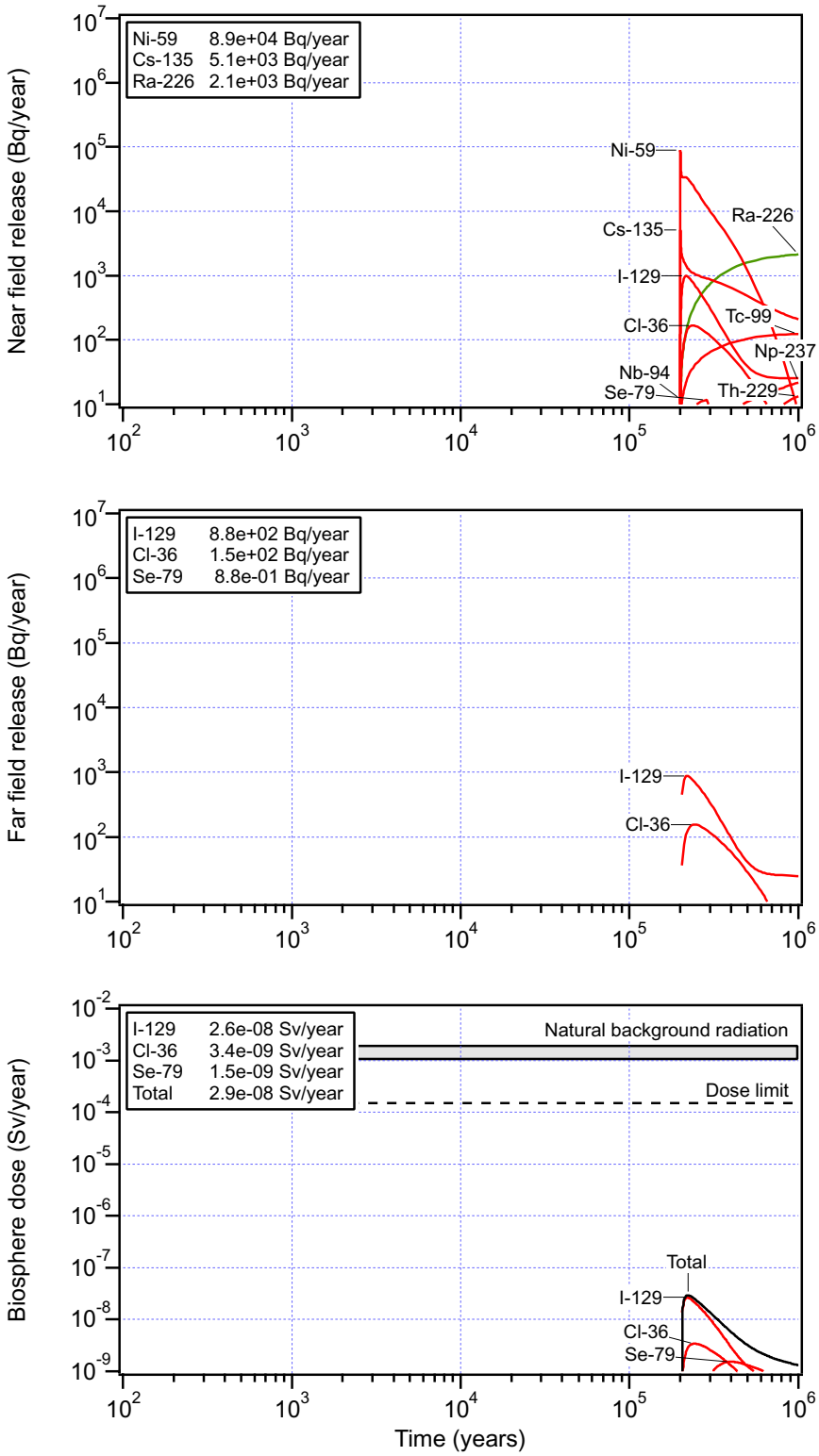

Figure 4-4. *Release from the near and far fields and biosphere doses as a function of time for the reasonable case for Beberg.*

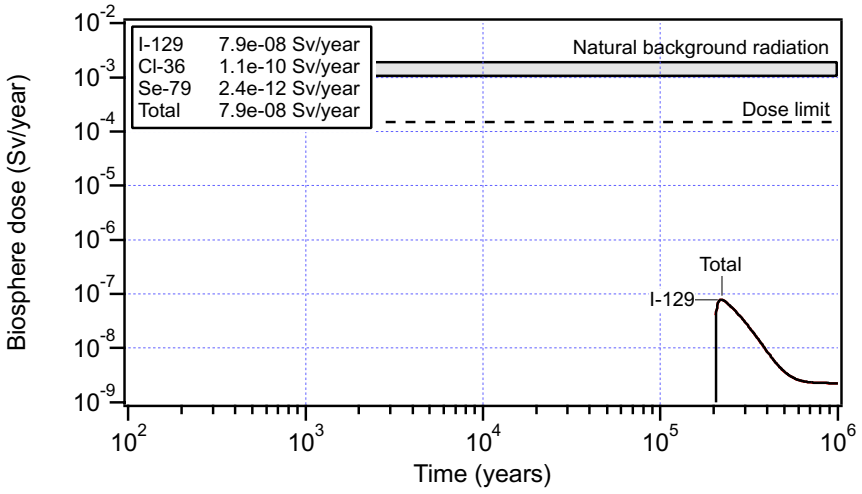

Figure 4-5. *Biosphere doses as a function of time for the reasonable case for Beberg, variation with EDF-factors for standard well.*

4.1.3 Ceberg

Reasonable cases for Ceberg are shown in Figures 4-6 (peat area) and 4-7 (standard well).

The release rate from the near field in the reasonable case is somewhat less from Ceberg than from the two other sites. This is due to the lower near-field water flux influencing the transport through the interface between the buffer/backfill and the rock.

The far-field release is similar to that of Beberg (both sites are non-saline). The same nuclides dominate and the shape of the curves are similar. The somewhat lower release in Ceberg is due to lower water fluxes and longer travel times.

The doses in the biosphere are dominated by I-129, Cl-36 and Se-79 that are all long-lived and rather easily transported through the barriers and far field. The total dose is about $1 \cdot 10^{-8}$ Sv/year for the reasonable case with EDF-factors for peat area and $5 \cdot 10^{-8}$ Sv/year for the variation with the standard well. For all times the doses are much lower than both the natural background and the dose limit. The doses are for all dominating nuclides lower than in Aberg and Beberg.

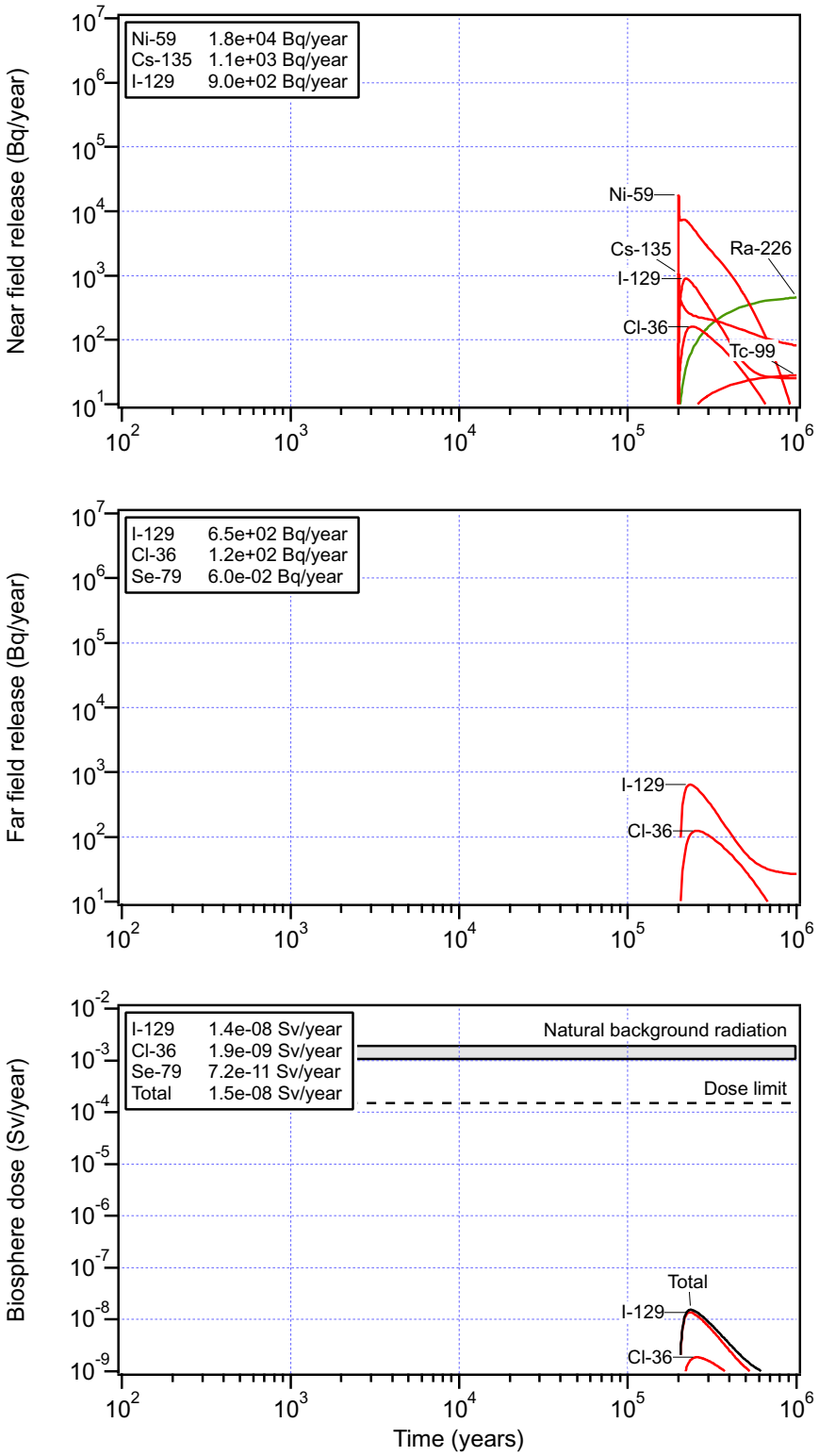

Figure 4-6. *Release from the near and far fields and biosphere doses as a function of time for the reasonable case for Ceberg.*

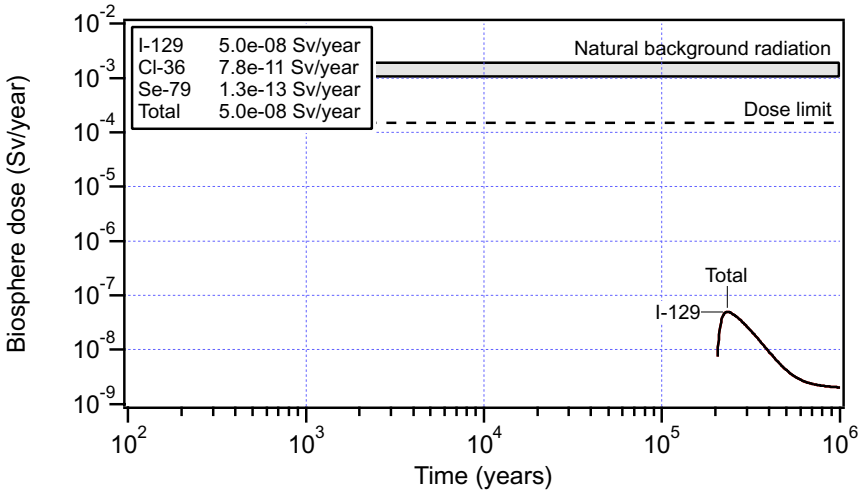

Figure 4-7. *Biosphere doses as a function of time for the reasonable case for Ceberg, variation with EDF-factors for standard well.*

4.2 Uncertainty cases

As described above the input data has been assigned reasonable values and to describe the uncertainty most parameters have also been assigned pessimistic values. The uncertainty cases have been set up to show the influence of the uncertainty for data related to different parts of the repository system by systematically giving them pessimistic values while all others are reasonable. The results also contribute to the understanding of the modelled system. In Table 4-2 a summary of the uncertainty cases is given. In the following the results for Aberg are described in detail. The results for Beberg and Ceberg are more briefly described and the figures for these sites are given in Appendices B and C, respectively.

Results for all parameters and sites are summarised in Section 4.2.8.

Table 4-2. **Summary of the uncertainty cases. All cases are performed for all sites. (P=Pessimistic estimate and PA=Peat area)**

Parameter	Uncertainty Cases							Remark
	UC1	UC2	UC3	UC4	UC5	UC6	UC7	
Near field								
Inventory								No P available
IRF		P						
Fuel conversion								No P available
Number of defective canisters	P							
Defect growth	P							
Delay time for transport	P							
Solubility		P						
Sorption in bentonite			P					
Sorption in backfill			P					
Near-field water flux q_0				P				
Q_{eq}-parameters				P				
Far field								
Diffusivity in rock						P		
Sorption in rock						P		
Travel time					P			
Flow-wetted surface					P			
Maximum penetration depth					P			
Peclet number					P			
Biosphere								
Choice of module	PA	PA	PA	PA	PA	PA	PA	
EDF for selected module							P	

4.2.1 Pessimistic canister related parameters

In this case the canister related parameters, i.e. the number of defective canisters, defect growth and delay time, are given pessimistic values while all other parameters are reasonable. There are hence initially five defective canisters in this case compared to one in the reasonable case. The delay time is only 300 years, i.e. a continuous water path connects the fuel and radionuclide transport occurs already at this time. The defect is initially small, i.e. 1 mm^2, and the release is thereby limited. The defect grows at 20 000 years and only offers small transport resistance thereafter. In the reasonable case the continuous water path is formed after 200 000 years, when also the size of the defect is large enough to offer only limited transport resistance.

Figure 4-8 shows the release from the near and far fields and the biosphere dose as a function of time for Aberg. Corresponding figures for Beberg and Ceberg are given in Appendices B and C, respectively.

The biosphere dose is also in this case dominated by long-lived, non or slightly sorbing nuclides and the dose is still low compared to the natural background and the dose limit. The increase in dose compared to the reasonable case is to a large extent dependent of the increase from one to five defective canisters. The dominating nuclides are all so long-lived that the difference between 20 000 years and 200 000 years for the large defect only give small influence on the size of the dose but of course the dose occurs earlier.

The results for Beberg and Ceberg show the same influence, mainly a higher dose corresponding to the increase from one to five defective canisters and also an earlier dose due to the assumed earlier growth of the defect.

A special case for Aberg with an initially large defect without any resistance for all time is given in Section 4.3.3.

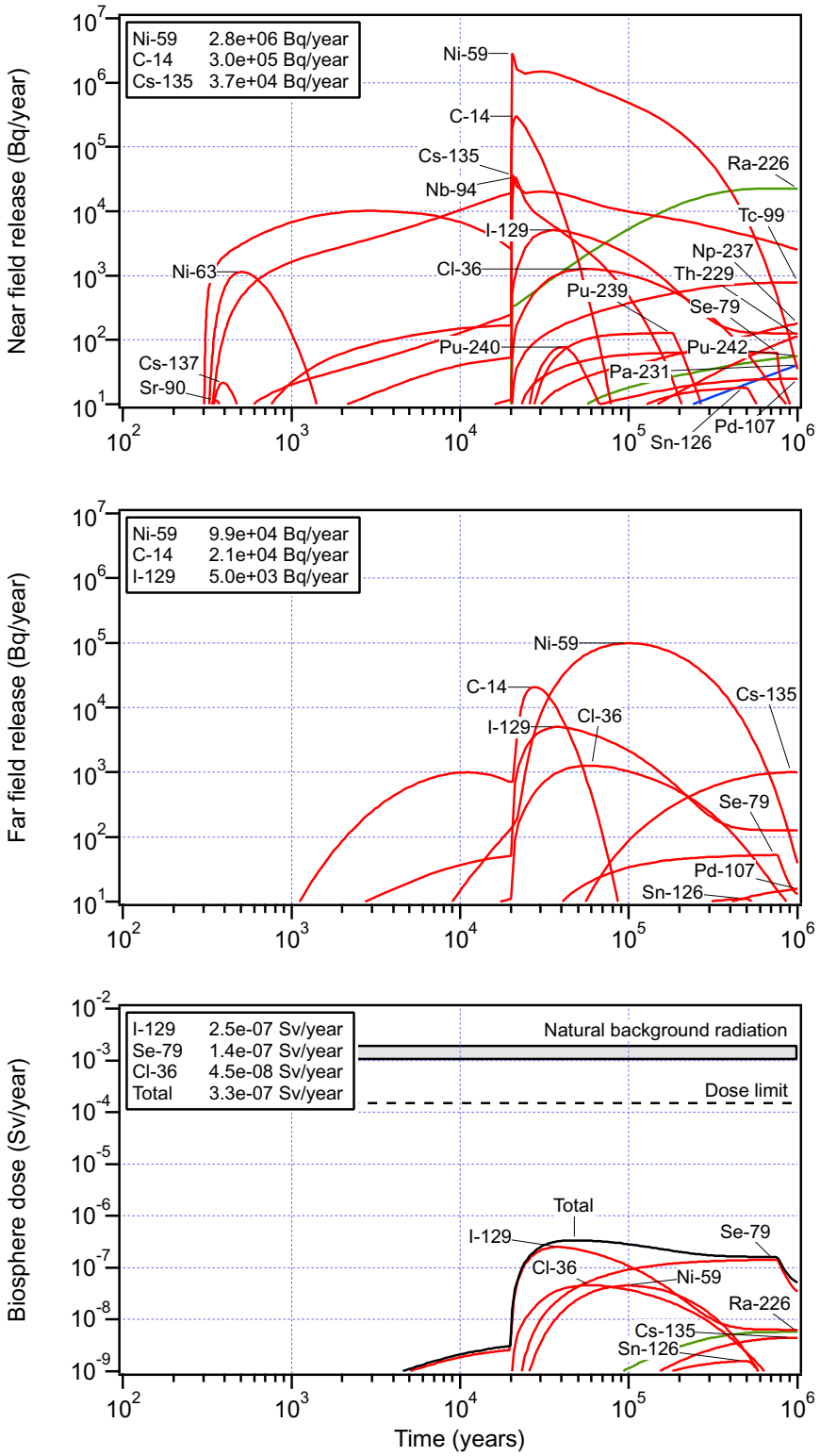

Figure 4-8. *Release from near and far fields and biosphere doses as a function of time for the uncertainty case with pessimistic canister related parameters for Aberg.*

4.2.2 Pessimistic fuel related parameters

The effects of pessimistic values on the instant release fraction, IRF, and on the solubilities are studied in this case. For Se-79 two different pessimistic solubilities have been assigned, see Section 3.6. The solubility limit $4 \cdot 10^{-6}$ mol/m^3 chosen as the highest calculated solubility, as for all the other nuclides, were used in this case.

Figure 4-9 shows the results for Aberg. Corresponding figures for Beberg and Ceberg are given in Appendices B and C, respectively.

The effect on the biosphere dose is rather small compared to the reasonable case. The maximum dose is about three orders of magnitude lower than the dose limit.

The increases in IRF for I-129 and Cl-36 by a factor of two give a corresponding increase in dose. These two nuclides have no solubility limits even in the reasonable case.

Se-79 is solubility limited both in this case and in the reasonable case. The increase in maximum dose for Se-79 is directly corresponding to the increase in solubility limit. A special case for Se-79 in Aberg without solubility limit but reasonable IRF has also been calculated. This case demonstrates the uncertainty of the redox state of Se-79. Potential oxidation of Se-79 during fuel conversion implies essentially infinite solubility. The maximum dose for Se-79 in that special case is $2.9 \cdot 10^{-8}$ Sv/year. In that case Se-79 is limited by the instant release fraction, IRF.

I-129, Se-79 and Cl-36 also dominate the doses for Beberg and Ceberg. I-129 and Cl-36 are influenced by a factor of two, directly corresponding to the increase of their IRF-values. The increase of Se-79 by a factor of about two is most likely due to the increase in solubility limit, as is the case for Aberg.

Two special cases for Aberg, one with immediate fuel dissolution and one without solubility limits, are presented in Section 4.3.1 and 4.3.2, respectively.

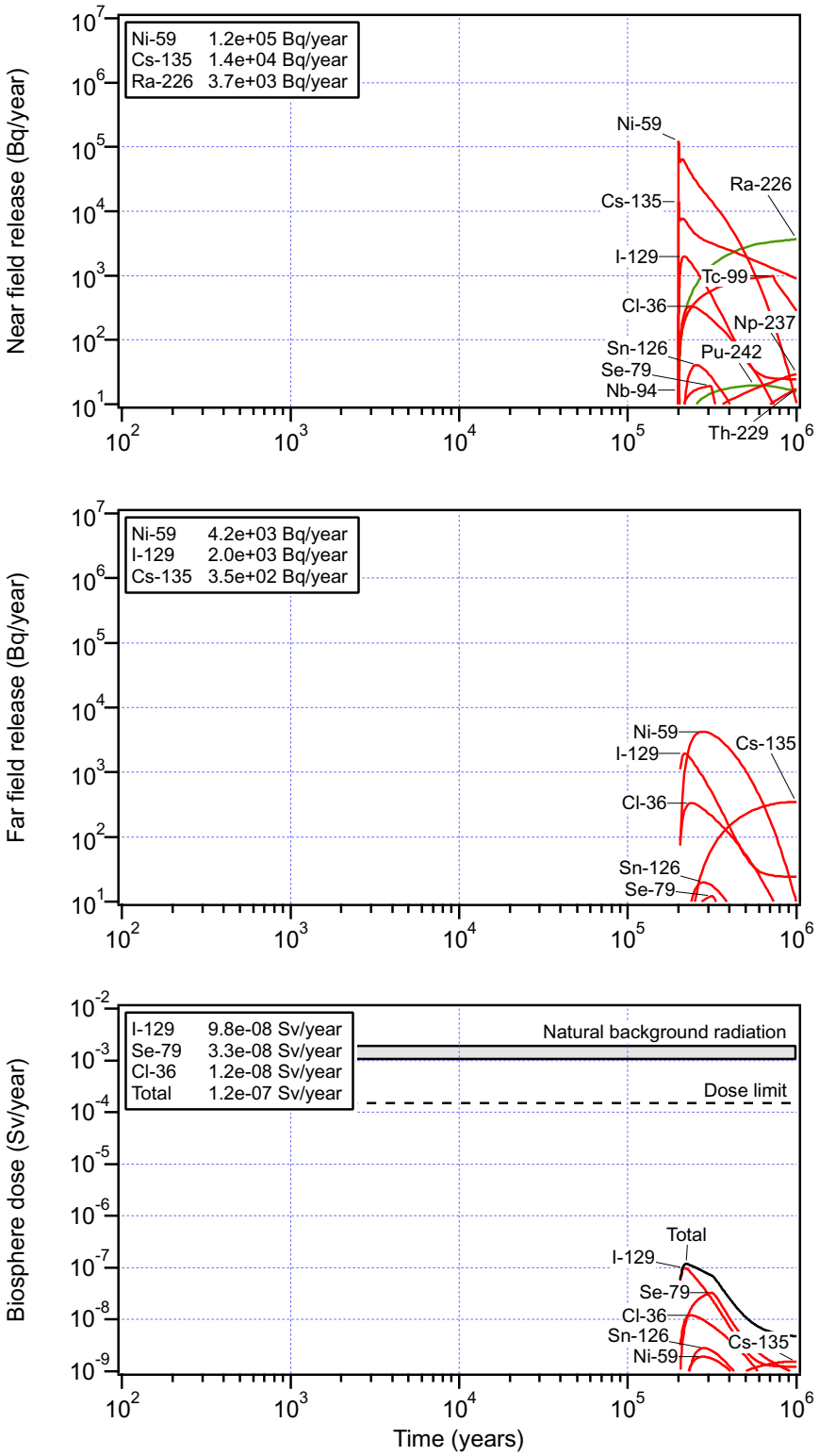

Figure 4-9. *Release from the near and far fields and biosphere doses as a function of time for the uncertainty case with pessimistic fuel related parameters for Aberg.*

4.2.3 Pessimistic sorption data in buffer and backfill

Pessimistic sorption data in the bentonite and the crushed rock-bentonite is used in this case. Figure 4-10 shows the result for Aberg. Corresponding figures for Beberg and Ceberg are given in Appendices B and C, respectively.

I-129 and Cl-36 are non-sorbing in both the reasonable and pessimistic estimate and are hence unchanged. Se-79 is only slightly affected. Sn-126 is influenced to a large extent due to a wide span in sorption data especially in bentonite. I-129 still dominates the total dose at the same level as in the reasonable case, i.e. well below the dose limit.

The effects are the same for Beberg and Ceberg even though the level of the dose from Sn-126 is lower due to a stronger retention in the rock at these two sites.

A special case for Aberg where the resistance in the buffer is negligible is presented in Section 4.3.4.

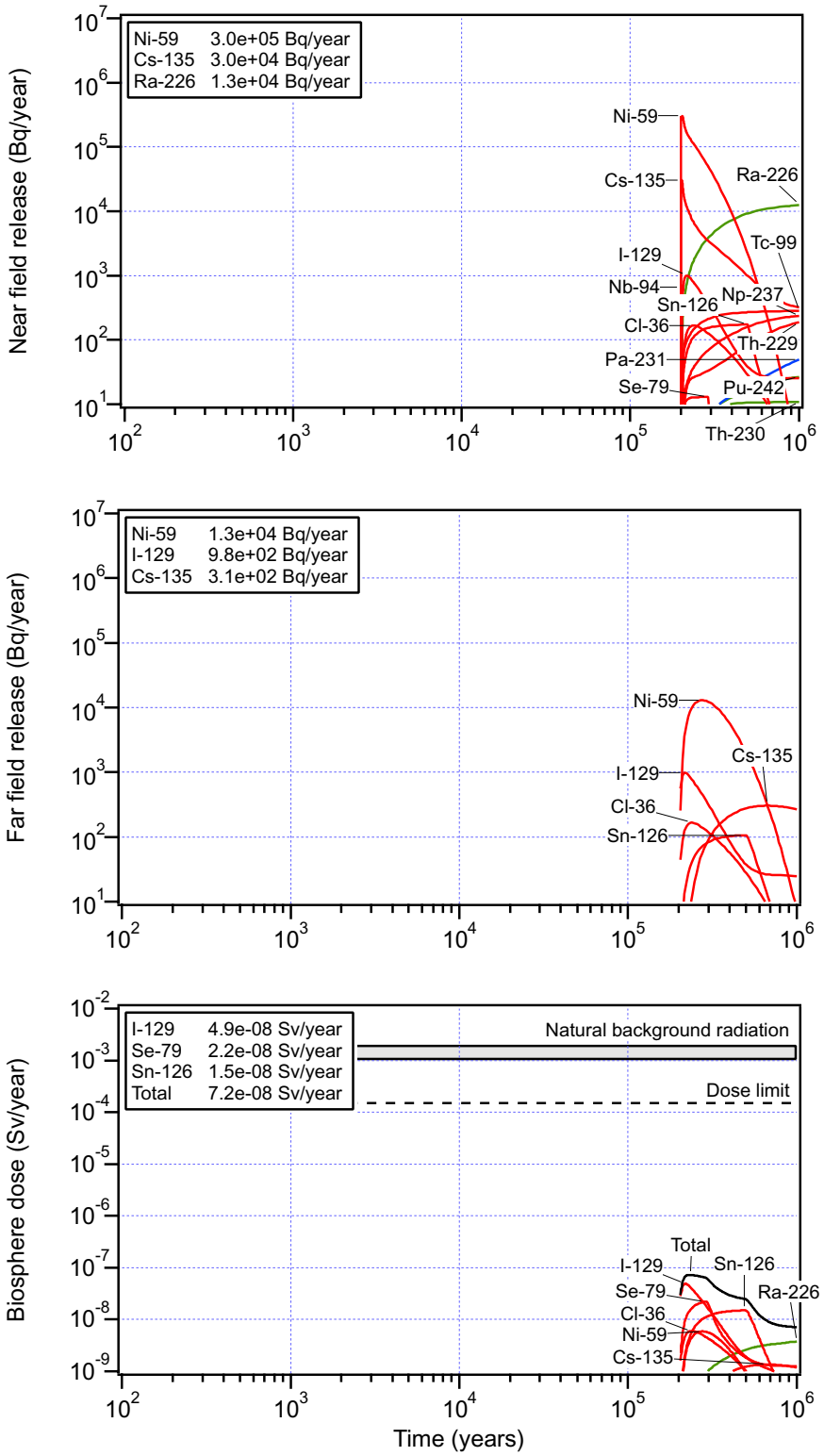

Figure 4-10. *Release from the near and far fields and biosphere dose as a function of time for the uncertainty case with pessimistic sorption in buffer and backfill for Aberg.*

4.2.4 Pessimistic connection between near field and rock

The connection between the near field and rock is determined by the water flux and the characteristics of the fractures/fracture zones that are in connection with the buffer or backfill. The parameters that are assigned pessimistic values in this case are the water flux and the Q_{eq}-parameters.

Figure 4-11 shows the results for Aberg. Corresponding figures for Beberg and Ceberg are given in Appendices B and C, respectively.

In the reasonable case the release from the near field of many of the nuclides are determined by the resistance in the connection between the near field and rock. Changing the parameters for this resistance implies that the release from the near field increases for nuclides like Ni-59, Cs-135 and Ra-226. The two nuclides that mostly contribute to the dose, I-129 and Se-79, are almost unaffected. This is since almost all resistance in the near field for these nuclides is in the buffer already in the reasonable case. Hence the maximum dose is about the same as in the reasonable case and well below the dose limit.

The same conclusions can be drawn for Beberg and Ceberg. The doses for these two sites are almost identical to the reasonable cases. Even though for example Ni-59, Cs-135 and Ra-226 are more easily transported through the near field, the retention in the rock is enough to reduce the dose from these nuclides to very low levels.

Finally it is noted that the difference between reasonable and pessimistic data for the water flux reflects an actual variability within a site.

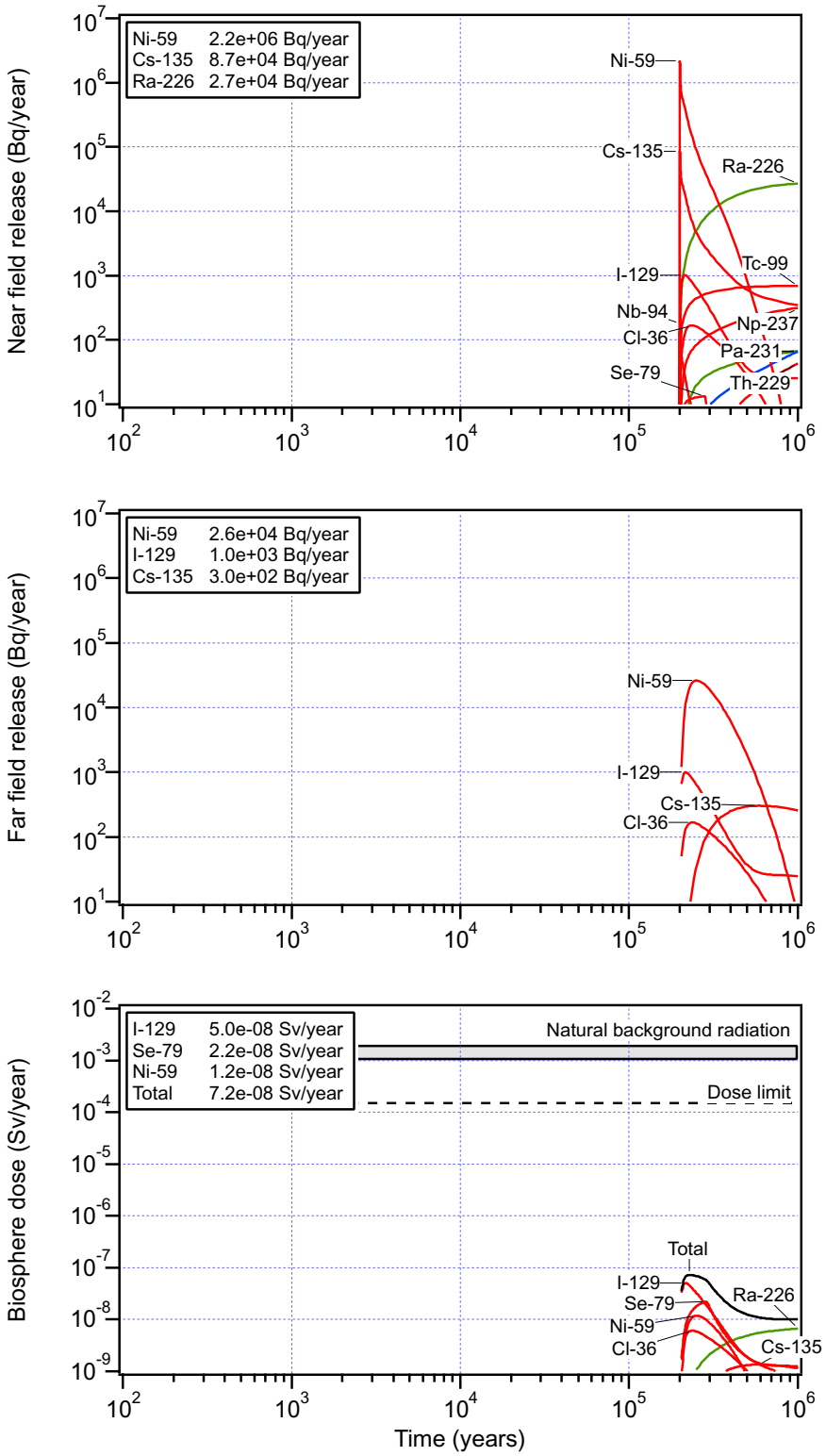

Figure 4-11. *Release from the near and far fields and biosphere doses as a function of time for the uncertainty case with pessimistic connection between near field and rock for Aberg.*

4.2.5 Pessimistic rock material parameters

Pessimistic sorption data and diffusivities in the rock are used in this case, while all other parameters are reasonable.

Figure 4-12 shows the results for Aberg. Corresponding figures for Beberg and Ceberg are given in Appendices B and C, respectively.

The near-field release is identical to the reasonable case, since all near field parameters are unchanged.

The far-field releases of Ni-59, Cs-135 and Ra-226 clearly show that these nuclides are less well retained in the rock with pessimistic sorption and diffusivity data.

The effect on the biosphere dose compared to the reasonable case is large for all sorbing nuclides e.g. Ni-59, Cs-135, Th-229 and Ra-226. The dose is in this case dominated by Ra-226. Even though the maximum dose is higher in this case compared to the reasonable case it is still more than two orders of magnitude lower than the dose limit.

The far-field release from Beberg shows that Ni-59 and Cs-135 are influenced to a large extent. They give, however, negligible contribution to the dose. The only notable change in dose compared to the reasonable case is for Se-79. The dose is still dominated by I-129. Slightly higher doses are obtained for the non-sorbing I-129 and Cl-36 due to the pessimistic diffusivity.

No difference can be seen in the far-field release for Ceberg compared to the reasonable case. The dose is still dominated by I-129. As in Beberg the pessimistic diffusivity implies somewhat higher doses for I-129 and Cl-36. Se-79 is influenced more, due to changes both in K_d and diffusivity.

The reason that the effects are less at Beberg and Ceberg is not mainly due to the fact that pessimistic chemical transport data are more favourable than in Aberg. Pessimistic data for Beberg are actually the same as for Aberg. The big effect at Aberg is due to the fact that flow-related transport data, which together with chemical transport data determine the retention for sorbing nuclides, are less favourable.

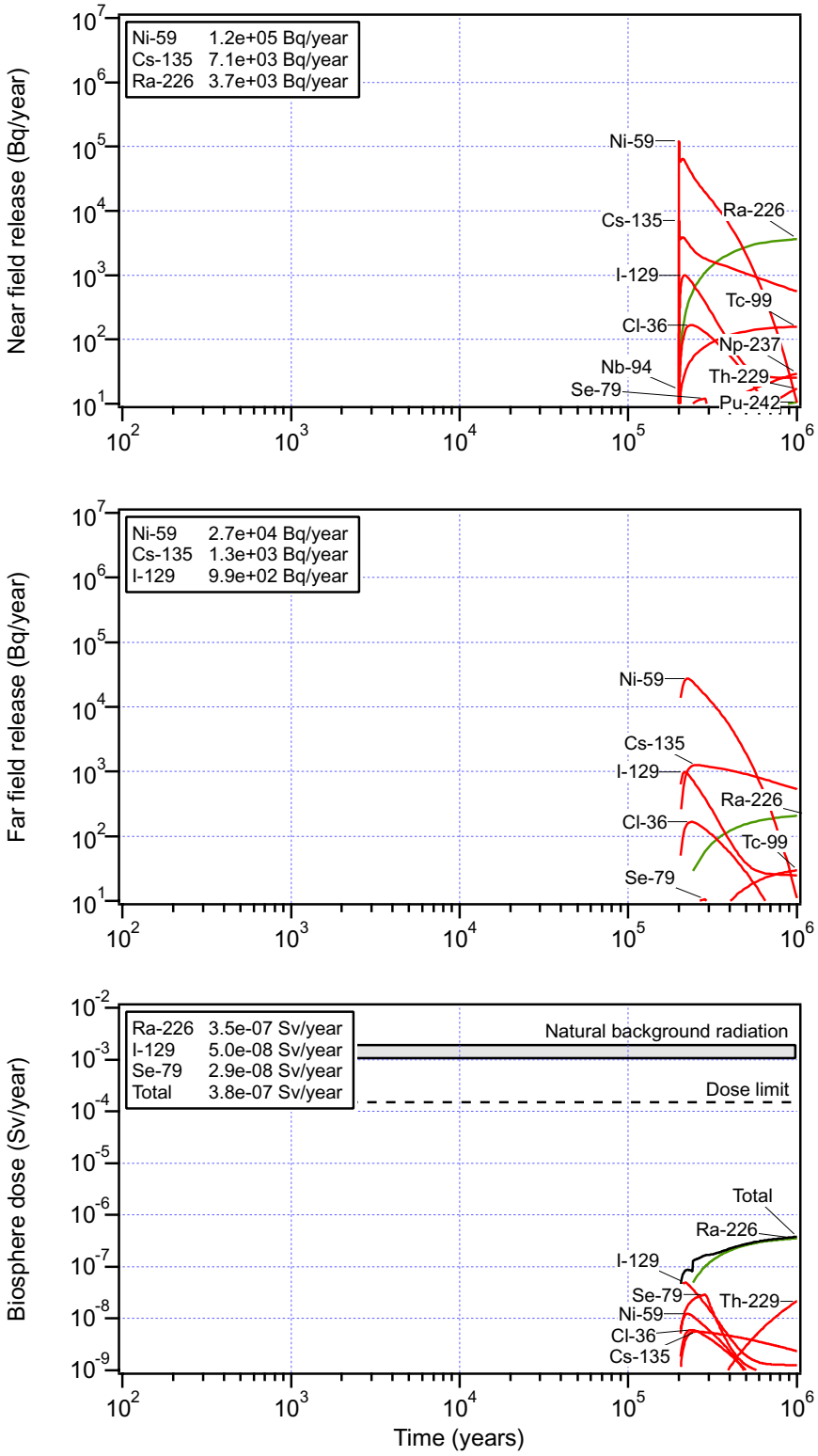

Figure 4-12. *Release from the near and far fields and biosphere doses as a function of time for the uncertainty case with pessimistic rock material parameters for Aberg.*

4.2.6 Pessimistic flow related parameters

In this case the flow related parameters are given pessimistic values and all others are assigned reasonable values. This means shorter travel times, decrease of a_w, decrease of the penetration depths and also a decrease of the Peclet number, see Table 4-3.

Tabell 4-3. Reasonable and pessimistic values for groundwater travel times and flow-wetted surface area.

	Groundwater travel time (years)		Flow-wetted surface area (m^{-1})	
	Reasonable	Pessimistic	Reasonable	Pessimistic
Aberg	10	0.8	10^4	10^3
Beberg	60	3.3	10^4	10^3
Ceberg	2000	400	10^3	10^3

Figure 4-13 shows the results for Aberg. Corresponding figures for Beberg and Ceberg are given in Appendices B and C, respectively.

The near-field release is identical to the reasonable case, since all near-field parameters are unchanged.

A comparison of near-field and far-field releases shows that the rock retention is negligible for the long-lived nuclides shown in the plots in this case.

The effect on the biosphere dose compared to the reasonable case is large for all sorbing nuclides. The non-sorbing nuclides I-129 and Cl-36 are not influenced by this change, since they already in the reasonable case passes through the rock with negligible delay. The dose is in this case totally dominated by Ra-226. The dose is more than one order of magnitude lower than the dose limit.

The results for Beberg are similar to those for Aberg. Ra-226 is the dose dominating nuclide.

The results for Ceberg are, however, almost the same as in the reasonable case. The dose from Se-79 shows an increase, but the dose is still dominated by I-129 at a very low level compared to the dose limit.

A special case for Aberg where the retention in the rock is not accounted is presented in Section 4.3.5.

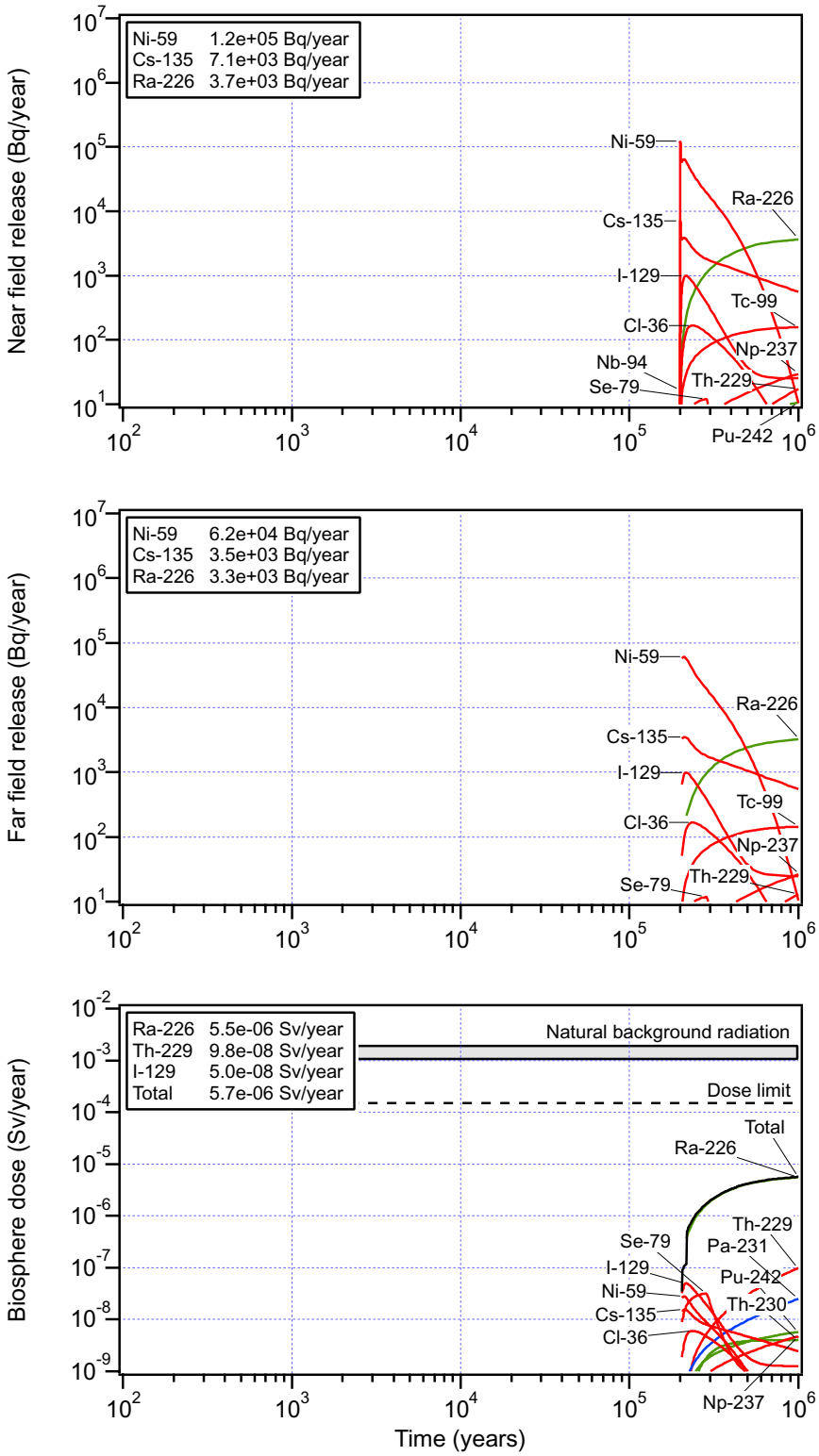

Figure 4-13. *Release from near and far fields and biosphere doses as a function of time for the uncertainty case with pessimistic flow related parameters for Aberg.*

4.2.7 Pessimistic dose conversion factors

In this case the dose conversion factors are assigned pessimistic values. The pessimistic values are chosen as the maximum EDF-factor for each nuclide among all modules, i.e. the peat area for almost all nuclides. The pessimistic EDF-factors are about one order of magnitude higher than the reasonable ones.

Figure 4-14 shows the results for Aberg. Corresponding figures for Beberg and Ceberg are given in Appendices B and C, respectively.

Since only the dose conversion factors are changed, the releases from the near field and far field are identical to the reasonable case.

The biosphere doses increase with a factor of about ten for most of the nuclides. This is directly corresponding to the increase of the EDF-factors. The maximum dose is more than two orders of magnitude below the dose limit.

The results for Beberg and Ceberg are similar to those of Aberg.

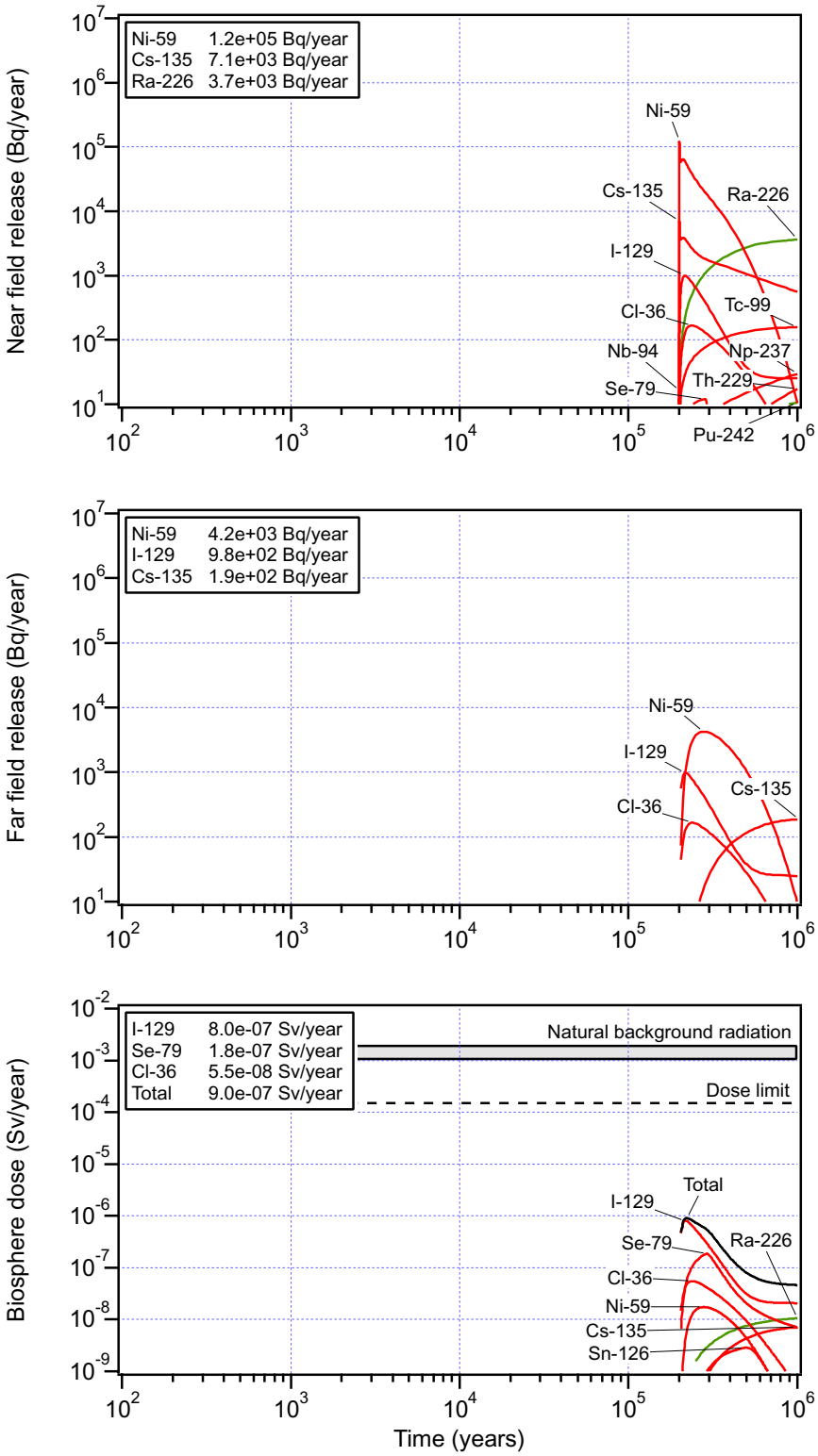

Figure 4-14. *Release from the near and far fields and biosphere doses as a function of time for the uncertainty case with pessimistic dose conversion factors for Aberg.*

4.2.8 Summary of uncertainty cases

In the uncertainty cases different groups of parameters are assigned pessimistic values. A complementary set of calculations with only single parameters with pessimistic values has been performed. In Figure 4-15 the change in maximum biosphere dose compared to the reasonable cases is shown for these cases.

Table 4-4. Summary of complementary uncertainty cases. (P=Pessimistic estimate and PA=Peat area).

Parameter	Complementary uncertainty cases													
	c1	c2	c3	c4	c5	c6	c7	c8	c9	c10	c11	c12	c13	c14
Near field														
Inventory														
IRF			P											
Fuel conversion														
Number of defective canisters	P													
Defect growth														
Delay time for transport		P												
Solubility				P										
Sorption in bentonite					P									
Sorption in backfill						P								
Near-field water flux q_0							P							
Q_{eq}-parameters														
Far field														
Diffusivity in rock													P	
Sorption in rock														P
Travel time								P		P				
Flow-wetted surface									P	P				
Maximum penetration depth												P		
Peclet number											P			
Biosphere														
Choice of module	PA	PA	PA	PA	PA	PA	PA	PA	PA	PA	PA	PA	PA	PA
EDF for selected module														

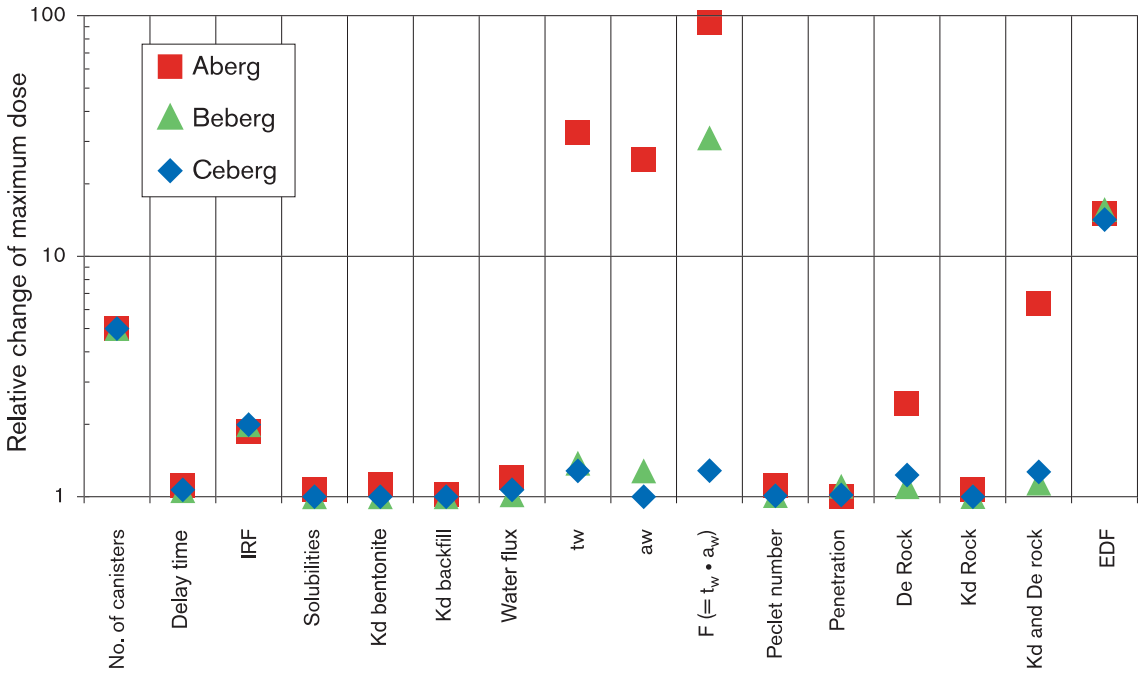

Figure 4-15. *The effect of varying different parameters based on the thoroughly reasonable cases.*

The figure shows that the greatest effects for Aberg are obtained for the number of initially defective canisters, the F factor (the product $t_w \cdot a_w$), sorption and diffusion in the rock (K_d and D_e) and the dose conversion factors (EDF). The other parameters have little influence on the result if they are varied alone, starting with the thoroughly reasonable case. The result is in agreement with the above discussion of the different parameter groups varied in the uncertainty cases. I-129 dominates the dose in almost all cases, except when t_w, a_w (or both t_w and a_w) or D_e in rock (or both D_e and K_d in rock) is pessimistic where Ra-226 is the dominating nuclide.

The figure shows that the greatest effect for Beberg are obtained for the number of initially defective canisters, the F factor (the product $t_w \cdot a_w$) and the dose conversion factors (EDF). I-129 dominates the dose in all but the case with a pessimistic F factor where Ra-226 is the dominating nuclide.

The effect at Ceberg is very small in all cases but those where the number of initially defective canisters and the dose conversion factors (EDF) are pessimistic. I-129 dominates the dose in all cases.

The estimated number of initially defective canisters could be improved with experience from future canister fabrication. The influence of uncertainties in the F factor differs between the sites. Here the result can thus be influenced by the choice of site. Within a site, the uncertainties can in part be reduced by investigating the site thoroughly, but a large part of the scatter in F-factors is caused by spatial variability within the site. This can only be partially reduced by suitable choices of canister positions, etc. The uncertainties surrounding the dose conversion factors should be possible to reduce with increased understanding of, and thereby improved modelling of, radionuclide dispersion in the biosphere.

These simple uncertainty analyses are complemented by the risk analyses in Section 5, where effects of combinations of reasonable and pessimistic data are systematically investigated.

4.3 Special cases for Aberg

To shed light on the roles of different barriers in the canister defect scenario, a number of special cases have been calculated:

- The fuel is completely dissolved when a continuous water pathway is created
- No solubility limitations
- Large initial canister defect
- Negligible diffusion resistance in the buffer
- Retention in the geosphere is neglected

None of the cases is realistic. They are included to illustrate the function of the barrier system. The changes that have been made in the models pertain only to radionuclide transport. The system's evolution in other respects, for example the hydromechanical consequences of a large initial canister defect, are not dealt with. The point of departure in all calculation cases is reasonable data for Aberg. In Table 4-5 the input data used in the different special cases are given.

Table 4-5. Summary of the special cases for Aberg (P=Pessimistic estimate, S=Special value and PA=Peat Area).

Parameter	Aberg, Special Cases				
	a00-irf100	**a00-csol**	**a00-nocanister**	**a00-nobuffer**	**a00-nofarf**
Near field					
Inventory					
IRF	S				
Fuel conversion	S				
Number of defective canisters					
Defect growth			S		
Delay time for transport			S		
Void					
Solubility		S			
Sorption in bentonite				S	
Diffusivity in bentonite				S	
Sorption in backfill					
Near field water flux q_0					
Q_{eq}-parameters					
Far field					
Diffusivity in rock					Not included
Sorption in rock					Not included
Travel time					Not included
Flow-wetted surface					Not included
Maximum penetration depth					Not included
Peclet number					Not included
Biosphere					
Choice of module	PA	PA	PA	PA	PA
EDF for selected module					

4.3.1 Immediate fuel dissolution, IRF=100

The influence of immediate fuel dissolution, i.e. the whole fraction of all nuclides is free for release immediately, is studied in this case. All other parameters are assigned reasonable values.

Figure 4-16 shows the release from the near and far fields and the biosphere dose as a function of time.

Some nuclides, I-129, Cl-36 and Cs-135, are influenced in proportion to the increase in IRF-value. The maximum dose from Se-79 is about the same as in the reasonable case, in both cases determined by the solubility limit. In the reasonable case the dose for longer times is lower since the slow fuel dissolution is not sufficient to uphold the solubility limit concentration. In the special case the dose continues at the level determined by the solubility limit.

The maximum dose of Ra-226 is in this case limited by the solubility, which can be seen as a plateau in the curves. Several additional nuclides are solubility limited in this case, compared to the reasonable case, this concerns Np-237, Pu-239 and Pa-231.

The most important conclusion from this case is that the fuel dissolution rate, which is surrounded by uncertainties, has a limited influence on the total function of the barrier system.

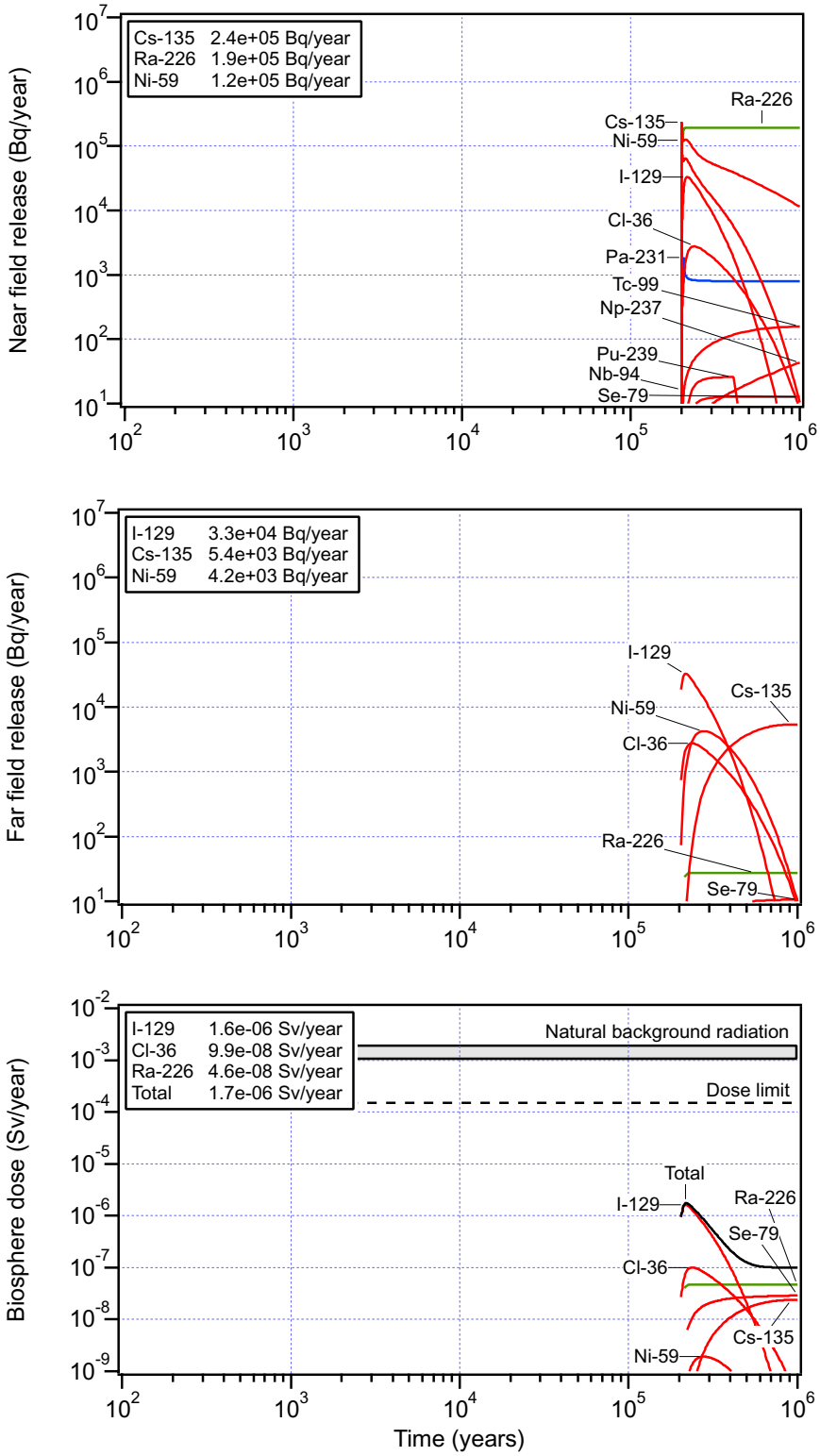

Figure 4-16. *Release from the near and far fields and biosphere doses as a function of time for the special case with immediate fuel dissolution for Aberg.*

4.3.2 No solubility limitations

The effect of disregarding all solubility limitations for the nuclides inside the canister is studied in this special case.

Figure 4-17 shows the release from the near and far fields and the biosphere dose as a function of time.

In this case many nuclides have much higher releases than in the reasonable case. The absence of a solubility limit for U-238 renders nuclides embedded in the matrix in the reasonable case free for release in this special case. In addition, the absence of solubility limits for other nuclides gives increased releases of species that are solubility limited in the reasonable case e.g. Pu-242, U-238, U-234, Th-230, Th-229, Pd-107, Se-79, Sn-126 and Tc-99. The nuclides Np-237 and Pa-231 are not solubility limited in the reasonable case, and hence limited by the dissolution rate of the uranium matrix. The dose is dominated by I-129.

Note that the release rate of Ra-226 from the near field decreases with time due to depletion of mother nuclides in the canister. The release rate from the far field is though increasing due to in-growth from mother nuclides released to the far field.

This case illustrates the importance of solubility limits, especially for the actinides. The value of the solubility limit may vary as illustrated by the span between reasonable and pessimistic values. The effect of pessimistic values has been illustrated in Section 4.2.2. The existence of solubility limits is however not questionable, since it is based on fundamental thermodynamics.

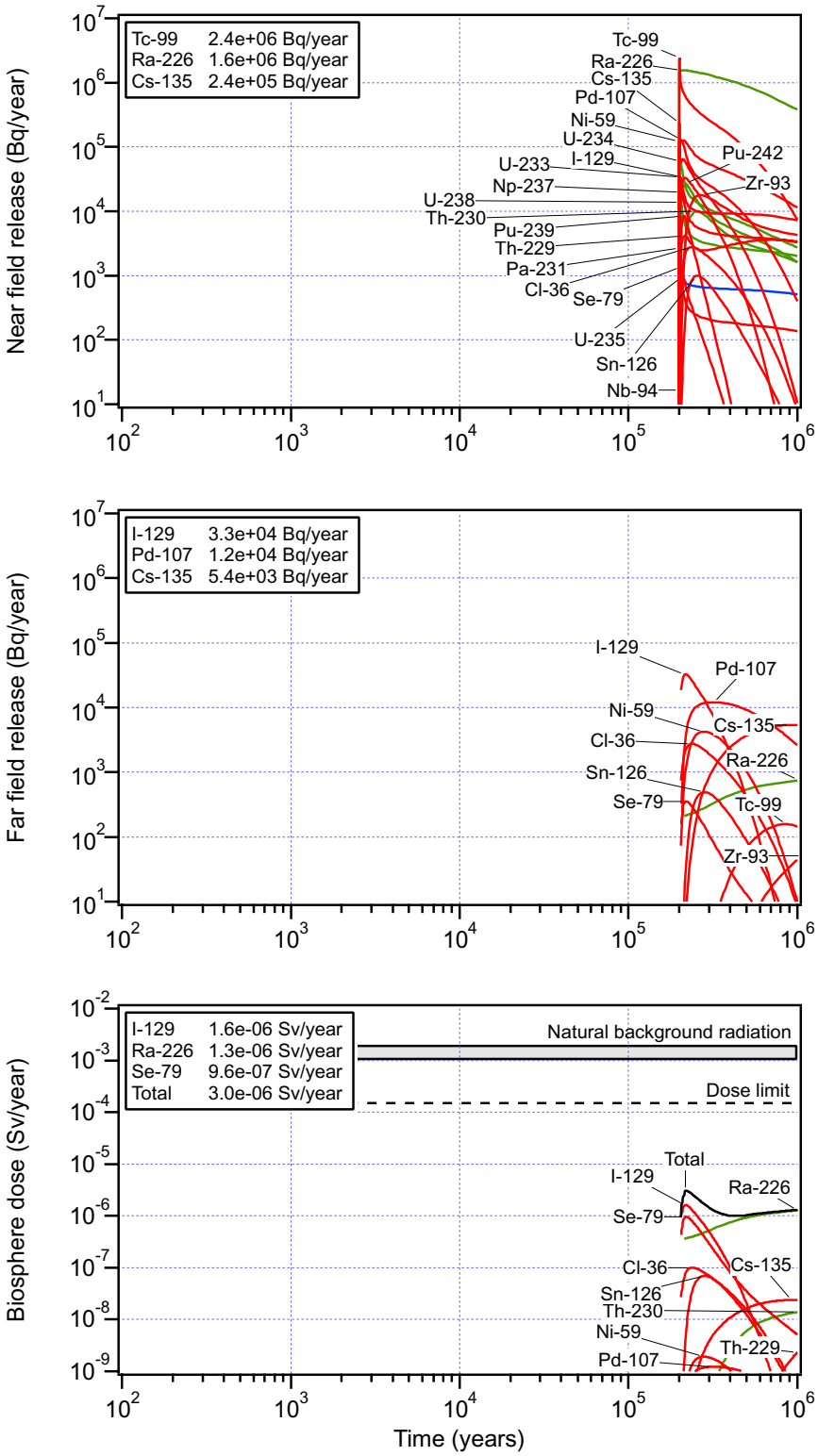

Figure 4-17. *Release from the near and far fields and biosphere doses as a function of time for the special case with no solubility limitations for Aberg.*

4.3.3 Large initial canister defect

In this case the canister is assumed to be initially defective and the defect large enough not to offer any transport resistance. The delay time is hence set to zero and the resistance in the hole is left out as well as the resistance in the connection between the hole and bentonite.

Figure 4-18 shows the release from the near and far fields and the biosphere dose as a function of time.

In this case the dose is dominated first by Sr-90, with a half-life of 29 years, thereafter by I-129 and finally by Se-79. Compared to other cases the biosphere dose is achieved early and continues at about the same level through almost the whole studied time period.

It can be concluded from this case that even with an initially unreasonably large canister defect the remainder of the system gives a sufficient protection and the dose is low compared to the dose limit.

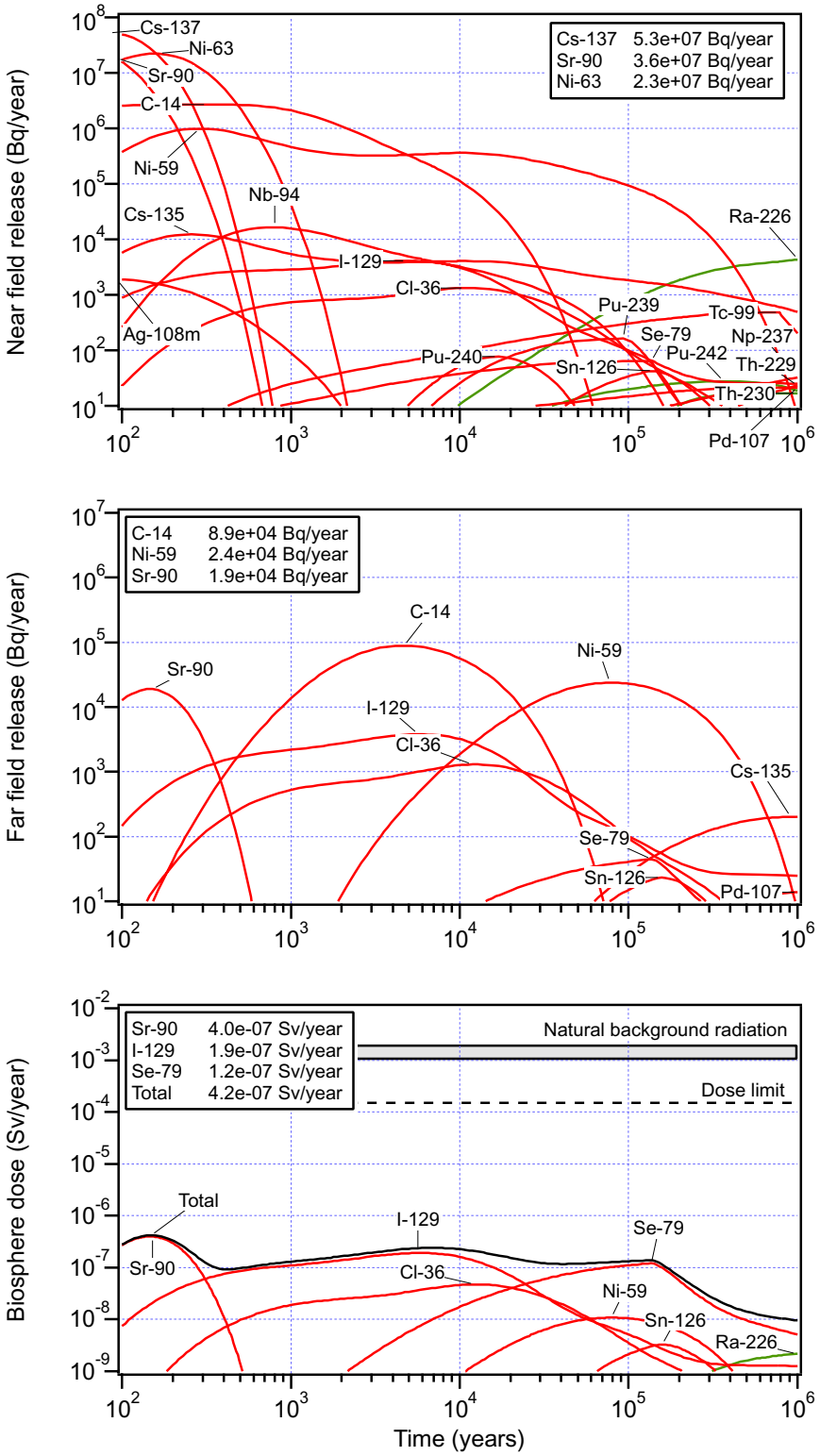

Figure 4-18. *Release from the near and far fields and biosphere doses as a function of time in the special case with large initial canister defect for Aberg. (Note that the scale is different for the near-field release compared to other figures in the report.)*

4.3.4 Negligible transport resistance in the buffer

In this case the effect of assigning a negligible transport resistance in the buffer is studied. The material in the buffer is replaced with water.

Figure 4-19 shows the release from the near and far fields and the biosphere dose as a function of time.

The effect is limited, since the transport resistances between the buffer and rock is dominating for many nuclides. Compared to the case with pessimistic sorption data in buffer and backfill, see Section 4.2.3, the releases are similar except for additional short initial pulses in this special case. These pulses result in about 10 times higher maximum doses from the three dominating nuclides, I-129, Cl-36 and Se-79. Compared to the reasonable case it is mainly Sn-126 and Ra-226 that is influenced. I-129 still dominates the total dose.

It can be concluded that the other barriers in the system gives a sufficient resistance to radionuclide transport even if the resistance in the buffer is neglected.

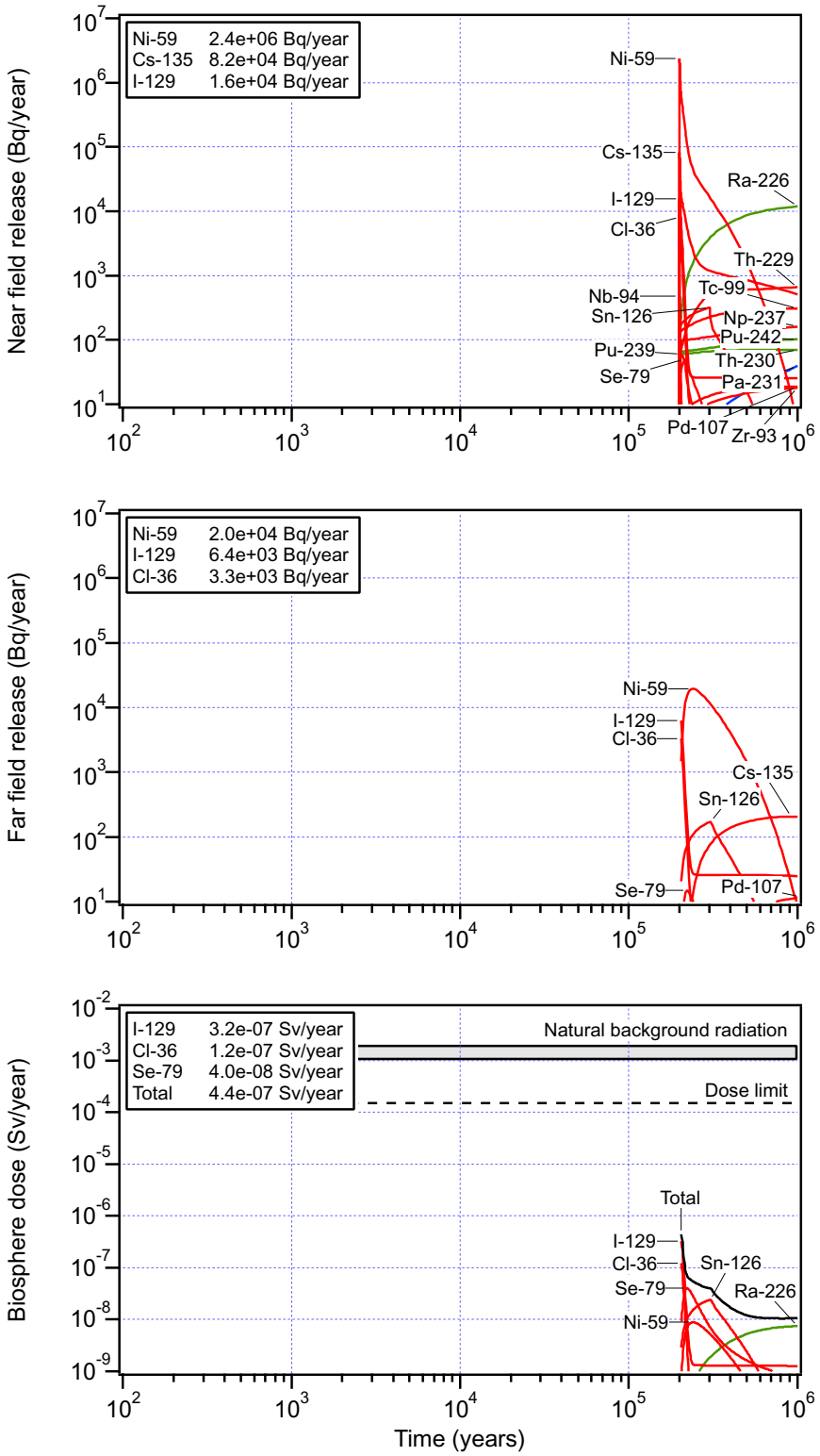

Figure 4-19. *Release from the near and far fields and biosphere doses as a function of time in the special case with negligible transport resistance in the buffer for Aberg.*

4.3.5 No retention in the rock

In this case the retention in the rock is totally neglected. This is done by using the near-field release rates directly in the dose calculations. The resistances between the buffer and rock described by Q_{eq}-values are assigned reasonable values.

Figure 4-20 shows the release from the near and far fields and the biosphere dose as a function of time.

The results are almost identical to the case with pessimistic flow related parameters in the rock, see Section 4.2.6. The effect on the biosphere dose compared to the reasonable case is large for all sorbing nuclides. The dose is totally dominated by Ra-226. This shows that retention in the rock is very important for the dose from Ra-226 as already concluded. The non-sorbing nuclides I-129 and Cl-36 are almost unaffected by the absence of retention in the rock.

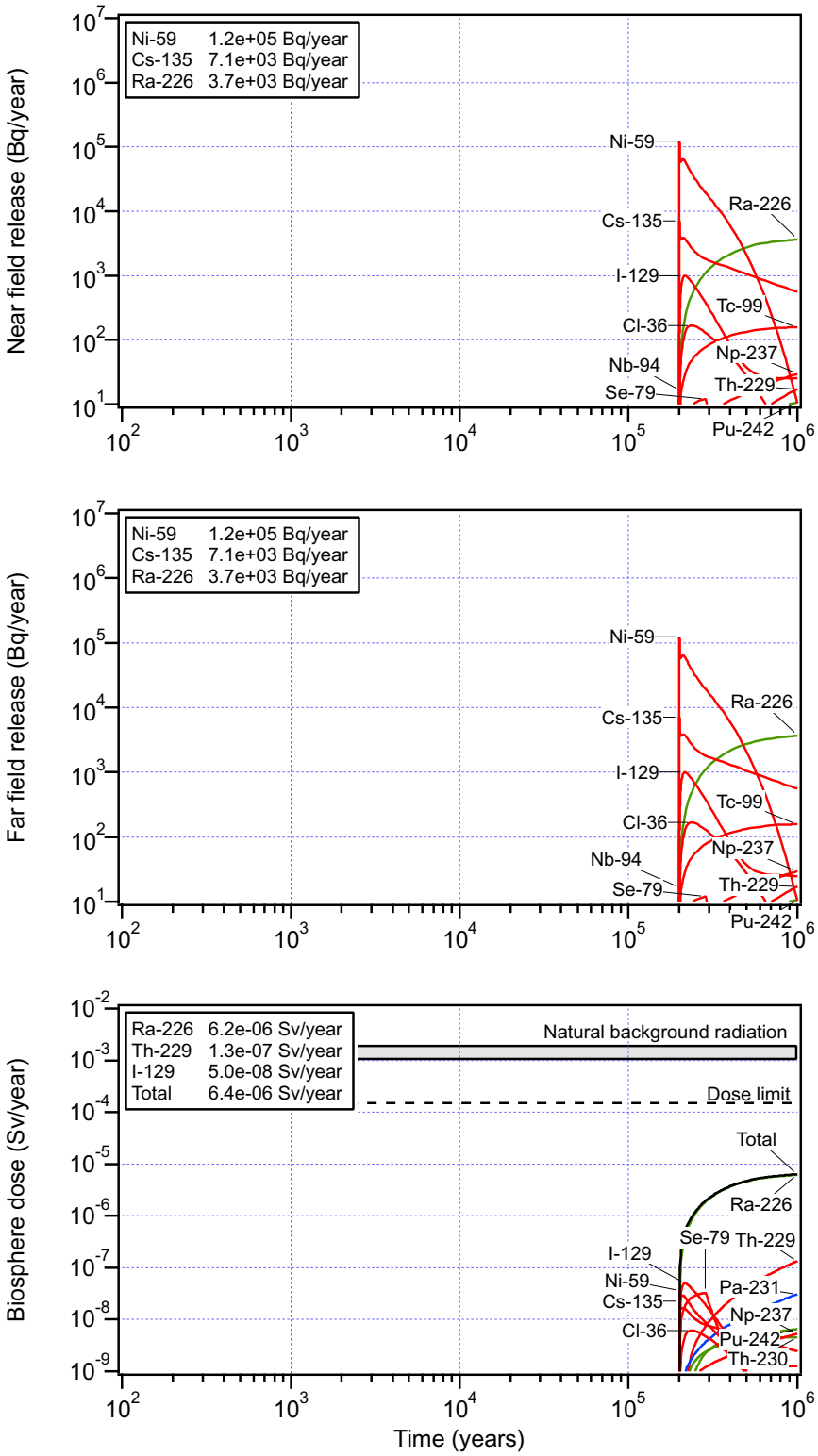

Figure 4-20. *Release from the near and far fields and biosphere doses as a function of time in the special case with no retention in the rock for Aberg.*

4.4 Glacial melting case for Aberg

In the canister defect scenario, which builds on the base scenario, today's climate is assumed to prevail. Expected future climate changes are treated in the climate scenario, see the SR 97 Main Report.

The glacial melting case treats those periods of the climate scenario where the hydraulic conditions are assumed to be less favourable than for the canister defect scenario, see the Main Report. According to the climate scenario, conditions at Aberg will be more favourable than for the canister defect scenario over most of the coming 100 000 years. However, when the ice-front passes and when Aberg lies in the melting zone of the ice sheet the groundwater flow may increase significantly. During these periods the sea covers Aberg. The Aberg glacial melting case considers the high flows caused by the ice sheet and combines this with the open coast biosphere module. This module has low dose conversion factors due to the high dilution.

A summary of the used input data is given in Table 4-6. The size and growth of the canister defect, the delay time and also the diffusivity in the rock are assigned pessimistic values. Several parameters are assigned special values not described in Chapter 3. This concerns the solubilities that are assigned the highest of the reasonable values for Aberg or Ceberg. This reflects the possible changes in solubility due to the possible changes of the groundwater composition. In addition the near-field water flux and the groundwater travel times are assigned values more pessimistic than the pessimistic values in the canister defect scenario. The near-field water flux is 0.4 m^3/m^2, yr and the groundwater travel time is 0.05 years. These values are based on a comparison of the regional groundwater flow calculations performed for present-day conditions (Svensson, 1997) and for subglacial conditions (Svensson, 1999). The latter calculations indicate that most of the exit points are in the ice tunnels, where transport further to the ice margin and out to the sea is fast. Some exit points are just in front of the ice margin. The dose conversion factors are hence chosen as the reasonable values for open coast.

Table 4-6. Summary of the input data to the glacial melting case for Aberg (P=Pessimistic estimate, S=Special value, OC=Open Coast).

Parameter	Aberg, Glacial melting
Near field	
Inventory	
IRF	
Fuel conversion	
Number of defective canisters	
Initial canister defects	P
Defect growth	P
Delay time for transport	P
Solubility	S
Sorption in bentonite	
Diffusivity in bentonite	
Sorption in backfill	
Near-field water flux, q_0	S
Q_{eq}-parameters	
Far field	
Diffusivity in rock	P
Sorption in rock	
Travel time	S
Flow-wetted surface	
Maximum penetration depth	
Peclet number	
Biosphere	
Choice of module	OC
EDF for selected module	

Figure 4-21 shows the release from the near and far fields and the biosphere dose as a function of time. The dose limit of 0.015 mSv/year, valid for the open coast, see Section 3.12, is indicated.

The near-field release has increased compared to the previously reported cases. This is mainly due to the influence of the very high near-field water flux. The high release rates before 20 000 years is due to the pessimistic assumption regarding the defect in the canister.

The far-field release is almost identical to the near-field release. This means that there is almost no retention in the far field, due to the extremely short groundwater travel time assumed to be valid for this scenario.

The calculated biosphere doses are less than 10^{-11} Sv/year for the whole time period as Aberg is assumed to be located beneath the surface of the sea which implies a great dilution in the biosphere.

Finally, it is noted that glacial melting conditions are expected to prevail only during limited time periods and not as a steady state condition as in this calculation case.

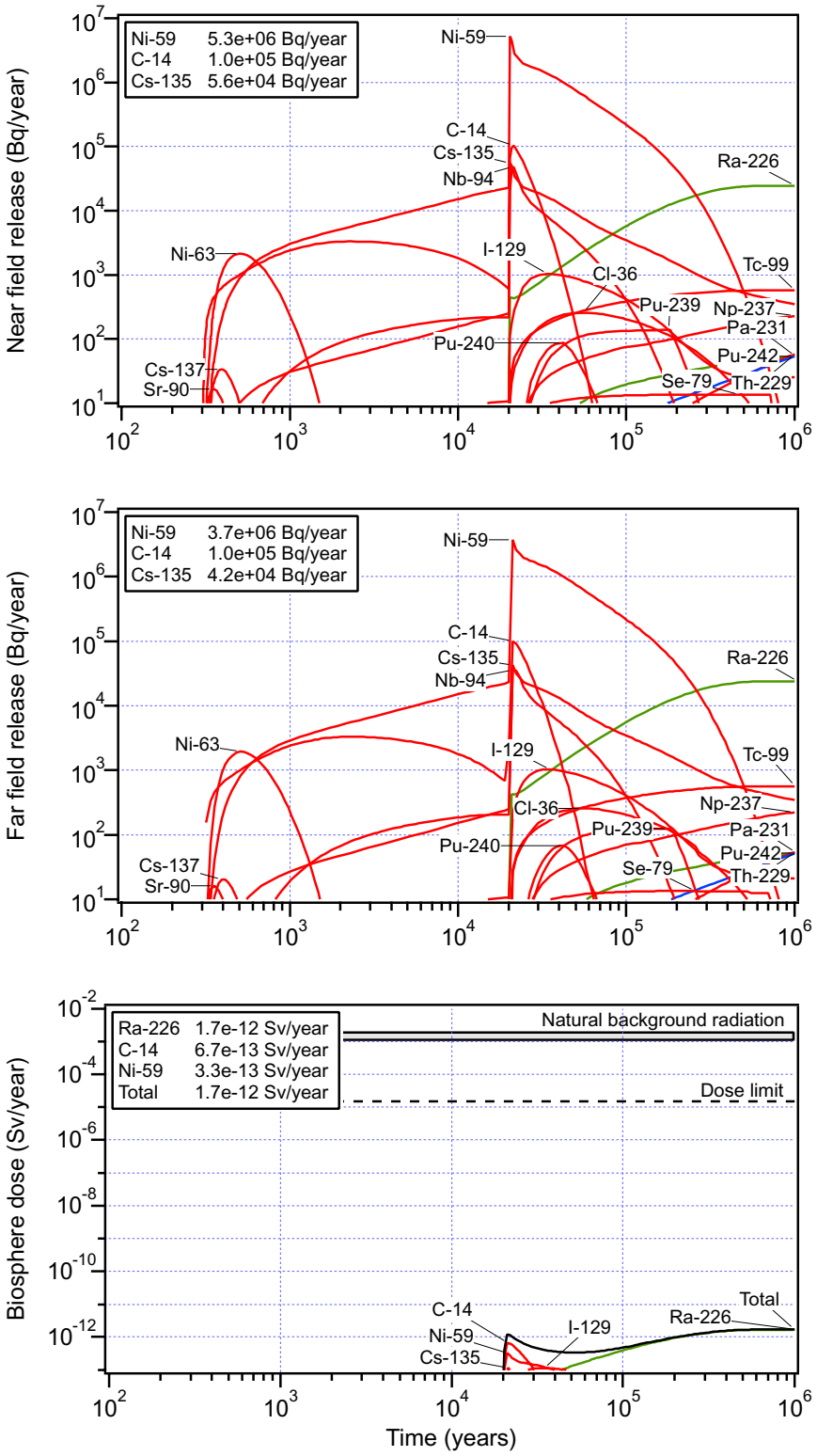

Figure 4-21. *Release from the near and far fields and biosphere doses as a function of time for the glacial melting case for Aberg. (Note that the scale for the biosphere dose differs from the other diagrams in the report. Note also the different level of the dose limit, valid for a large population.)*

5 Probabilistic calculations

The stipulated criterion for repository safety is a risk measure, i.e. a summation of products of probabilities and consequences for different alternatives for repository evolution.

The purpose of the probabilistic calculations is to judge the risk associated with the canister defect scenario. The risk in a situation where a number of different outcomes are possible is defined as the sum of the partial risks for each outcome. The partial risk is in turn the product of probability and consequence for the outcome in question. Mathematically, the risk R is expressed as:

$$R = \sum_i p_i k_i$$

where p_i and k_i are the probability and consequence, respectively, for outcome i. The risk R is thereby by definition the mean of all consequences.

As regards the risk in the canister defect scenario, different data choices for the models give rise to the different outcomes. The consequence is chosen as the maximum annual dose that arises during a million years. The risk is thereby the mean of the maximum doses in all realizations.

Calculations reported so far show only the consequence in the form of dose for different choices of data for the models. To be able to calculate a risk, the probability of different data sets must also be estimated.

Calculated distributions are only available for the near-field water fluxes and groundwater travel times, see Table 3-1. Most of the data are only estimated with a reasonable and a pessimistic value, i.e. the number of defective canisters, solubilities, IRFs, diffusion and sorption data in bentonite and backfill, diffusion data, sorption data, flow-wetted surface area and maximum penetration depth in the rock, as well as EDFs in the biosphere.

As was stated earlier in Chapter 3 the pessimistic values are chosen as an upper limit of the parameters negative influence on the calculation result. Many pessimistic values must thus be regarded as highly improbable. Even the reasonable values are often cautiously chosen.

Based on the above, a probability of 0.9 is assigned to reasonable data and 0.1 to pessimistic data for most parameters where no distributions are available. The situation is illustrated in Figure 5-1. Instead of guessing what a whole distribution looks like, a rough estimate is made of the probability of reasonable versus pessimistic data. (The graduation of the x-axis is arbitrary in this illustration; reasonable and pessimistic values can sometimes differ by several orders of magnitude.) The reasonableness of the assigned probabilities can only be judged by studying the procedure used in the selection of reasonable and pessimistic values in each individual case, which is reported in (Andersson, 1999). The probability values 0.9 and 0.1 are based on a general study of this type and are deemed to be a conservative choice.

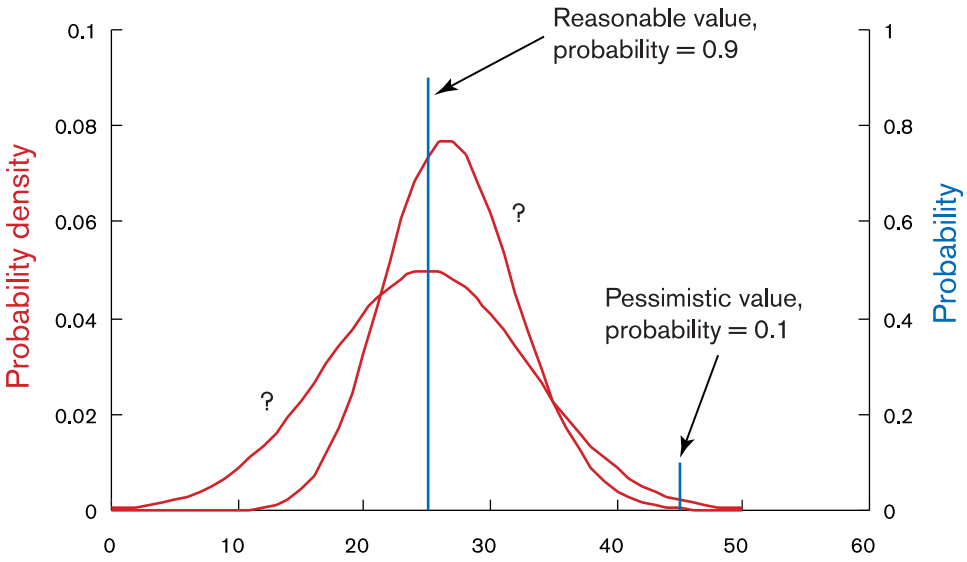

Figure 5-1. *Illustration of the probabilities used for input data where distributions are lacking. (The scale on the X-axis is arbitrary.)*

The defect growth, delay time for transport, Q_{eq}-parameters, penetration depth and Peclet number are assigned pessimistic values. The reason is technical and related to limitations in current versions of the calculation programs. The influence of the difference between pessimistic and reasonable values on the calculation result is limited for these parameters.

Two different biosphere modules are chosen for the EDF-factors: peat area and standard well. For both these the average values are used as reasonable values and the maximum values are used as pessimistic values, see Table 3.16 and 3.18.

Near-field water fluxes and groundwater travel times are correlated, according to the results of the hydrological calculations. Other input data to the probabilistic calculation are not correlated, which is not entirely correct. Co-variations can occur between different nuclides as regards e.g. EDFs so that these data should at least be partially correlated. There is, however, nearly always one nuclide that completely dominates the maximum dose in a given realization. By not correlating such data, more realizations will contain a pessimistic value for at least one nuclide, which makes it pessimistic not to include such correlations.

The nuclides in the risk calculation are reduced for capacity reasons to those which might conceivably under some circumstances make significant contributions to the maximum dose, namely Ni-59, Nb-94, Sn-126, I-129, Pu-239 and the decay chain U-238 → U-234 → Th-230 → Ra-226.

The reported results for the probabilistic calculations include 5000 realizations. A total of 6400 realizations were executed, but the mean values, i.e. the risk, were not influenced by the last 1400 realizations, see Figure 5-2.

In Figure 5-3 and 5-4 the distribution functions for the maximum biosphere doses are given for peat area and standard well, respectively. The mean values for each distribution, i.e. the risk at the three sites, are indicated in the figures and also given in Table 5-1.

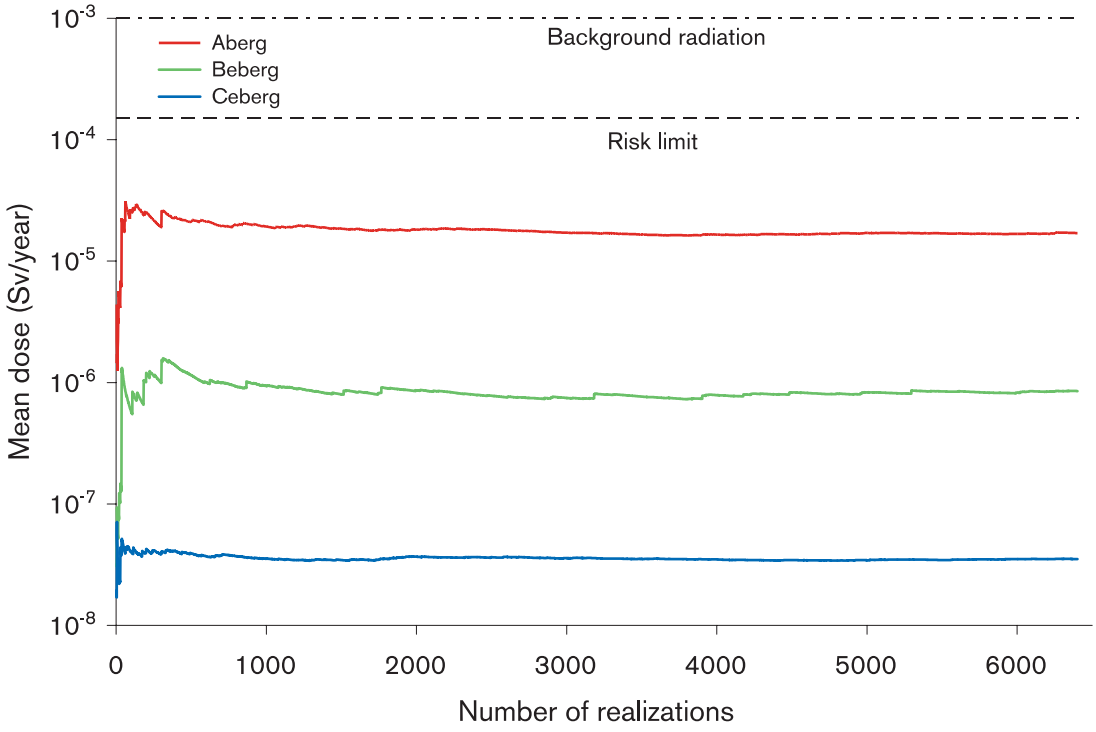

Figure 5-2. *Mean dose in peat area at Aberg, Beberg and Ceberg as a function of the number of realizations.*

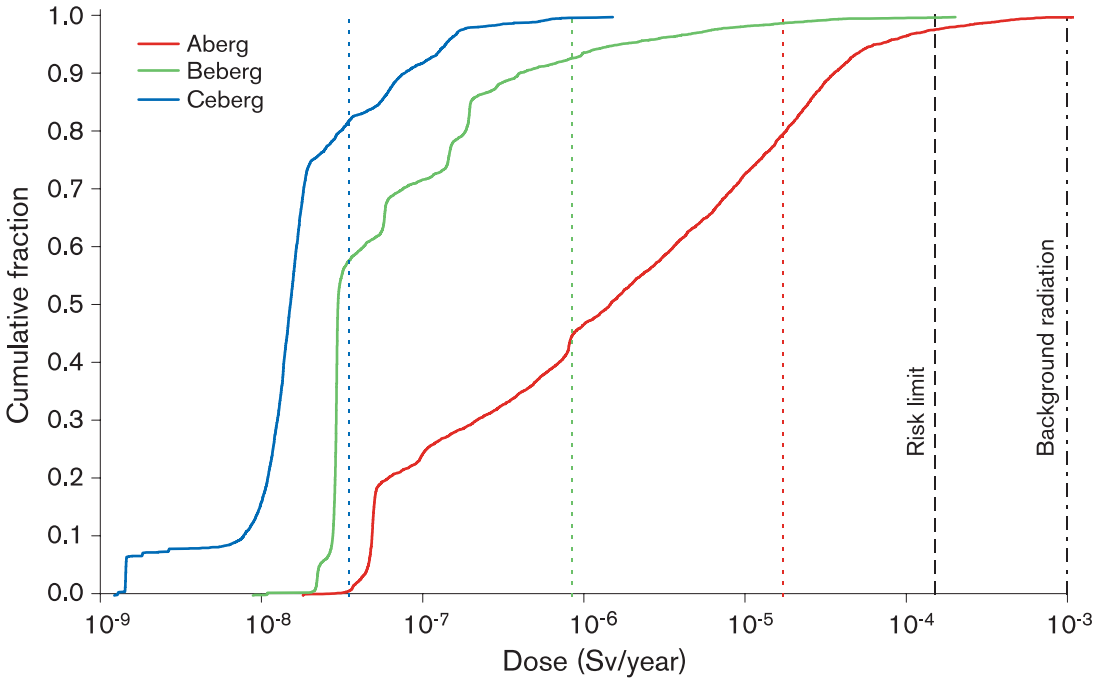

Figure 5-3. *Distribution functions for the maximum dose in peat area at Aberg, Beberg and Ceberg. The mean values for each distribution, i.e. the risk at the three sites, are also indicated as coloured vertical lines.*

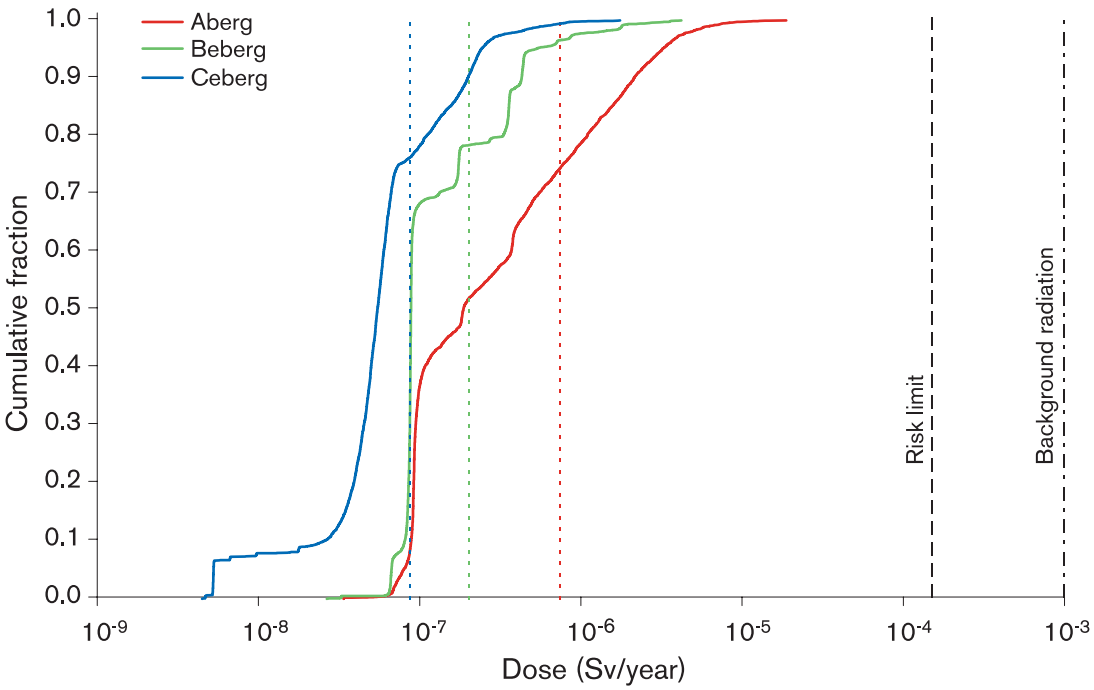

Figure 5-4. *Distribution functions for the maximum dose in standard well at Aberg, Beberg and Ceberg. The mean values for each distribution, i.e. the risk at the three sites, are also indicated as coloured vertical lines.*

Table 5-1. Calculated risks for the ecosystems peat area and standard wells at the different site.

	Calculated risk (Sv/yr)	
	Peat area	**Standard well (300 l/h)**
Aberg	$1.7 \cdot 10^{-5}$	$7.3 \cdot 10^{-7}$
Beberg	$8.3 \cdot 10^{-7}$	$2.0 \cdot 10^{-7}$
Ceberg	$3.4 \cdot 10^{-8}$	$8.5 \cdot 10^{-8}$

The mean values should be compared with the risk limit in the figures. The risk limit applies to the most exposed individuals in a regional group, which is also true for the EDFs used for well and peat area. The mean values for all sites lie well below the risk limit, in both the well and peat area cases. It is also apparent that the safety margin differs between the sites, it is largest in Ceberg and smallest in Aberg.

It is also worth noting for the well case that all realizations for all sites are more than one order of magnitude below the dose that corresponds to the risk limit in these calculations, i.e. the distributions in Figure 5-4 never come close to the risk limit.

Nearly all realizations that give significant maximum doses in the risk calculations are dominated either by I-129 or, if retention in the rock is weak, by Ra-226. A large canister defect is created after 20 000 years (pessimistic value in all realizations). The maximum dose of I-129 comes shortly thereafter.

The maximum dose of Ra-226 never arises until after more than 100 000 years, however, for fundamental reasons: Ra-226 is not present in the fuel initially, but is formed by chain decay of the initial content of U-238 and U-234. The nature of the decay chain is such that the rate of formation of Ra-226 does not become significant until after around 100 000 years.

The shape of the distributions in the risk calculations also illustrates differences in the repository's "insensitivity" to variations in parameters. Regard the distribution for peat area at Ceberg in Figure 5-3. It has a nearly vertical section around a dose of 10^{-8} Sv/yr where the cumulative fraction of realizations goes from 0.1 to over 0.7, i.e. over 60 percent of the realizations give rise to doses of around 10^{-8} Sv/yr. These realizations include a large number of parameter combinations that all give equivalent results of around 10^{-8} Sv/yr, which is also the maximum dose for the case where all parameters are chosen as reasonable, Figure 4-6.

The dose is lower in about ten percent of the realizations. These realizations have groundwater travel times that are longer than those chosen as reasonable. If pessimistic data had been compensated with "favourable" data, the fraction with lower doses would be greater. Several realizations give equal dose at a very low level. These all have a groundwater travel time of 100 000 years. This time has been assigned to particles in the groundwater flow model that have exit points at the bottom or sides of the model area instead of at the surface (Walker and Gylling, 1999).

The other barely 30 percent of the realizations have results over 10^{-8} Sv/yr. Only for these realizations are the parameter combinations sufficiently disadvantageous to affect the result significantly in an unfavourable direction.

The corresponding "vertical" range at Beberg lies around $3 \cdot 10^{-8}$ Sv/yr (around the maximum dose for the reasonable case) and includes around 60 percent of the realizations. Approximately 40 percent of the realizations have less favourable results. These also span a considerably larger dose range than the equivalent realizations for Ceberg.

The "vertical" part of the curve for Aberg lies around $5 \cdot 10^{-8}$ Sv/yr (around the maximum dose for the reasonable case) and includes only 20 percent of the realizations. In 80 percent of the realizations, the parameter combinations are less favourable in Aberg.

The above exposition illustrates two points:

- Aberg is most and Ceberg least sensitive to parameter variations. The "height" of the nearly vertical section can be said to be a measure of the repository's robustness on the site in question.
- The distributions also illustrate the fact that data that are more favourable than the reasonable data have not been included (except for travel times and water fluxes): A very small fraction of the realizations have a more favourable result than the case with thoroughly reasonable values, i.e. a very small fraction lie to the left of the "vertical" part of the respective distribution.

Similar observations can be made for the well case, Figure 5-4. Note that the distributions have a different shape, despite the fact that they are the result of the same realizations as for the peat case. The releases from the far field are exactly the same, but other nuclides dominate the doses for the well. This means that the far-field releases undergo a different turnover in the biosphere, and the effects of different parameter combinations in fuel, buffer and far field are different than in the peat case.

As regards robustness as well, differences between the sites mainly show up in a very long time perspective, for the same reasons as in the above risk discussion.

The three realizations with the highest maximum doses for Aberg for peat area are all dominated by Ra-226, the dose conversion factor for Ra-226 is pessimistic for all of them as well as the flow wetted surface. In all three realizations five canisters are defective, which implies that it is highly probable that at least one of them has a short groundwater travel time. In the realization with the highest dose all five defective canisters contribute to the dose, but in the second highest only two and in the third one contribute with 80% of the dose. The realization with the highest dose has a maximum dose about 100 times higher than the mean value for Aberg.

The three realizations with the highest maximum doses for Beberg for peat area are not as uniform as for Aberg. The maximum dose is dominated by Ra-226 and the dose conversion factor for Ra-226 is pessimistic for all of them. For the realization resulting in the highest dose there is only one defective canister, but with a very short groundwater travel time. The realization with the second highest dose has several pessimistic parameters, sorption data in bentonite and rock for Ra-226, flow wetted surface and only one defective canister, but with a short groundwater travel time. The realization with the third highest dose has five defective canisters, two of them with short groundwater travel time, pessimistic flow wetted surface and pessimistic diffusivity in rock for Ra-226. The realization with the highest dose has a maximum dose about 200 times higher than the mean value for Beberg.

The three realizations with the highest maximum doses for Ceberg for peat area are more varied. The realization resulting in the highest dose is dominated by Sn-126, with the following pessimistic parameters: five canisters are initially defective, sorption data in bentonite and rock for Sn-126 as well as IRF for Sn-126. The dose conversion factor for Sn-126 is however not pessimistic. The realization with the second highest maximum dose is dominated by I-129. The pessimistic parameters are five initially defective canisters, one of them with short groundwater travel time (resulting in 87% of the dose), IRF for I-129 and dose conversion factor for I-129. The realization with the third highest maximum dose is dominated by Sn-126. The pessimistic parameters are in this realization five initially defective canisters, sorption data in bentonite and rock for Sn-126. The dose conversion factor for Sn-126 is however not pessimistic. The realization with the highest maximum dose has a maximum dose about 40 times higher than the mean value for Beberg.

In order to shed light on the importance of Ra-226, the result of the risk calculation can also be evaluated with Ra-226 excluded. The results are shown in Figure 5-5 and Table 5-2. The results are influenced greatly for the peat area at Aberg and Beberg, in other cases more marginally.

The effect would have been roughly the same if the risk calculation had been done for a period of 100 000 years instead of a million years, since significant doses from Ra-226 come after roughly 100 000 years and for other nuclides that dominate the dose picture shortly after the canister defect has become large, i.e. 20 000 years.

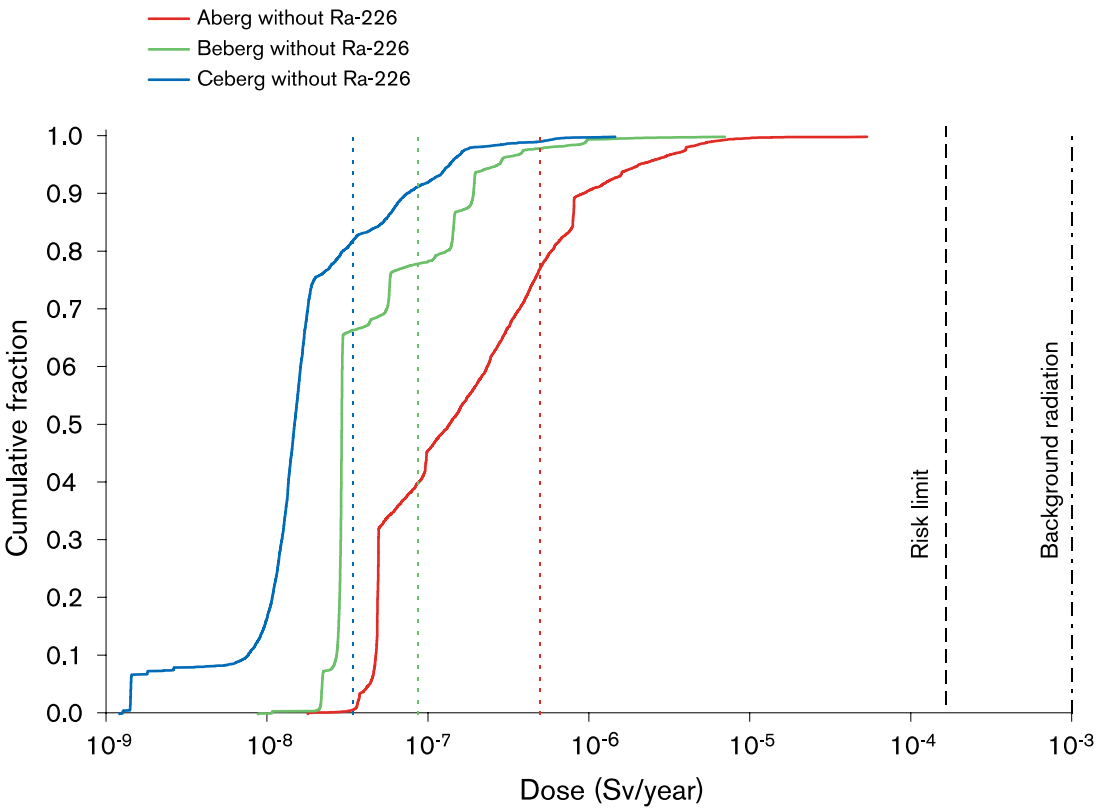

Figure 5-5. *Distribution functions for the maximum dose* ***without Ra-226*** *in peat area at Aberg, Beberg and Ceberg. The mean values for each distribution, i.e. the risk at the three sites, are also indicated as coloured vertical lines.*

Table 5-2. Relative risks for peat area and standard well with and without Ra-226. The risks are expressed as fractions of the acceptance criterion for the most exposed individuals, i.e. 0.15 mSv/yr.

	Peat area with Ra-226	without Ra-226	Well with Ra-226	without Ra-226
Aberg	0.11	0.003	0.005	0.001
Beberg	0.006	0.0006	0.001	0.001
Ceberg	0.0002	0.0002	0.0006	0.0006

In summary, the three sites are relatively equivalent during the initial 100 000 years. The differences between the sites are roughly a factor of ten and the risks are always less than one percent of the risk limit, for both well and peat ecosystem. The same conclusion applies to the well case for the period between 100 000 and one million years. With a peat ecosystem, the risk increases at Aberg and Beberg by a factor of 20 and 10, respectively, but is always well below the risk limit. An important reason why this outcome is obtained for the peat area is accumulation of Ra-226 in peat, a process which is included in the biosphere model. To put the result in perspective, it can be noted that certain peat bogs in Sweden exhibit sharply elevated concentrations of Ra-226, which comes naturally from the bedrock (Ek et al., 1982).

The results should also be viewed in the light of the fact that extensive glaciations are to be expected in Sweden within a period of a hundred thousand years, which is the subject of the climate scenario in the SR 97 Main Report.

6 Discussion and conclusions

The reasonable cases demonstrate the function of the repositories expressed as biosphere doses calculated with reasonable input data throughout. The biosphere doses are for all three hypothetical repository sites at least 3 orders of magnitude less than the dose limit.

The maximum biosphere dose is in most cases dominated by the long-lived non-sorbing I-129. In some uncertainty and special cases as well as in many realizations in the probabilistic calculations Ra-226 or Sn-126 dominate the maximum biosphere dose. Ra-226 is a naturally occurring radionuclide that is formed by in-growth from the chain decay of U-238 in the fuel matrix. Ra-226 is also in many cases the dominating nuclide at longer times.

The uncertainty cases demonstrate the importance of different parameters. Changing one parameter or some few parameters to pessimistic while all others are reasonable show that the biosphere doses never exceed the dose limit.

The analysis shows that the most important parameters in the near field are the number of defective canisters and the instant release fraction. The influence from varying one parameter never changes the doses as much as an order of magnitude. In the far field the most important uncertainties affecting release and retention are associated with permeability and connectivity of the fractures in the rock. These properties affect several parameters. Highly permeable and well connected fractures imply high groundwater fluxes and short groundwater travel times. Sparsely connected or highly variable fracture properties implies low flow wetted surface along migration paths. It should, however, be remembered that the far-field parameters have little importance if the near-field parameters take their reasonable values. In that case almost all radionuclides will be contained in the near field. The dose rate in the biosphere is essentially controlled by the possibilities of dilution. If the release occurs to an inner bay or open coast, the dose rates will be several orders of magnitude lower than if the release occurs to a drinking water well or peat area.

For Aberg uncertainty and/or variability in the parameters related to the far-field transport have the greatest influence on the result. Changing at least one of the far-field parameters diffusivities, flow-wetted surface or the groundwater travel time yields a release dominated by Ra-226 instead of I-129. The maximum biosphere dose is influenced to a large extent, but is at least one order of magnitude less than the dose limit. In addition to the far-field parameters the number of defective canisters and the dose conversion factors significantly influence the result. These two parameters influence the dose in proportion to the change in input data and I-129 is still the dominating nuclide.

Also for Beberg the parameters related to the far-field transport are the most important, although the impact of the uncertainty/variability is less than for Aberg. Changing both the flow-wetted surface and the groundwater travel time yields a release dominated by Ra-226 instead of I-129 and a significantly increased maximum biosphere dose. All other changes of input data give I-129 as the dose dominating nuclide. As for Aberg the number of defective canisters and the dose conversion factors significantly influence the result.

The uncertainty calculations for Ceberg show that uncertainty/variability in the far-field transport data are of minor importance. As for the other two sites the number of defective canisters and the dose conversion factors significantly influence the result. I-129 dominates the maximum biosphere dose in all the uncertainty calculations for Ceberg.

The special cases for Aberg demonstrate the principle of several barriers concerning radionuclide transport. Not even these cases with extreme and unreasonable assumptions concerning individual barrier functions result in unacceptable consequences. These cases also increase the understanding of the system modelled, for example which nuclides are solubility limited and the relative importance of different barriers for the different nuclides.

The probabilistic calculations are performed with the conservative estimate that the pessimistic values will become reality is 0.1 throughout. The near-field water fluxes and groundwater travel times are assigned correlated calculated distributions from the groundwater flow calculations.

If the release takes place to a standard well, the risk at Aberg is less than one hundredth of the acceptance criterion if the calculation is performed for a time span of one million years. The risk at Beberg is approximately one-fifth, and at Ceberg one-tenth, of the risk at Aberg.

In the case of release to a peat area, the sites differ in roughly the same way for times up to around 100 000 years. For a million years, the risk at Aberg then increases by approximately a factor of 40, at Beberg by a factor of ten and at Ceberg only marginally. The natural radionuclide Ra-226 dominates the consequences for the peat area for times over 100 000 years.

The dominating nuclide in most of the realizations for Aberg is Ra-226, while I-129 dominates most of the realizations for Beberg and Ceberg.

A more comprehensive discussion of the results of the radionuclide transport calculations with implications for the future research etc. is given in the SR 97 Main Report, Section 9.11.13.

7 References

Andersson J., Hermansson J., ElertM., Gylling B., Moreno L. and Selroos J-O. (1998) Derivation and treatment of the flow wetted surface and other geosphere parameters in the transport models FARF31 and COMP23 for use in safety assessment, SKB report R-98-60, Swedish Nuclear fuel and Waste Management Co, Stockholm.

Andersson J. (1999) Data and data uncertainties - Compilation of data and data uncertainties for radionuclide transport calculations, SKB Technical report TR-99-09, Swedish Nuclear fuel and Waste Management Co, Stockholm.

Bond A., Hoch A., Jones G., Tomczyk A., Wiggin R. and Worraker W. (1997) Assessment of a spent fuel disposal canister. Assessment studies for a copper canister with cast steel inner component, SKB Technical report TR 97-19, Swedish Nuclear fuel and Waste Management Co, Stockholm.

Bruno J., Cera E., de Pablo J., Duro L., Jordana S. and Savage D. (1997) Determination of radionuclide solubility limits to be used in SR 97. Uncertainties associated to calculated solubilities. SKB Technical report TR 97-33, Swedish Nuclear fuel and Waste Management Co, Stockholm.

Bäckblom G. (1996) Preliminär utformning av djupförvarets närområde, SKB AR D-96-011, Swedish Nuclear fuel and Waste Management Co, Stockholm. (In Swedish).

Carbol P. and Engkvist I. (1997) Compilation of radionuclide sorption coefficients for performance assessment, SKB report R-97-13, Swedish Nuclear fuel and Waste Management Co, Stockholm.

Ek J., Evans S. and Ljungqvist L. (1982) Variation in radioactivity, uranium and radium-226 contents in three radioactive springs along their out-flows in northern Sweden. SKBF/KBS TR 82-13, Swedish Nuclear fuel and Waste Management Co, Stockholm.

Elert M., Neretnieks I., Kjellbert N. and Ström A. (1992) Description of the transport mechanisms and path-ways in the far field of a KBS-3 type repository. SKB Technical report TR 92-09, Swedish Nuclear fuel and Waste Management Co, Stockholm.

Eriksson L., Hermasson H., Elert M., Lindgren M. and Widén H. (1999) FARF31 Version 1.1 - Including the capability of nuclide specific diffusivity coefficients, SKB report TS-99-15, Swedish Nuclear fuel and Waste Management Co, Stockholm.

Firestone R.B. et al. (1998) Table of Isotopes, Eight Edition, 1198 Update, Lawrence Berkely National Laboratory, University of California

Gylling B., Walker D. and Hartley L. (1999) Site-scale groundwater flow modelling of Beberg, SKB Technical report TR-99-18, Swedish Nuclear fuel and Waste Management Co, Stockholm.

Håkansson R. (1998) Beräkning av nuklidinnehåll, resteffekt, aktivitet samt doshastighet för utbränt kärnbränsle, Studsvik Nuclear, NR-96/079, rev. 1998-11-16. (In Swedish).

Johnsson L.H. and Tait J.C. (1997) Release of segregated nuclides from spent fuel, SKB Technical report TR 97-18, Swedish Nuclear fuel and Waste Management Co, Stockholm.

Lindgren M. and Widén H. (1998) Discretization in COMP23 for SR97, SKB report R-98-03, Swedish Nuclear fuel and Waste Management Co, Stockholm.

Lindgren M. and Widén H. (1999) Preparation of inventory data files for SR 97 calculations with PROPER, SKB report R-99-63, Swedish Nuclear fuel and Waste Management Co, Stockholm.

Moreno L. (1999) Impact of the water flow rate in the tunnel of the release of radionuclides, SKB report R-99-##, Swedish Nuclear fuel and Waste Management Co, Stockholm.

Moreno L. and Gylling B. (1998) Equivalent flow rate concept used in near field transport model COMP23 - Proposed values for SR 97, SKB report R-98-53, Swedish Nuclear fuel and Waste Management Co, Stockholm.

Neretnieks I. (1986) Stationary transport of dissolved species in the backfill surrounding a waste canister in fissured rock: Some simple analytical solutions. Nuclear Technology, vol. 72, pp. 194-200.

Nordlinder S., Berström U. and Mathiasson L. (1999) Ecosystem specific dose conversion factors for Aberg, Beberg and Ceberg, SKB Technical report TR-99-15, Swedish Nuclear fuel and Waste Management Co, Stockholm.

Norman S. and Kjellbert N. (1990) FARF31- A far field radionuclide migration code for use in the PROPER package, SKB Technical report TR 90-01, Swedish Nuclear fuel and Waste Management Co, Stockholm.

Ochs M. (1997) Review of a report on diffusion and sorption properties of radionuclides in compacted bentonite, SKB report R-97-15, Swedish Nuclear fuel and Waste Management Co, Stockholm.

Ohlsson Y. and Neretnieks I. (1997) Diffusion data in granite. Recommended values, SKB Technical report TR 97-20, Swedish Nuclear fuel and Waste Management Co, Stockholm.

Romero L. (1995) The near-field transport in a repository for high-level nuclear waste, Ph.D Thesis, TRITA-KET R21, The Royal Institute of Technology, Stockholm, Sweden.

Romero L., Thompson A., Moreno L., Neretnieks I., Widén H. and Boghammar A. (1999) COMP23/NUCTRAN User's Guide, SKB R-99-64, Swedish Nuclear fuel and Waste Management Co, Stockholm.

SKB91 (1992) SKB91 - Final disposal of spent nuclear fuel. Importance of the bedrock for safety, SKB Technical report TR 92-20, Swedish Nuclear fuel and Waste Management Co, Stockholm.

SKI SITE-94 (1996) SKI SITE-94, Deep repository performance assessment project, SKI Report 96:36, Swedish Nuclear Power Inspectorate, Stockholm.

SR95 (1995) SR95 - Template for safety reports with descriptive examples, Swedish Nuclear fuel and Waste Management Co, Stockholm.

Svensson U. (1997) A regional analysis of groundwater flow and salinity distribution in the Äspö area. SKB Technical report TR 97-09, Swedish Nuclear fuel and Waste Management Co, Stockholm.

Svensson U. (1999) Subglacial groundwater flow at Äspö as governed by basal melting and ice tunnels. SKB report R-99-38, Swedish Nuclear fuel and Waste Management Co, Stockholm.

TILA-99, Vieno T. and Nordman H. (1999) Safety assessment of spent fuel disposal in Hästholmen, Kivetty, Olkiluoto and Romuvaara, TILA-99. POSIVA 99-07, Posiva Oy, Helsinki, Finland.

Walker D. and Gylling B. (1998) Site-scale groundwater flow modelling of Aberg, SKB Technical report TR-98-23, Swedish Nuclear fuel and Waste Management Co, Stockholm.

Walker D. and Gylling B. (1999) Site-scale groundwater flow modelling of Ceberg, SKB Technical report TR-99-13, Swedish Nuclear fuel and Waste Management Co, Stockholm.

Yu J.-W. and Neretnieks I. (1997) Diffusion and sorption properties of radionuclides in compacted bentonite, SKB Technical report TR 97-12, Swedish Nuclear fuel and Waste Management Co, Stockholm.